CFD Applications in Wind Energy

Sørensen, Niels N.

Publication date:
2010

CFD Applications in Wind Energy

Glasgow - 2010

Niels N. Sørensen

Wind Energy Division · Risø DTU

RISØ-DTU, 09-09-2010

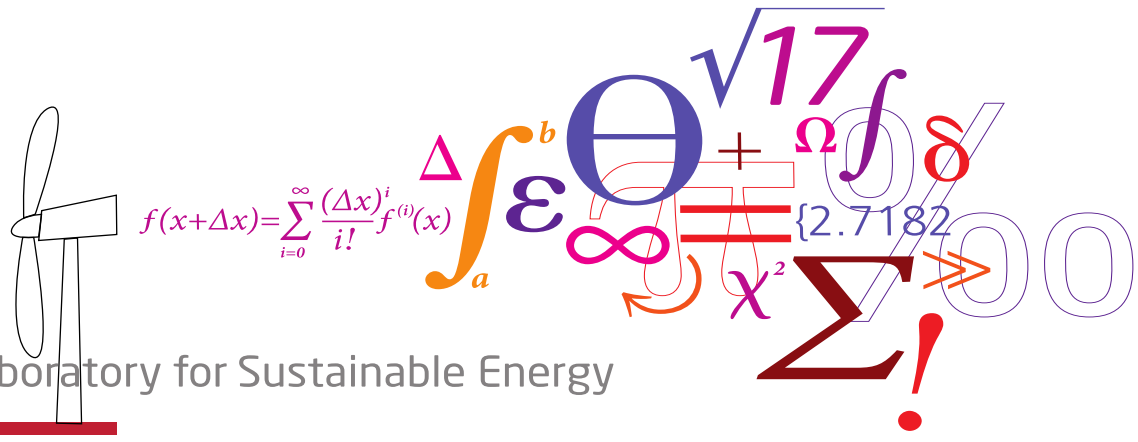

Risø DTU
National Laboratory for Sustainable Energy

Outline

1. The EllipSys Code
2. Grid Generation
3. Airfoil Aerodynamics
   - Performance
   - Dynamic airfoil computations
4. Rotor Aerodynamics
   - Rotors in axial flow
   - Yawed flow
   - Rotors in shear
5. Wind turbine related flow
   - Deep stall aerodynamics
   - Flow in the Nacelle region
   - Loads during standstill
   - Dynamic stall during standstill
6. Conclusion

The original philosophy

The code has been developed with wind energy application in mind over the last 20 years, by MEK DTU and here at Risø-DTU

- Accurate
- Consistent and convergent
- Stable
- Conservative
- Versatile
- Fast and Scalable

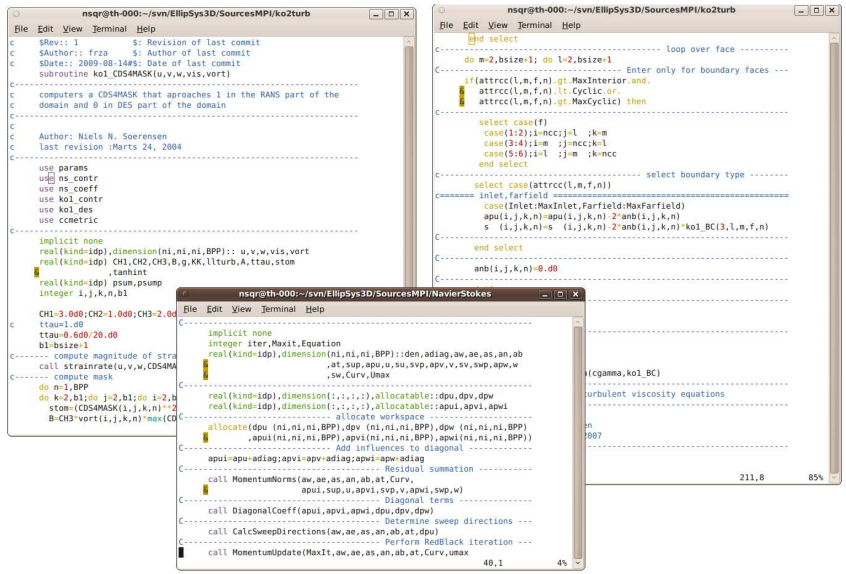

Niels N. Sørensen,
Risø DTU

Components of the solver

- Incompressible Navier-Stokes equations
- Pressure/Velocity formulation, using pressure correction technique
- Finite volume method
- Structured multi-block patched grids/overset grids
- Steady/Unsteady algorithms (SIMPLE/PISO) with sub-iterations
- Cartesian or polar velocity components
- Fixed, Moving Frame, Moving Mesh
- Turbulence modelling, RANS and LES/DES
- Transition modeling, e^n and $\gamma - Re_\theta$ correlation based model
- Acceleration Techniques
  - Grid sequence for the total algorithm
  - Multi-grid fort the solution of the pressure Poisson equation
- Parallellized using MPI for distributed computers

Discritization choices

- A second order implicit three point backward scheme is used along with sub-iterations

$$\frac{\partial \phi}{\partial t} = \frac{3\phi^t - 4\phi^{t-} + \phi^{t-2}}{2\Delta t}$$

- Diffusive terms are treated by central differences (2. order accurate)
- Convective terms
  - Upwind Differencing Scheme (UDS)
  - Second Order Upwind Differencing Scheme (SUDS)
  - Second Order Central Differencing Scheme (CDS)
  - Quadratic Upwind Interpolation for Convective Kinematics (QUICK)
  - Fourth Order Central Differencing (CDS4)

Hyperbolic Grid Generation

2D

$$\begin{aligned} \vec{r}_\xi \cdot \vec{r}_\eta &= 0 \\ \hat{n} \cdot (r_\xi \times r_\eta) &= \Delta S \\ \hat{n} \cdot \vec{r}_\eta &= 0 \end{aligned}$$

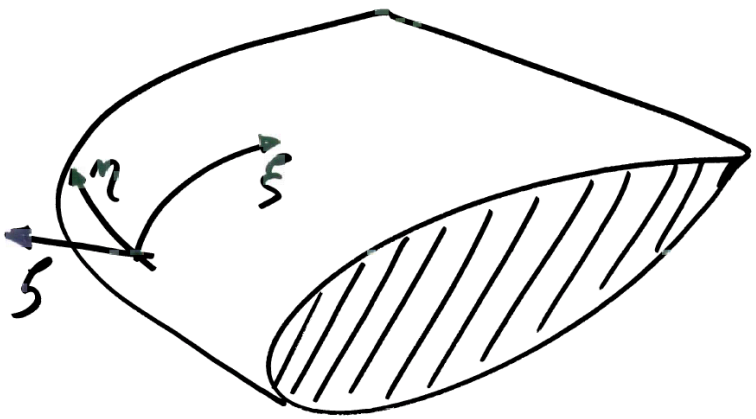

3D

$$\begin{aligned} \vec{r}_\xi \cdot \vec{r}_\zeta &= 0 \\ \vec{r}_\eta \cdot \vec{r}_\zeta &= 0 \\ J &= \Delta V \end{aligned}$$

Where:

$$J = \begin{vmatrix} x_\xi & x_\eta & x_\zeta \\ y_\xi & y_\eta & y_\zeta \\ z_\xi & z_\eta & z_\zeta \end{vmatrix}$$

Niels N. Sørensen,
Risø DTU

Hyperbolic Grid Generation

- The hyperbolic grid generation is a fast marching algorithm
- It produces meshes with good orthogonality and smoothness
- Easy to control stretching near the surfaces
- Lack of control of the exact position of the boundary
- By blending the hyperbolic method with a transfinite technique in the farfield, the location of the outer boundary can be controlled.

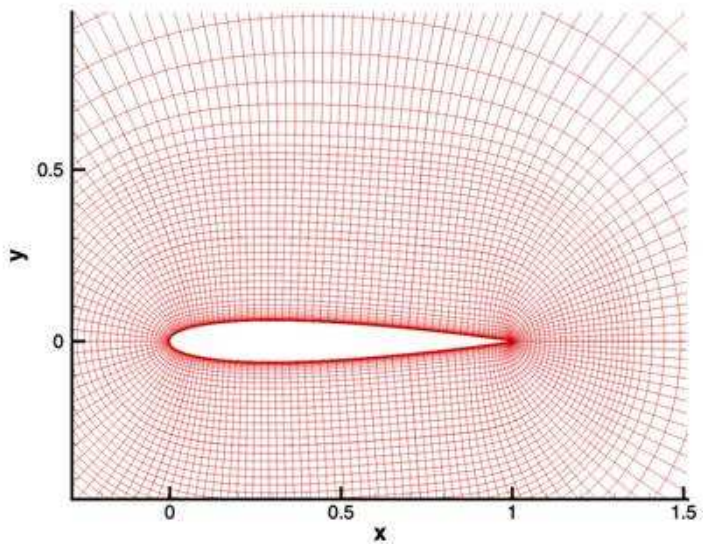

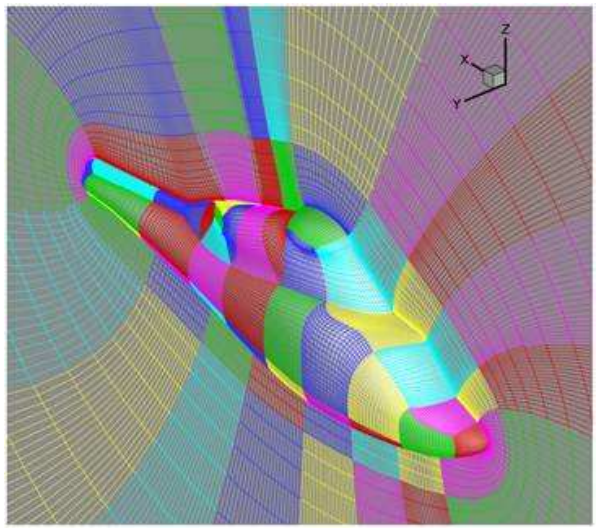

Niels N. Sørensen,
Risø DTU

Multi-element Airfoils

- An example of a combination of the hyperbolic technique with a transfinite technique is the present multi-element airfoil

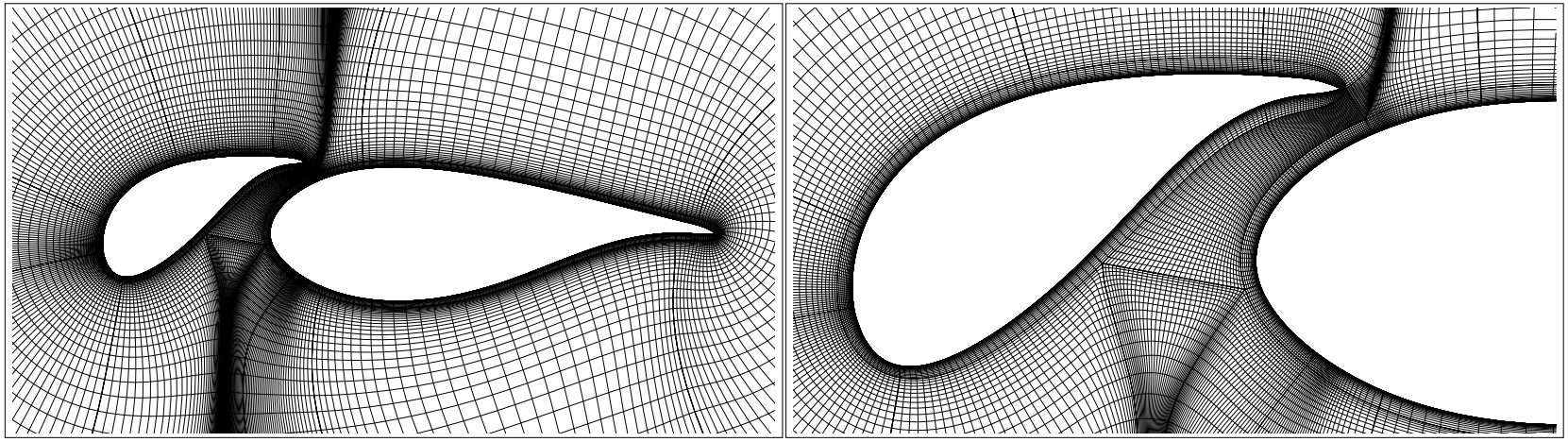

Niels N. Sørensen,
Risø DTU

NACA64-418

- 2D computation
- O-grid with 2048 $\times$ 384 cells, figure shows 384 $\times$ 384
- Reynolds Number 6 $\times$ 10^6
- Grid refinement study at 6 degrees angle of attack
- $k-\omega$ SST and $\gamma - Re_\theta$ transitions model

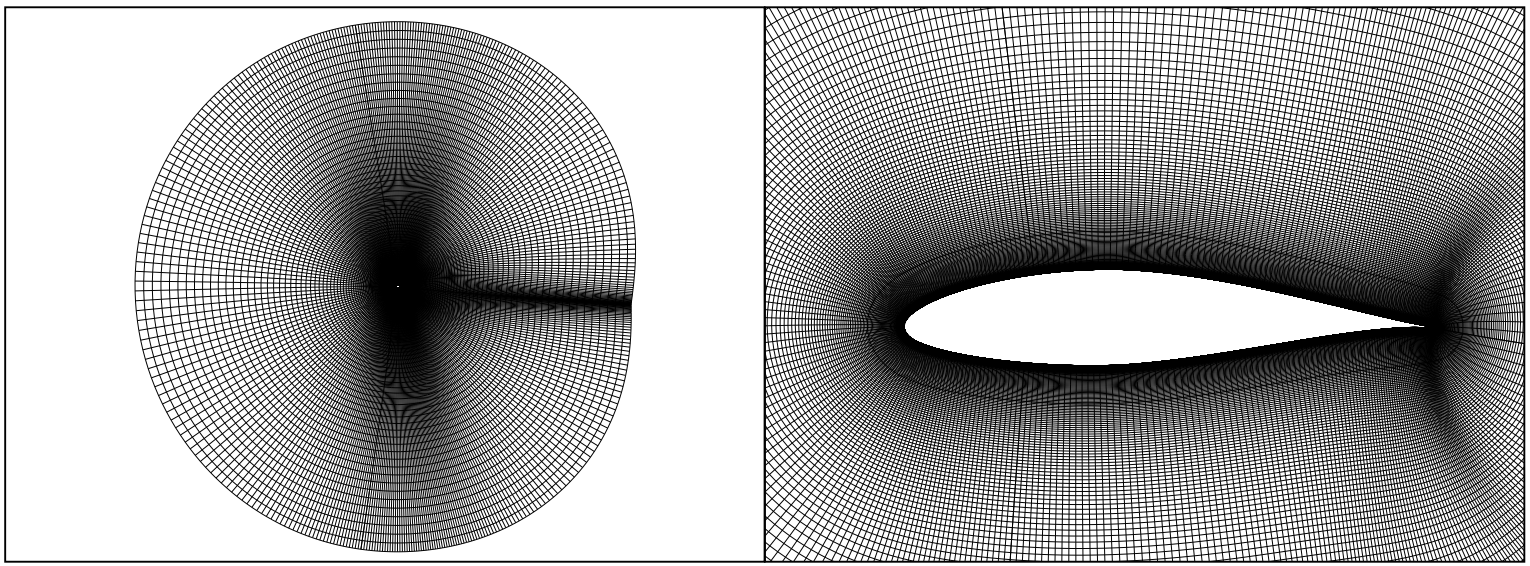

NACA64-418

- The lift and drag is well predicted in the linear region (384 $\times$ 384)
- In stall the agreement between experiment and computations are not perfect

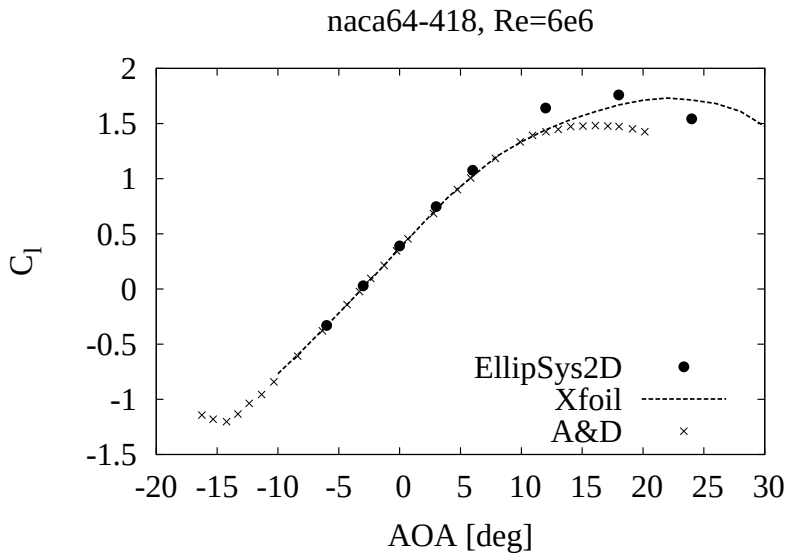

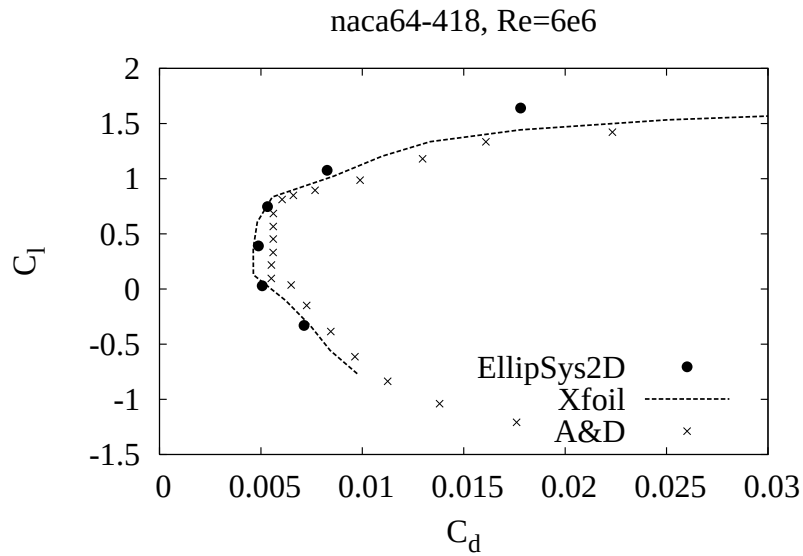

Niels N. Sørensen,
Risø DTU

NACA64-418

The formal order of the code is 2, and the computations show

Coarsening Level	p_{C_l}	p_{C_d}	p_{C_m}
1+2+4	1.88	1.89	1.95

The result on the different grid levels, AOA 6 deg.

Coarsening Level	C_l	C_d	C_m
8	1.04093	0.01098340	0.174302
4	1.05689	0.00845596	0.177110
2	1.05317	0.00818944	0.176174
1	1.05216	0.00811763	0.175933
Richardson	1.05178	0.00809826	0.175849

Dynamic stall

- Dynamic stall is important in connection with vibration analysis of turbines
- Dynamic stall computations can be performed for prescribed or coupled to an aeroelastic model
- The present example is prescribed motion according to an experiment of Galbraith et. al.
- The present computations is performed fully turbulent in an moving frame

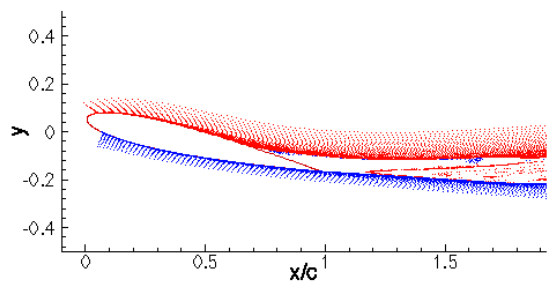

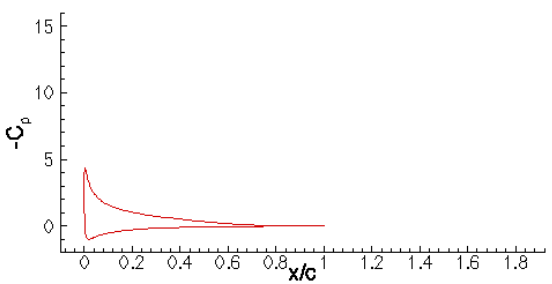

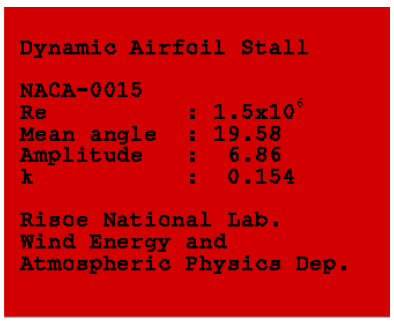

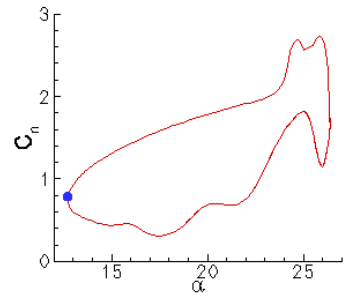

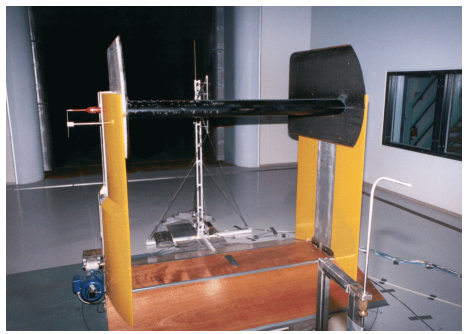

Airfoil with moving flap

- Recently there has been an increased interest in localized control on wind turbine blades
- A typical approach is deforming trailing edge

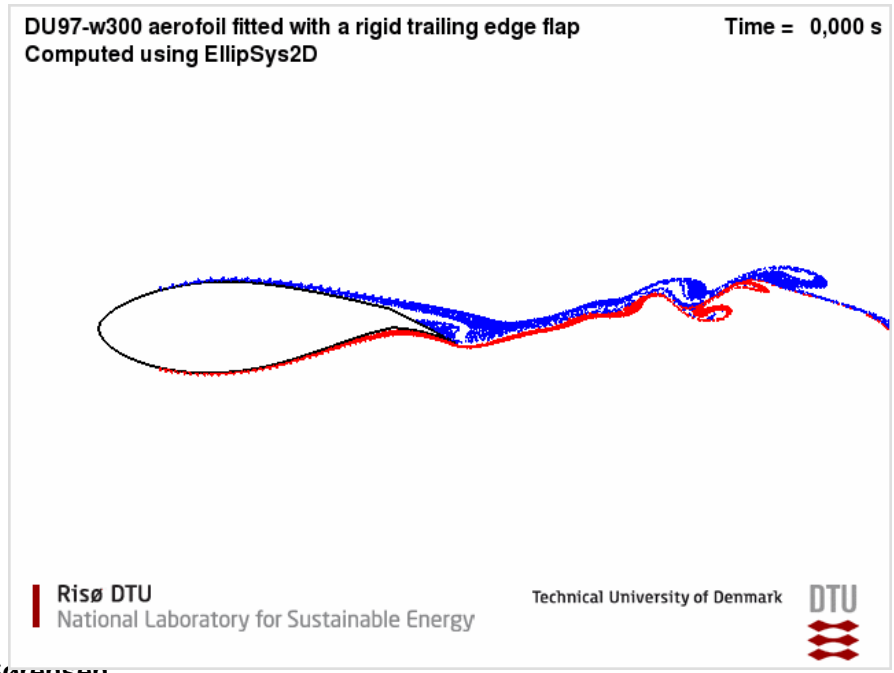

NREL Phase-VI

Parameters:

- 2 Bladed rotor based on the S809 airfoil
- Rotor diameter 10.06 m
- Rotational speed 72 RPM
- Tip pitch 3 deg., pointing leading edge into the wind
- Wind speeds (7,10,11,13,15, 20, 25)m/s
- Inflow turbulence is reported to be around 0.5% in the tunnel.

Nrel Phase-VI

Cyclic rotor grid:

- 3.1 million grid cells
- Grid resolution Chord-wise 256, span-wise 64, and normal 128, plus a tip patch of 64×64
- Domain radius corresponding to 9 rotor diameters
- Wall normal cell size corresponding to $y^+ < 2$

Can be used only for axial flow computations

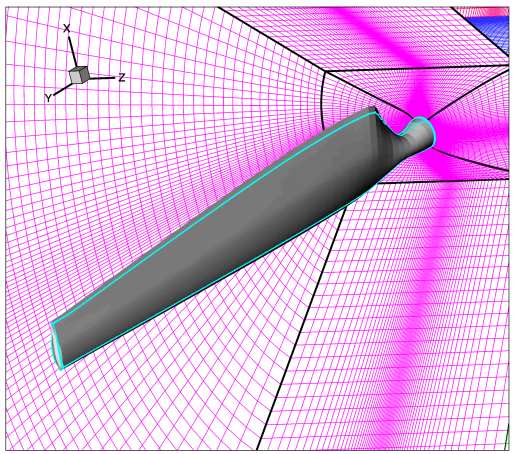

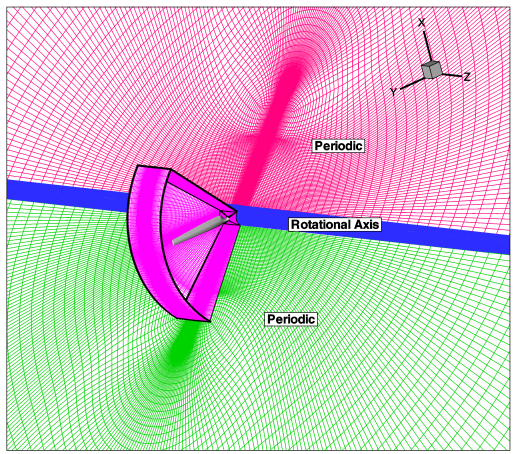

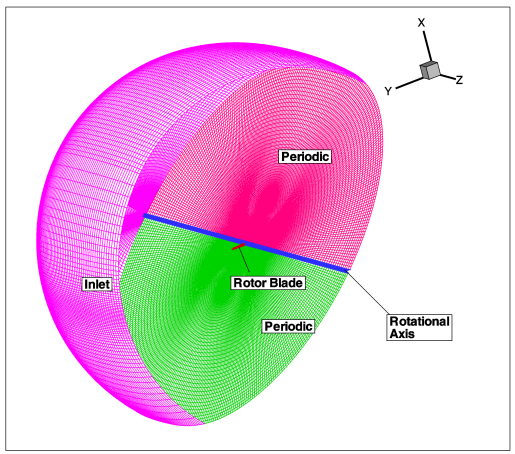

Niels N. Sørensen,
Risø DTU

Nrel Phase-VI

Full rotor grid:

- 5.4 million grid cells
- Grid resolution Chord-wise 256, span-wise 64, and normal 128, plus a tip patch of 64×64
- Domain radius corresponding to 9 rotor diameters
- Wall normal cell size corresponding to $y^+ < 2$

Can be used both for axial and yaw computations

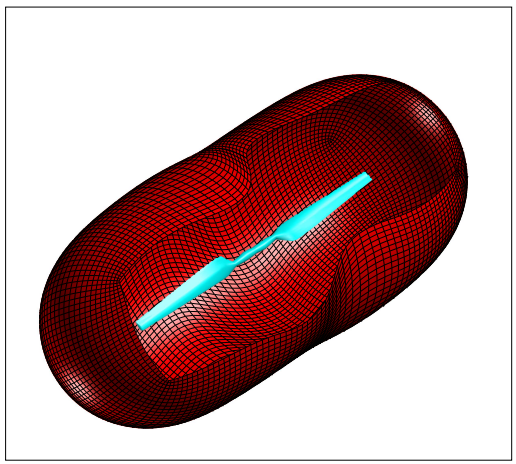

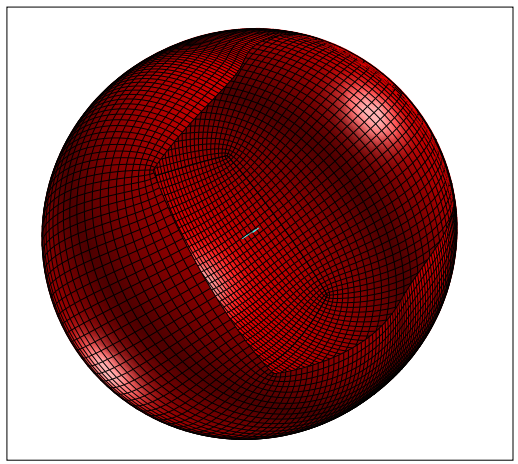

Nrel Phase-VI, Prediction of shaft torque

- Blind prediction of the NREL Phase-VI rotor
- The shaft torque is equivalent to the power production

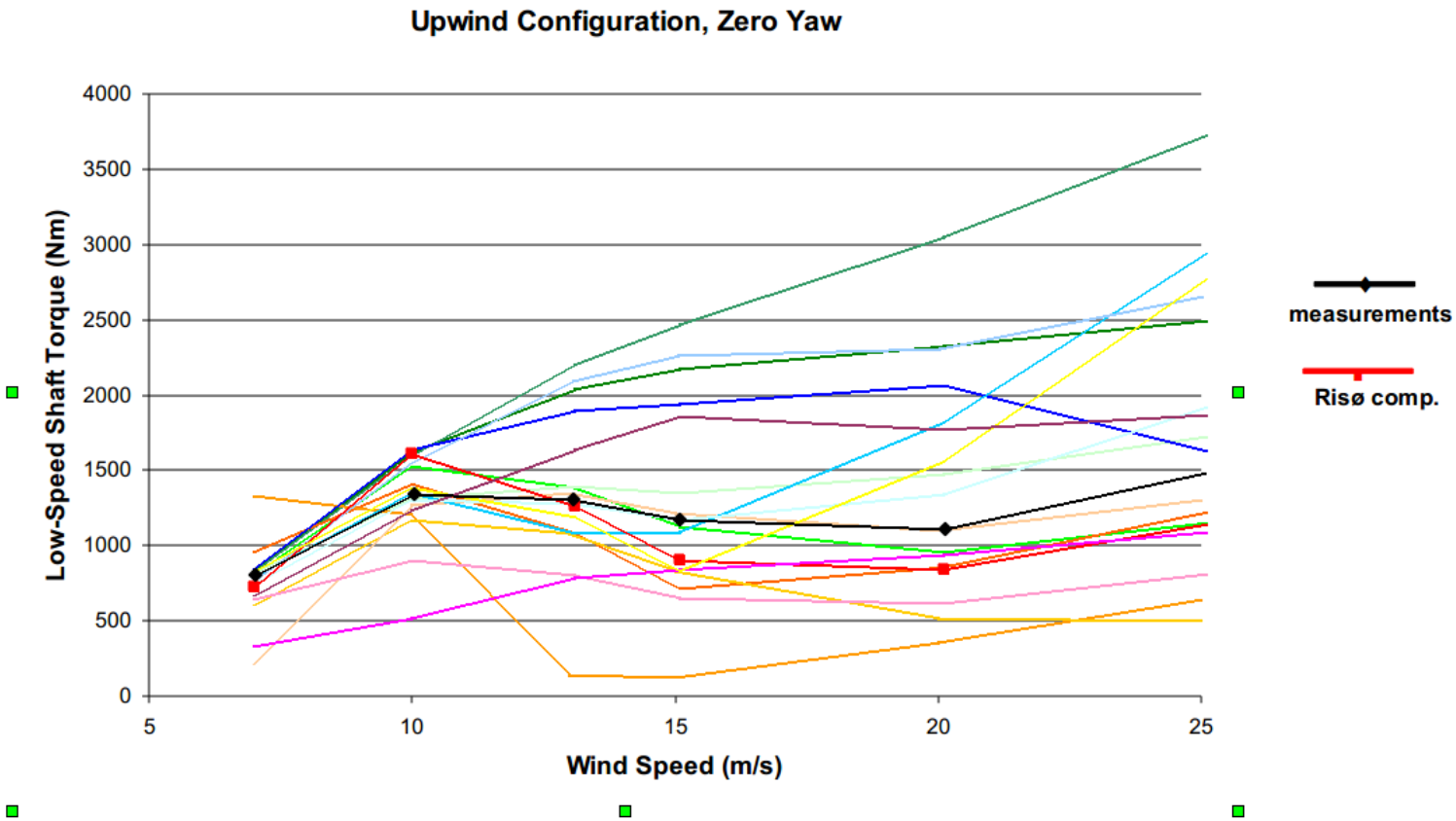

Niels N. Sørensen,
Risø DTU

Nrel Phase-VI, span-wise distributions of force coefficients

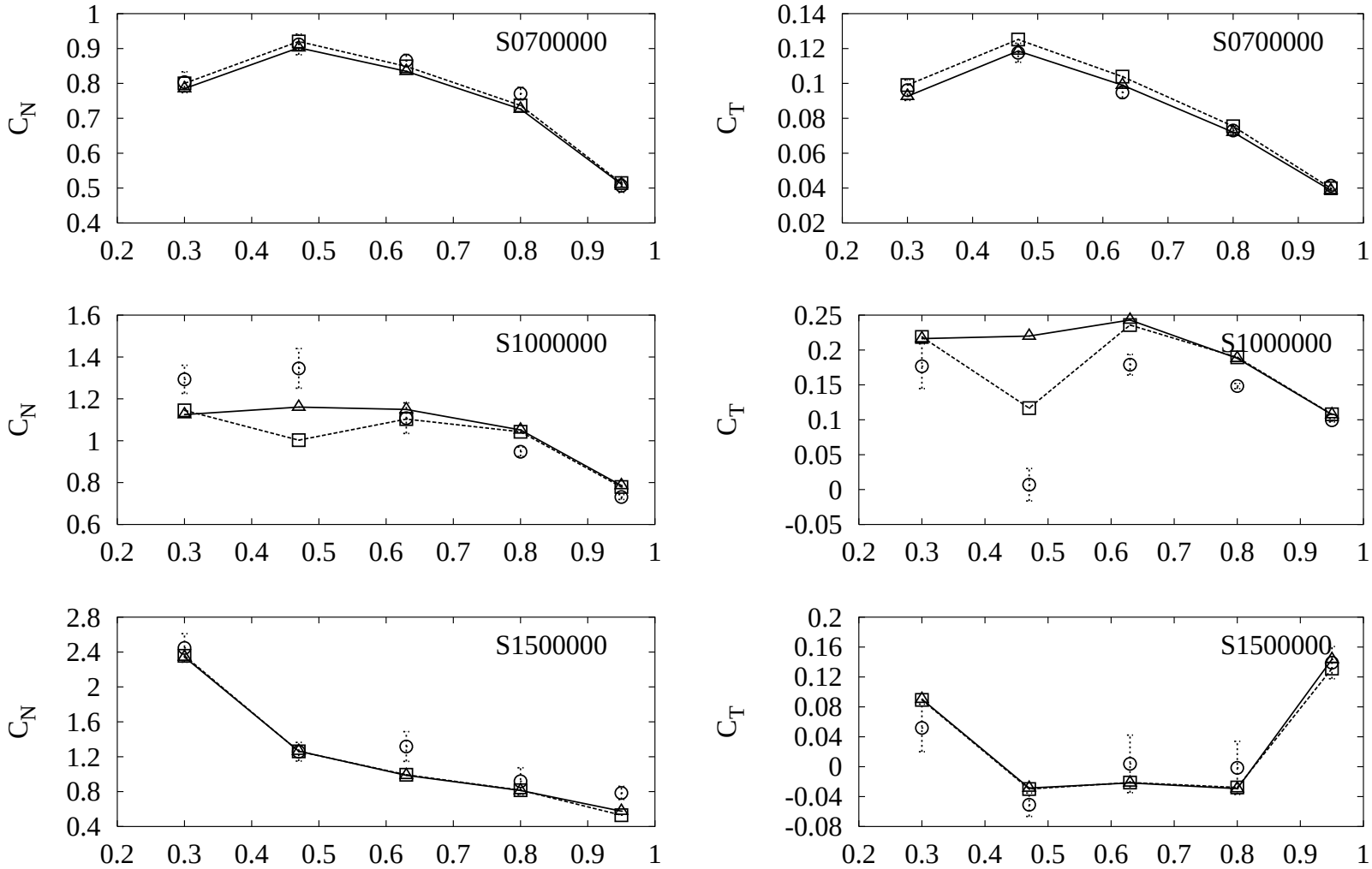

Niels N. Sørensen,
Risø DTU

Nrel Phase-VI, span-wise distributions ... (2)

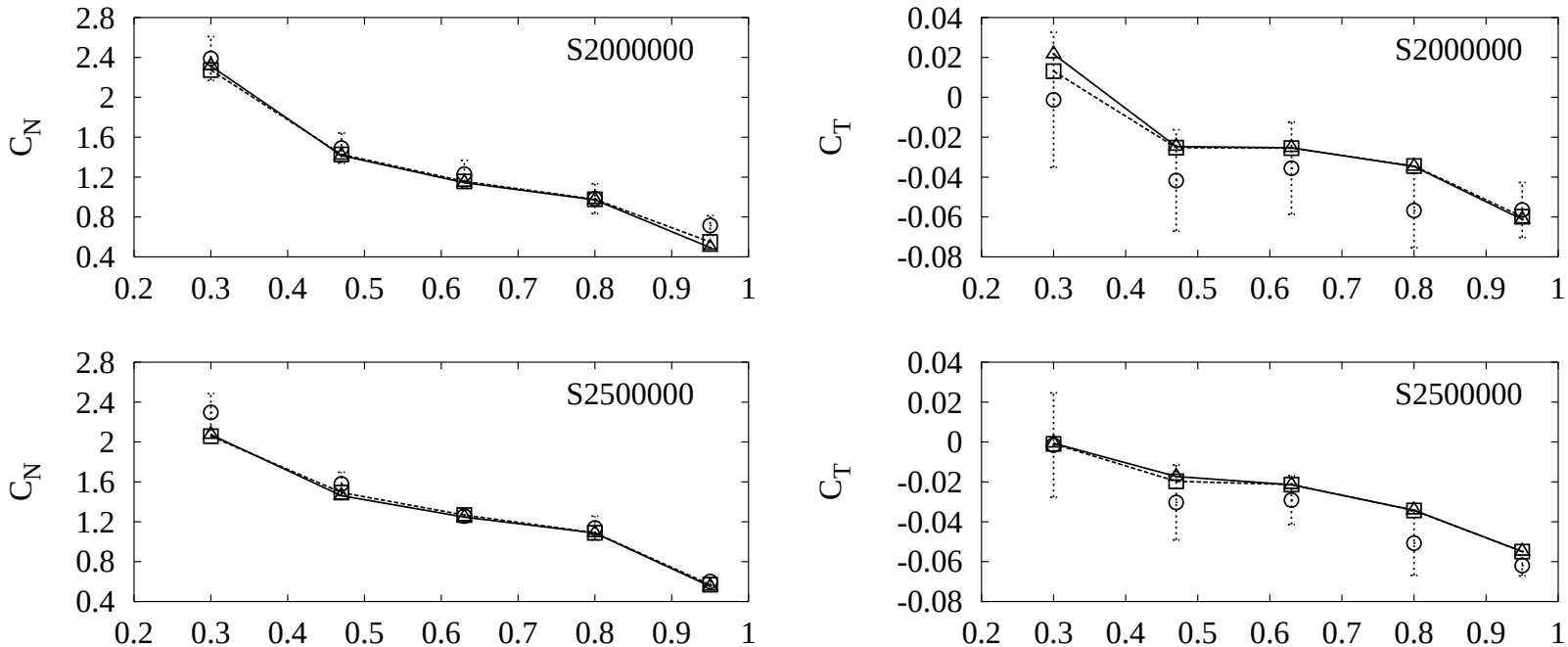

Niels N. Sørensen,
Risø DTU

Nrel Phase-VI, W=7 m/s

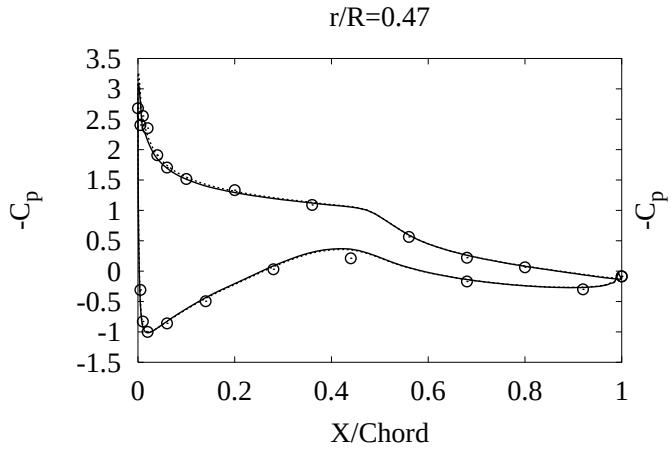

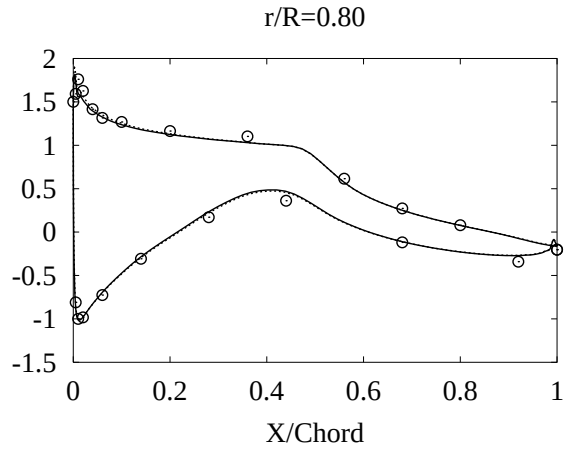

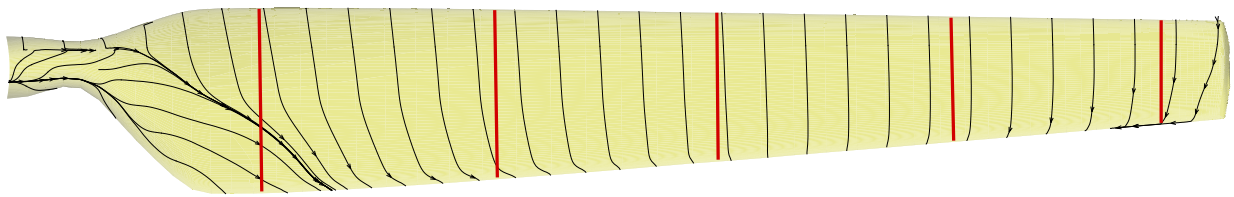

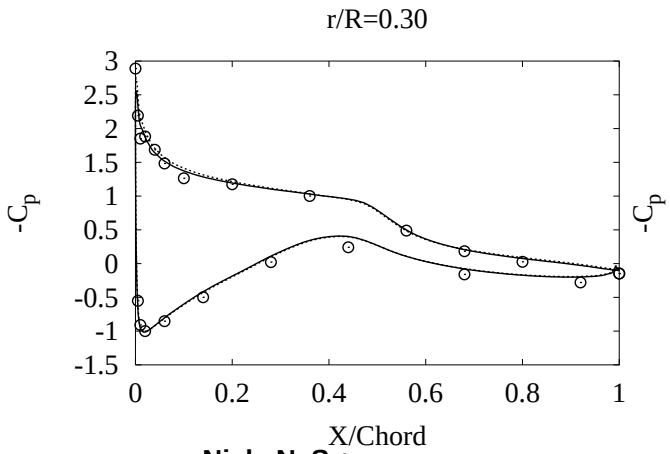

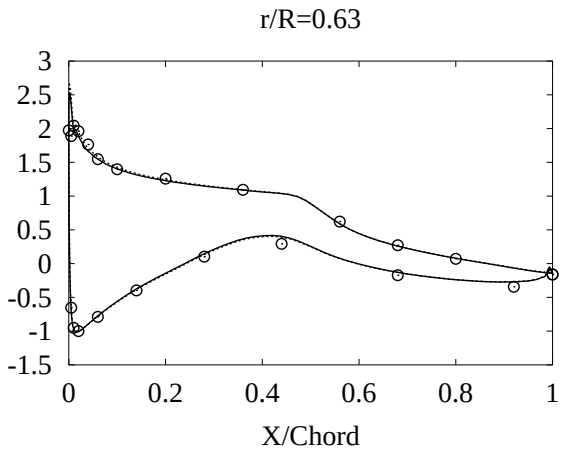

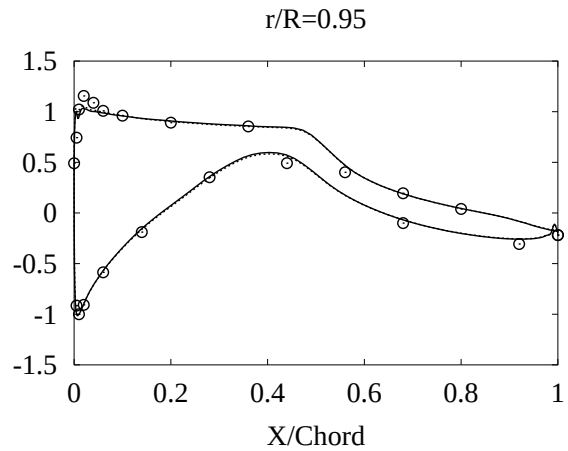

Niels N. Sørensen,
Risø DTU

Nrel Phase-VI, W=10 m/s

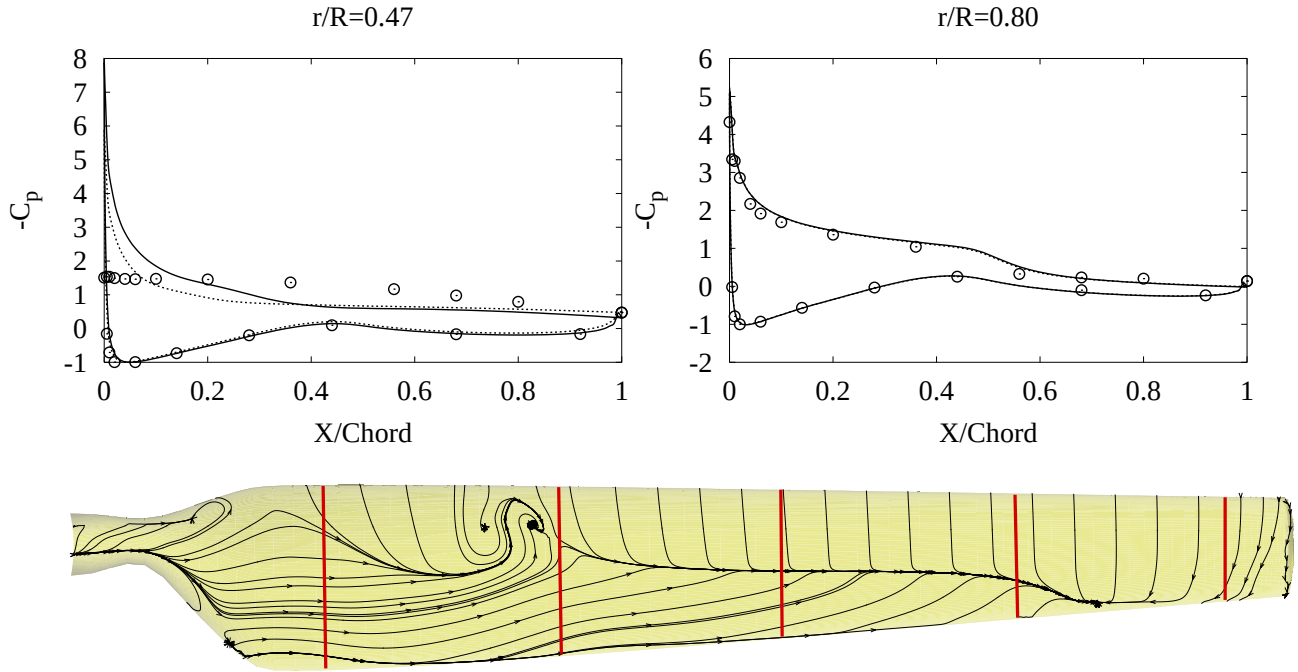

Niels N. Sørensen,
Risø DTU

Nrel Phase-VI, W=20 m/s

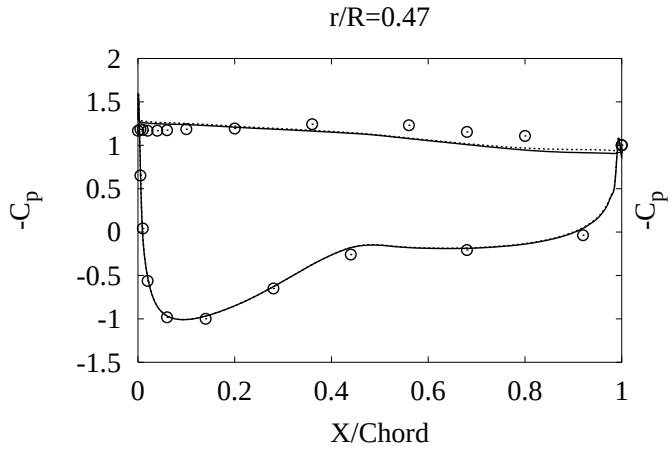

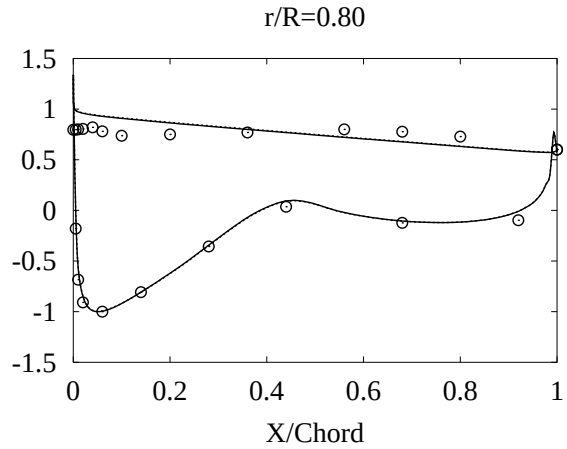

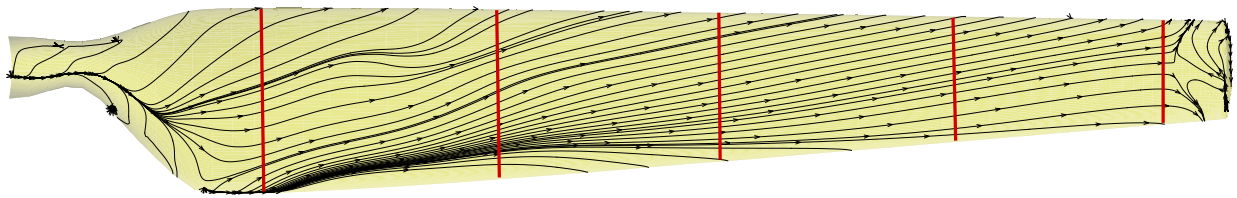

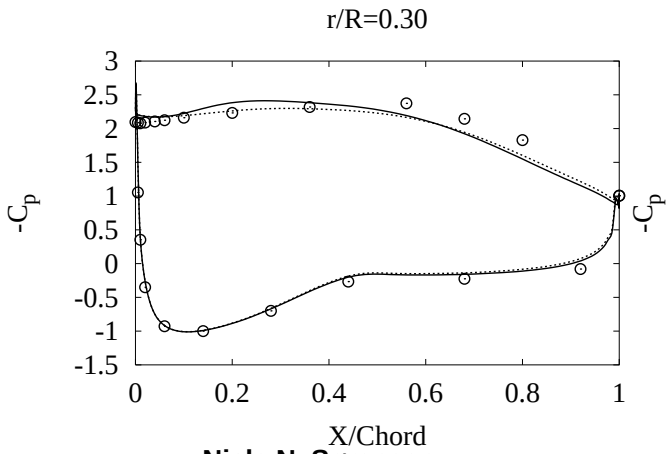

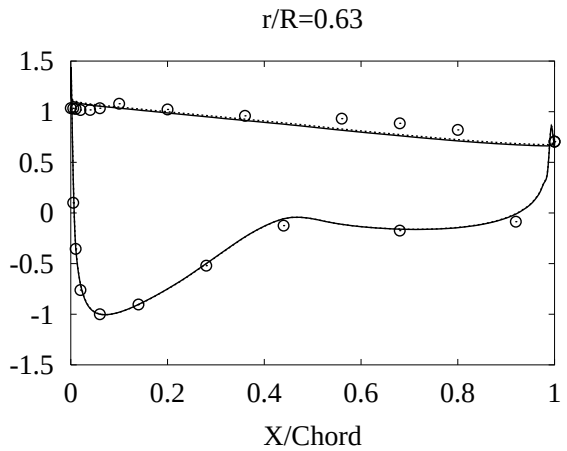

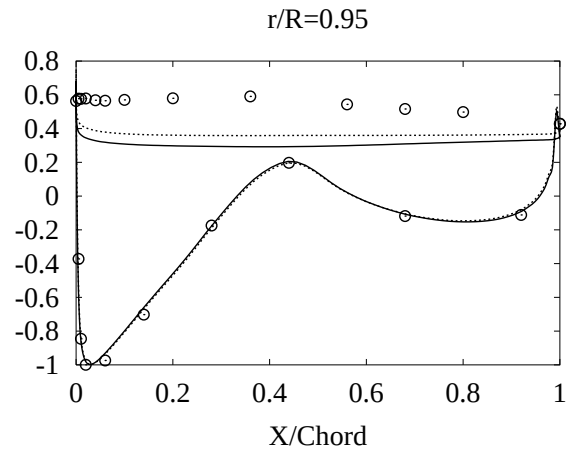

Nrel Phase-VI, including transition

With the availability of the $\gamma - Re_\theta$ transition model, we have investigated the influence on transition on the Phase-VI rotor

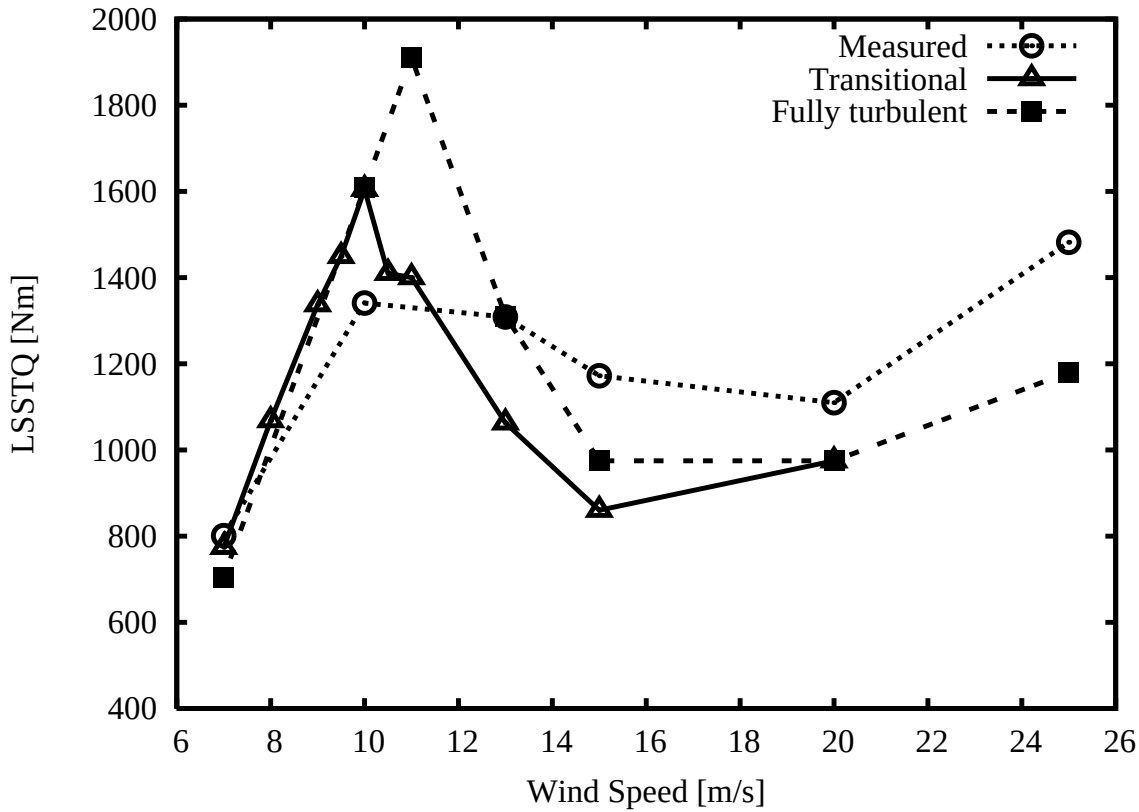

The influence of transition is strong around onset of stall, but very weak else where

Nrel Phase-VI, including transition

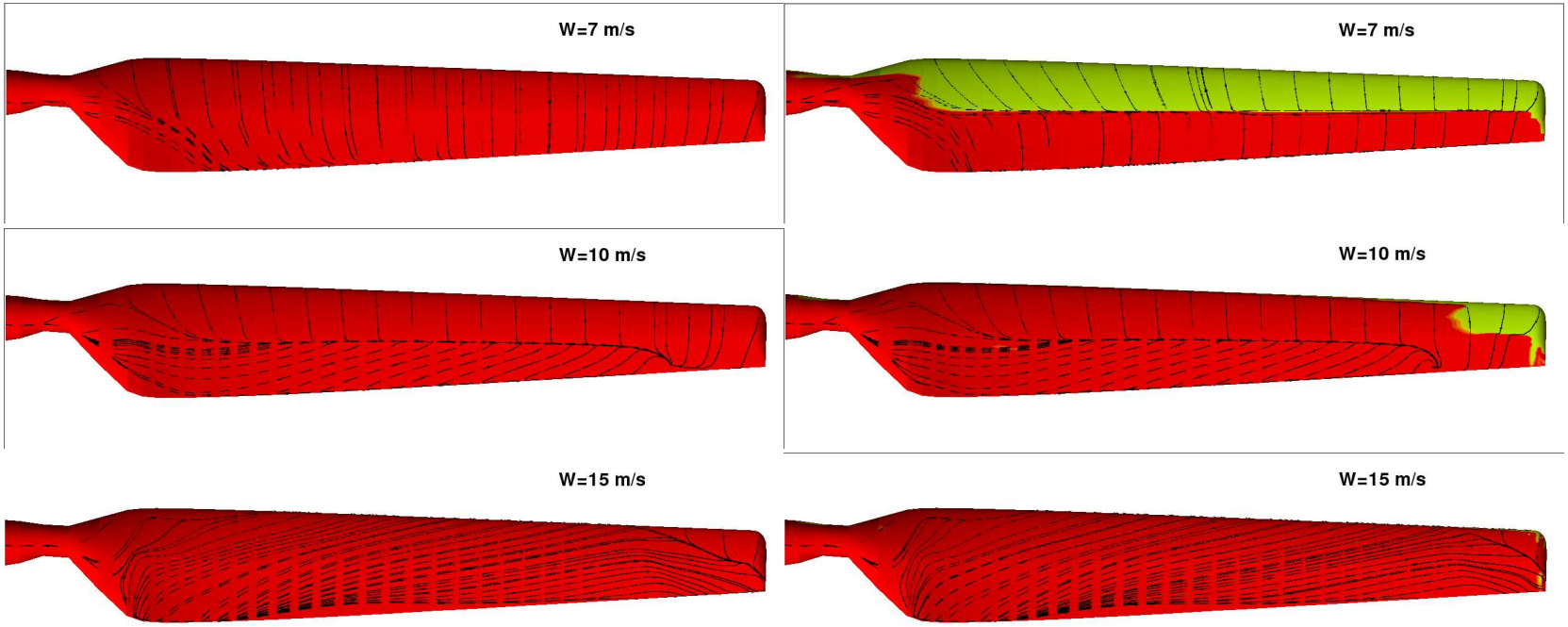

Niels N. Sørensen,
Risø DTU

Nrel Phase-VI, DDES including transition

We have previously performed DES computations of the NREL Phase-VI rotor without very much effect on the quality of the results.
At the moment we are investigating the combination of DDES and transition for the Phase-VI rotor

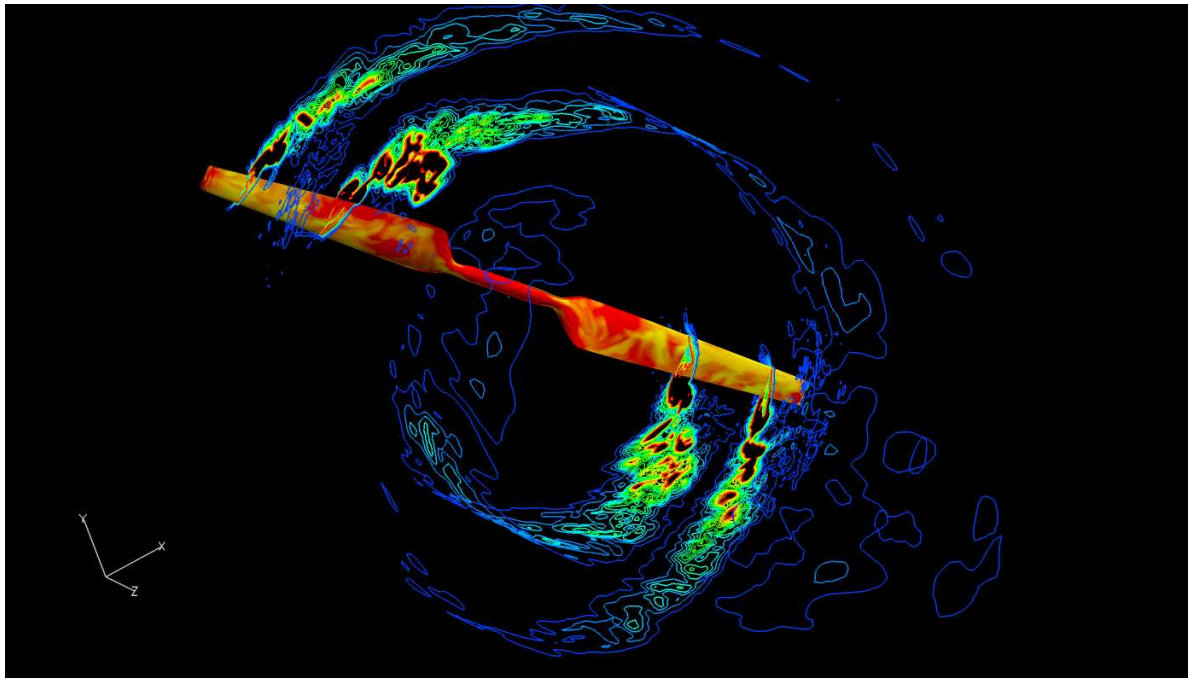

Nrel Phase-VI, yaw computations

Parameters:

- Rotational speed 72 RPM
- Tip pitch 3 deg., pointing leading edge into the wind
- Wind speeds 15 m/s
- Yaw error [10: 30: 60] degrees

Variation of the geometrical angle of attack

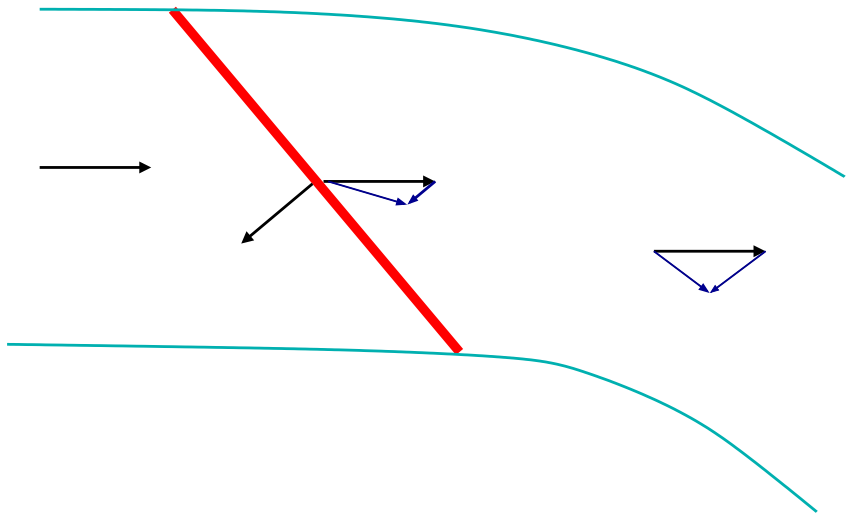

Nrel Phase-VI, yaw computations

Parameters:

- Rotational speed 72 RPM
- Tip pitch 3 deg., pointing leading edge into the wind
- Wind speeds 15 m/s
- Yaw error [10: 30: 60] degrees

Variation of the geometrical angle of attack

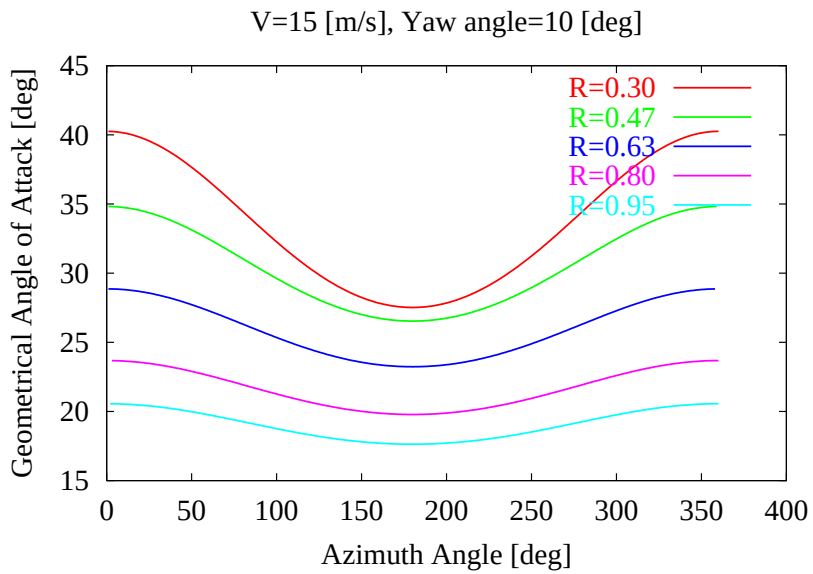

Niels N. Sørensen,
Risø DTU

Nrel Phase-VI, yaw computations

Parameters:

- Rotational speed 72 RPM
- Tip pitch 3 deg., pointing leading edge into the wind
- Wind speeds 15 m/s
- Yaw error [10: 30: 60] degrees

Variation of the geometrical angle of attack

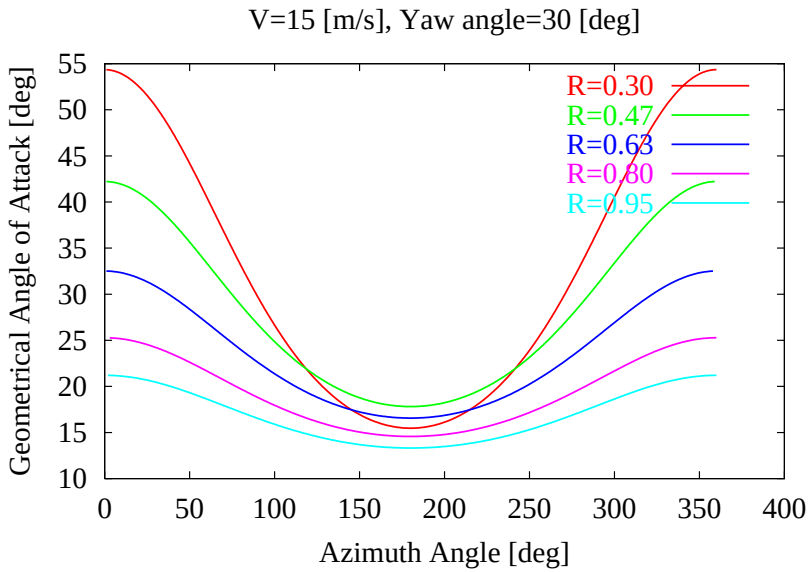

Niels N. Sørensen,
Risø DTU

Nrel Phase-VI, yaw computations

Parameters:

- Rotational speed 72 RPM
- Tip pitch 3 deg., pointing leading edge into the wind
- Wind speeds 15 m/s
- Yaw error [10: 30: 60] degrees

Variation of the geometrical angle of attack

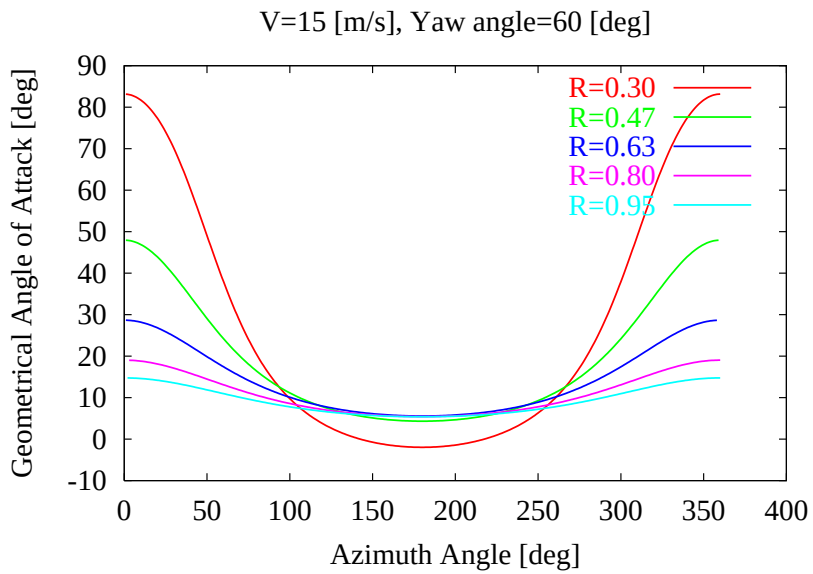

Niels N. Sørensen,
Risø DTU

Nrel Phase-VI, C_n at W=15 m/s, 10 deg yaw error

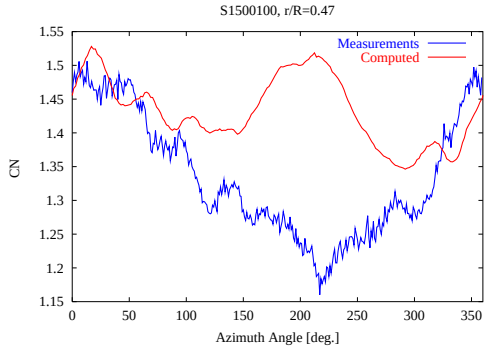

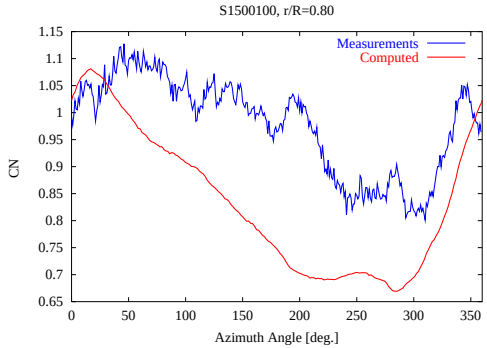

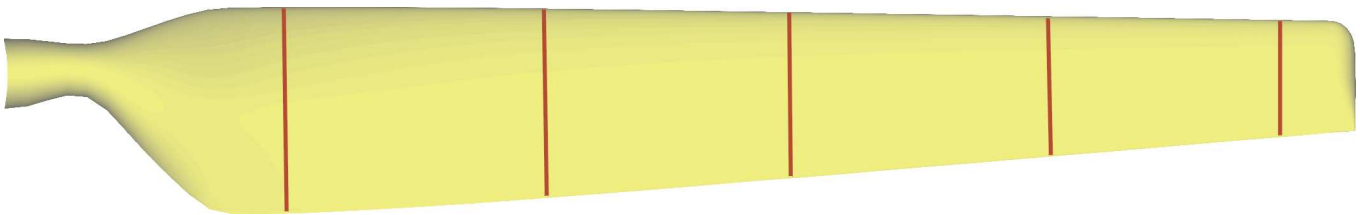

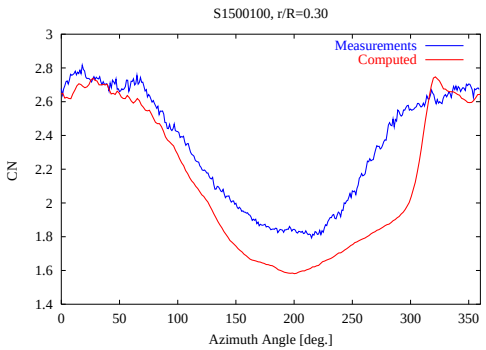

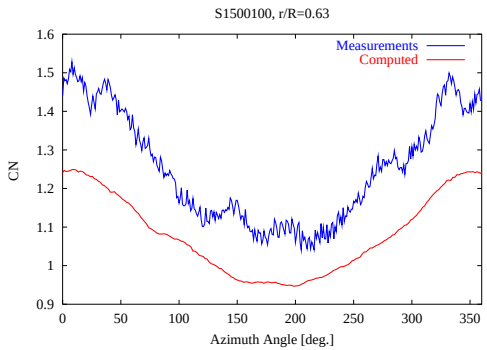

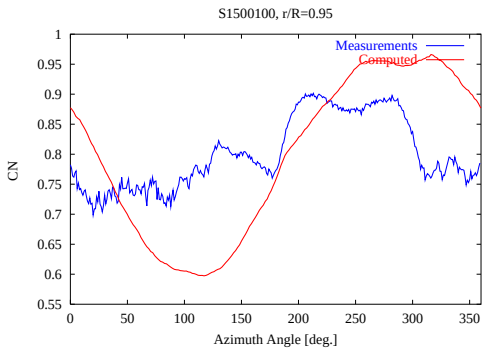

Niels N. Sørensen,
Risø DTU

Nrel Phase-VI, C_t at W=15 m/s, 10 deg yaw error

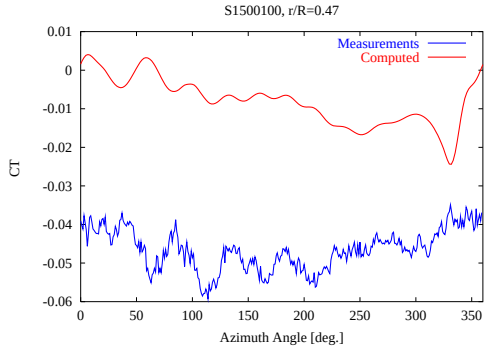

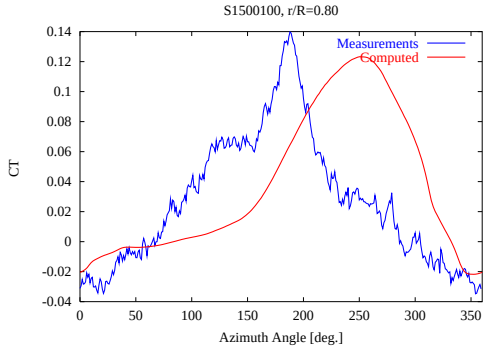

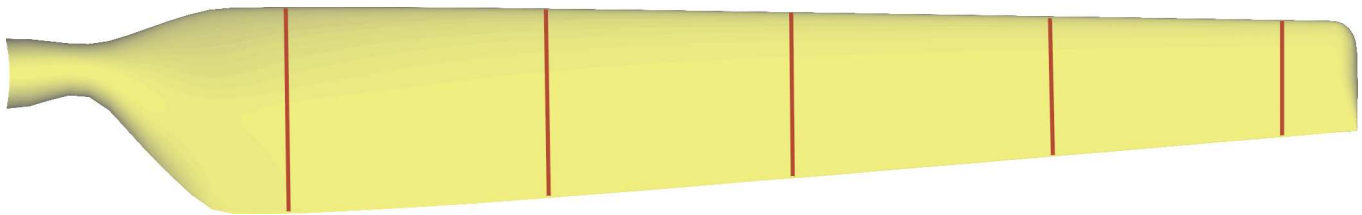

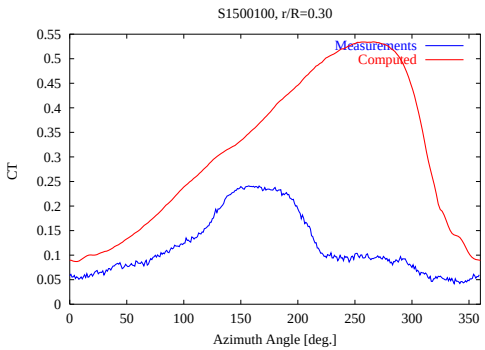

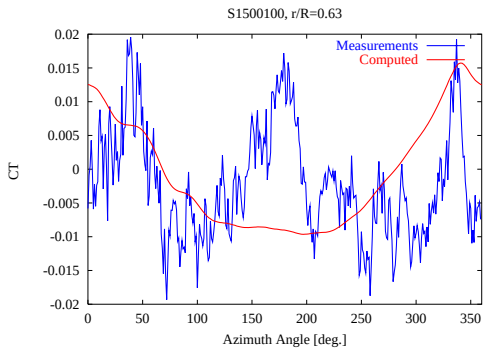

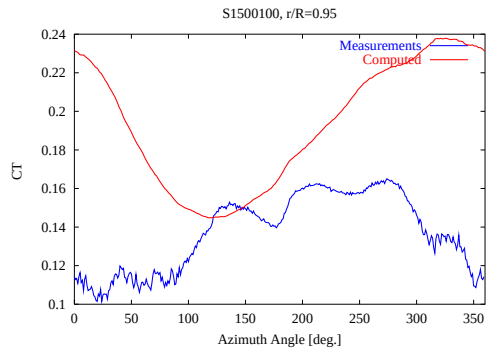

Niels N. Sørensen,
Risø DTU

Nrel Phase-VI, C_n at W=15 m/s, 30 deg yaw error

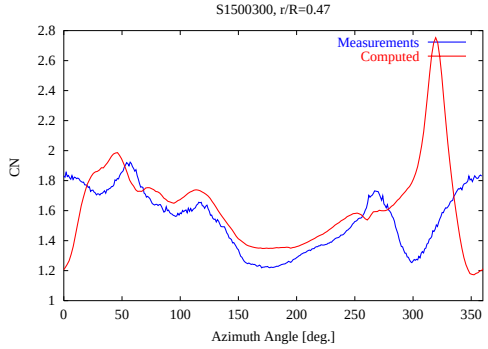

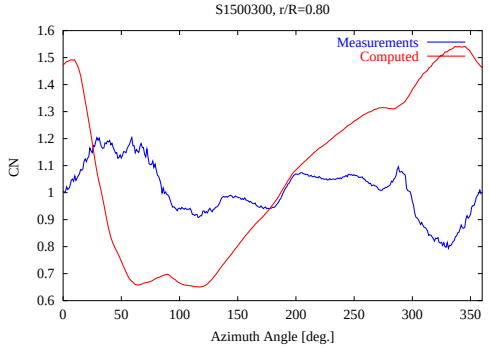

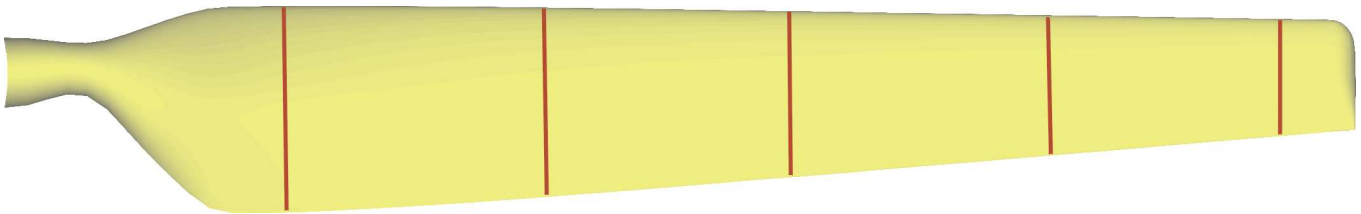

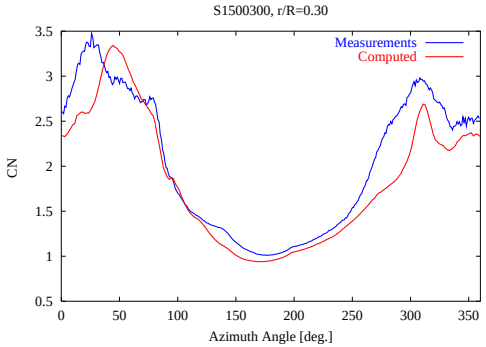

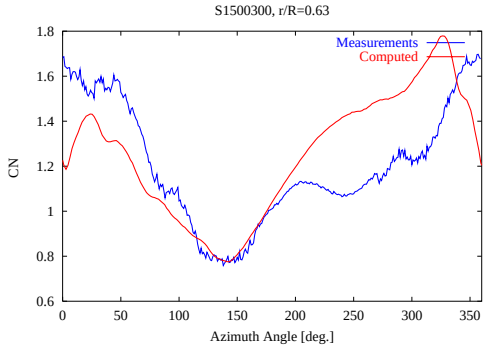

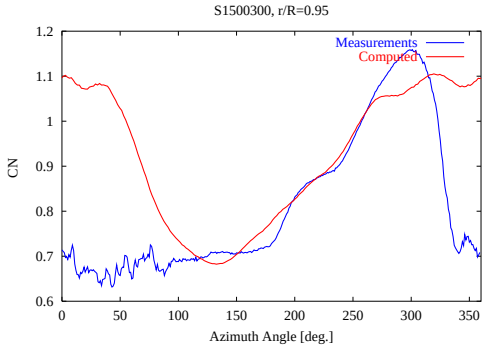

Niels N. Sørensen,
Risø DTU

Nrel Phase-VI, C_t at W=15 m/s, 30 deg yaw error

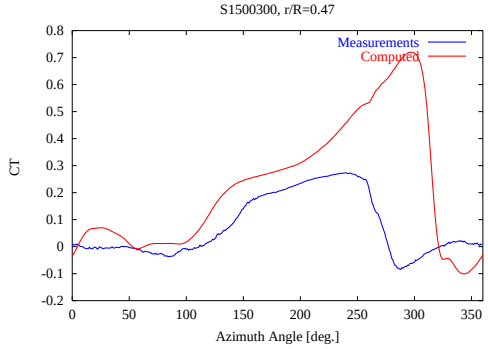

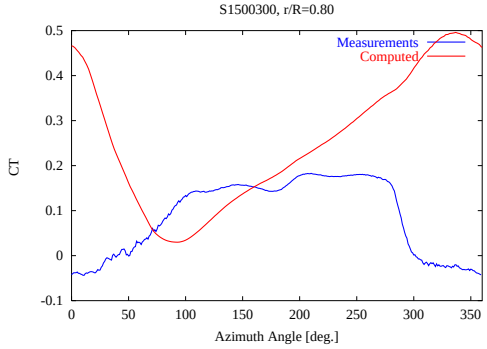

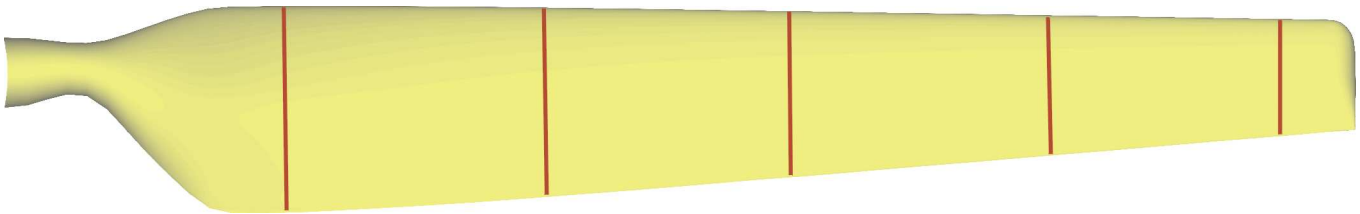

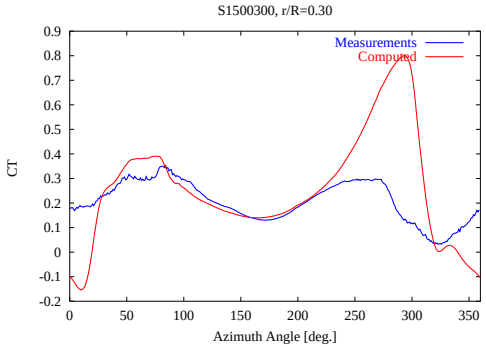

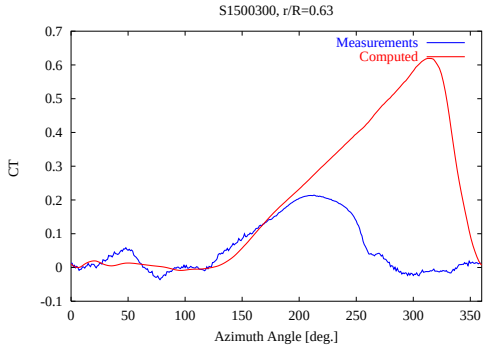

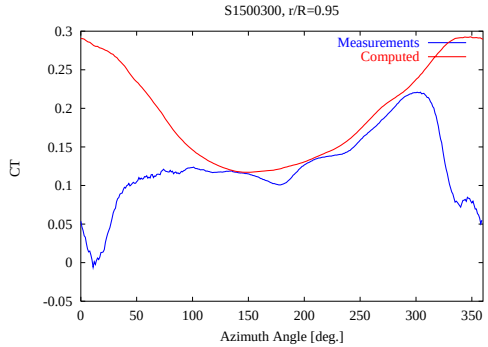

Niels N. Sørensen,
Risø DTU

Nrel Phase-VI, C_n at W=15 m/s, 60 deg yaw error

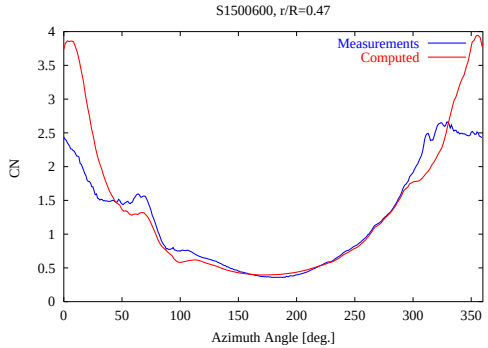

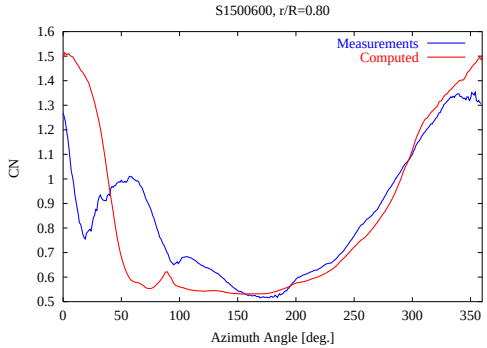

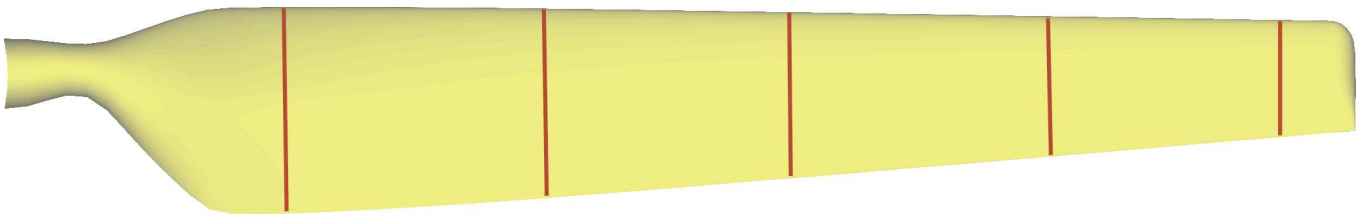

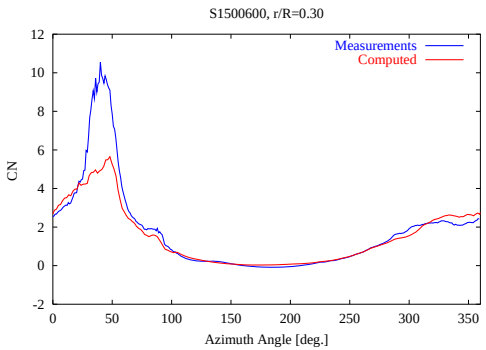

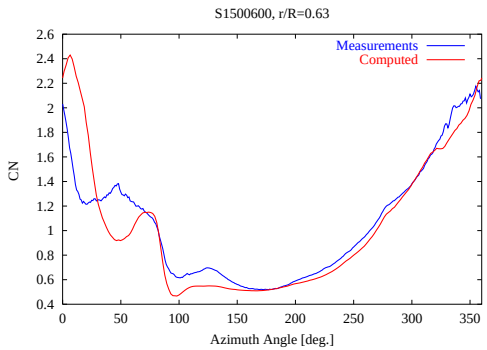

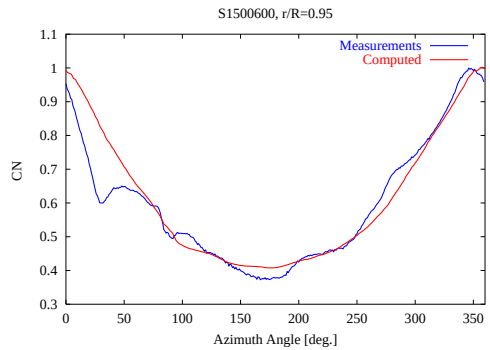

Niels N. Sørensen,
Risø DTU

Nrel Phase-VI, C_t at W=15 m/s, 60 deg yaw error

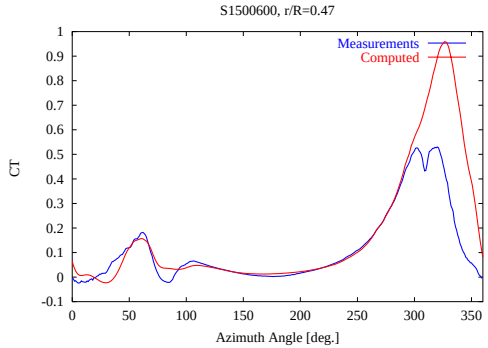

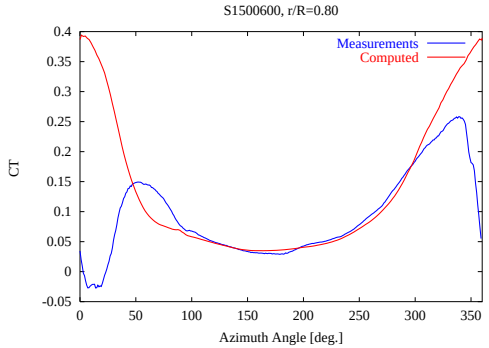

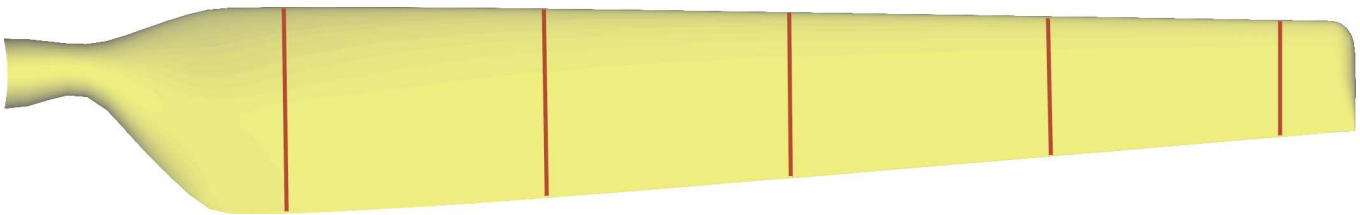

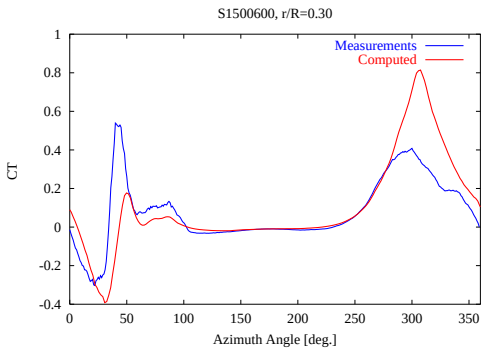

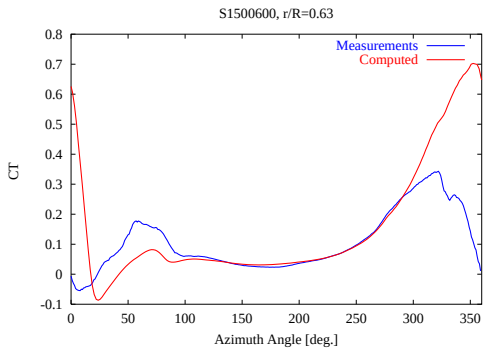

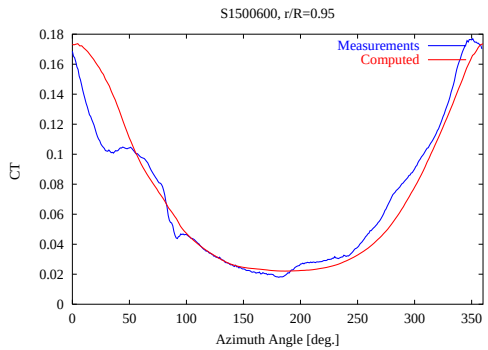

Niels N. Sørensen,
Risø DTU

Nrel Phase-VI, yaw computations

The wake flow at 30 degrees yaw error

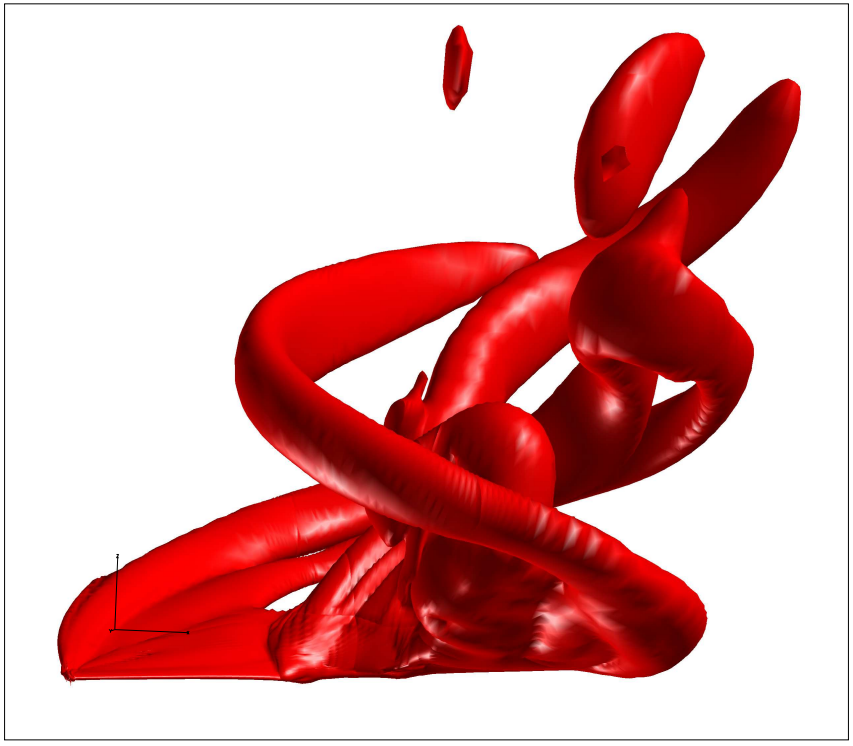

Effect of Inflow Shear

Boundary Conditions

- Ambient turbulence intensity is usually very low at night.
- We can use standard boundary conditions on turbulence quantities, resulting in virtually laminar inflow on the turbine.
- Pure power law shear with an exponent of 0.55 and hub height velocity of 8 m/s.

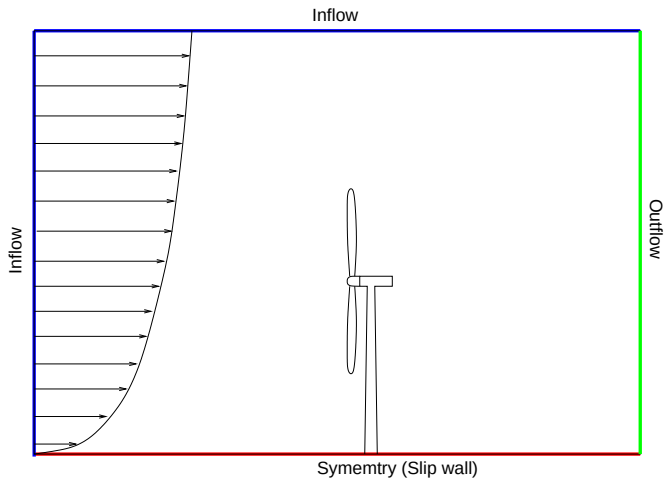

$$U(z) = U_{hub}\,(z/z_{hub})^{\alpha} \qquad (1)$$

Computational Mesh

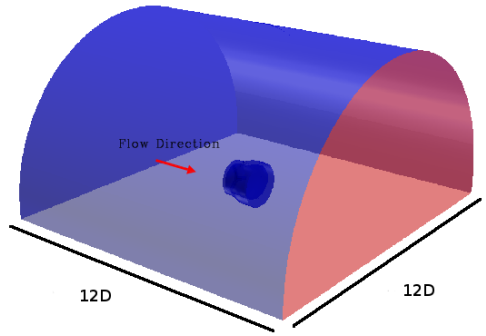

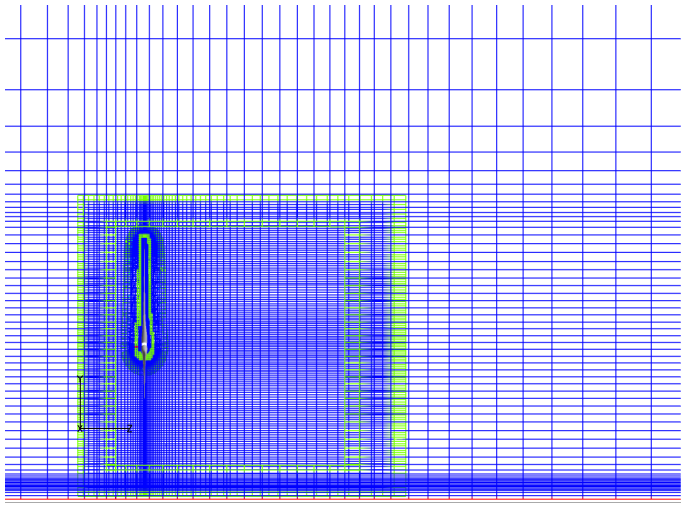

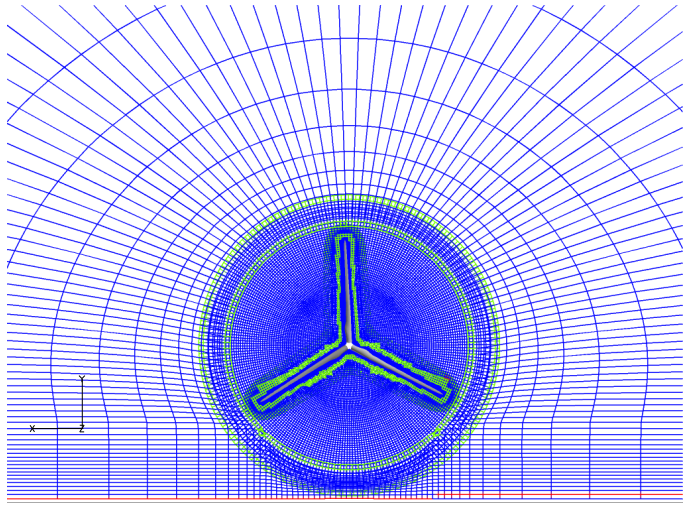

Niels N. Sørensen,
Risø DTU

Convergence of Unsteady Simulations

- Unsteady simulations of rotor flows require prohibitively long to converge without the use of acceleration techniques.
- “Standard” CFD simulations allow for the use of grid and time step sequencing that greatly reduces the computational time.
- The overset grid method limits the use of grid sequencing to ∼two levels.
- Time step sequencing is therefore primarily used:
  - Grid level 2: 20 revs with 150 time steps per rev (2.4° per time step).
  - Grid level 2: 10 revs with 1500 time steps per rev (0.24° per time step).
  - Grid level 1: 3-5 revs with 3000 time steps per rev (0.12° per time step).
- Generally, the solution is fully converged on level 2, which is computed in roughly 48 hours on 20 nodes (4 cores each).

Blade Tangential Forces

- Hysteresis effects give rise to a 11° phase lag relative to the blade position.
- Vortex shedding on the inner part of the rotor causes the fluctuating tangential force.

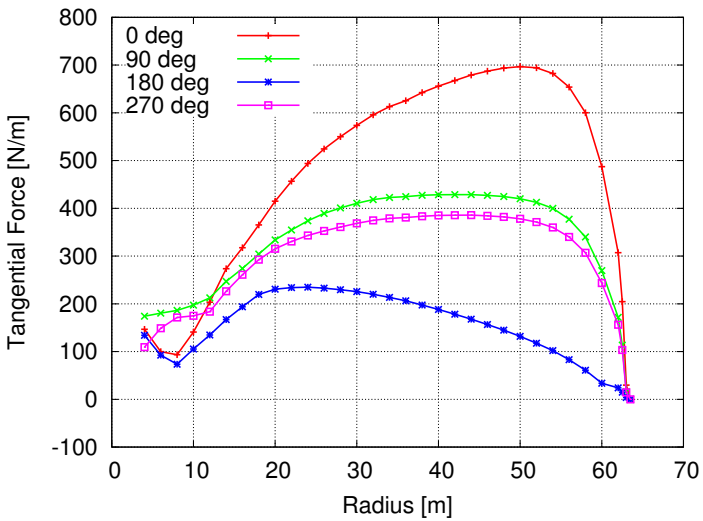

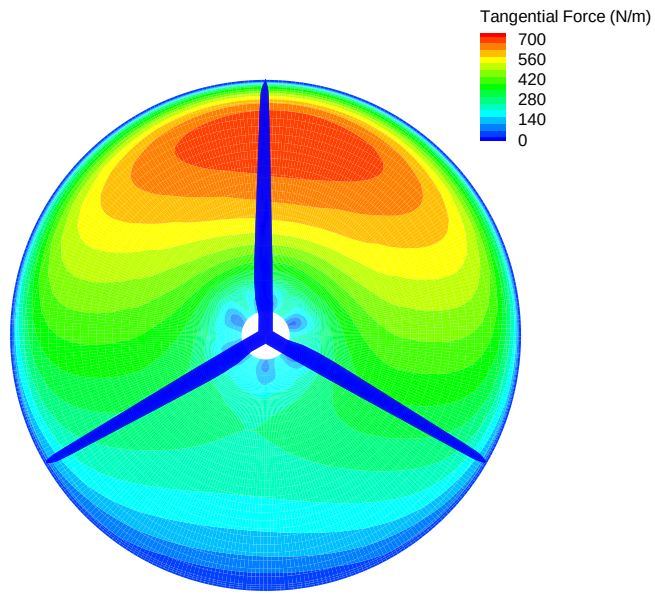

Niels N. Sørensen,
Risø DTU

Blade Tangential Forces

- Hysteresis effects give rise to a 11° phase lag relative to the blade position.
- Vortex shedding on the inner part of the rotor causes the fluctuating tangential force.
- Comparison of HAWC2 and EllipSys3D does not give an entirely consistent prediction of the torque generated in shear (HAWC solid, EllipSys3D dotted).

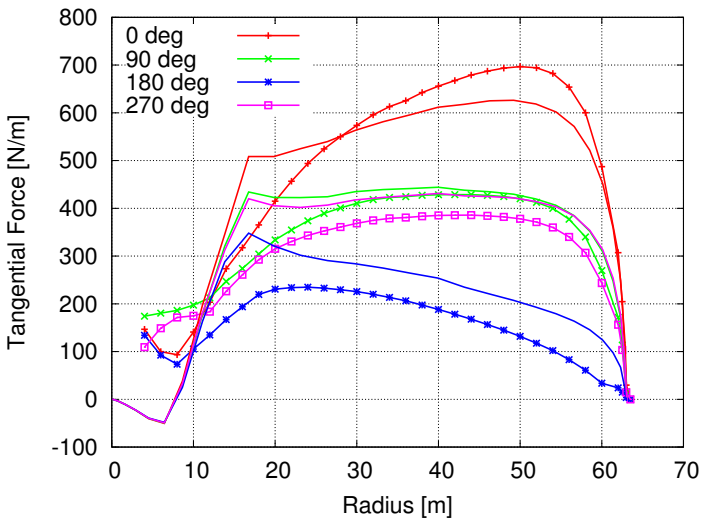

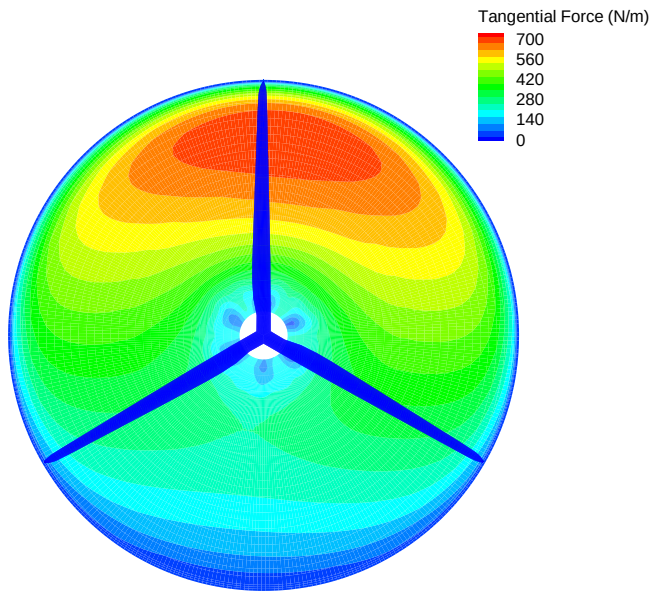

Niels N. Sørensen,
Risø DTU

Blade Tangential Forces

- Hysteresis effects give rise to a 11° phase lag relative to the blade position.
- Vortex shedding on the inner part of the rotor causes the fluctuating tangential force.
- Comparison of HAWC2 and EllipSys3D does not give an entirely consistent prediction of the torque generated in shear (HAWC solid, EllipSys3D dotted).
- However, comparisons with the ACL results by MEK DTU are considerably more consistent (ACL solid, EllipSys3D dotted).

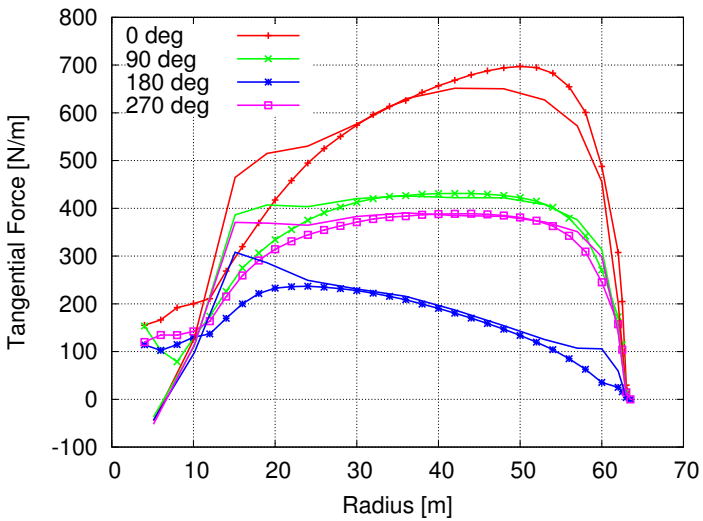

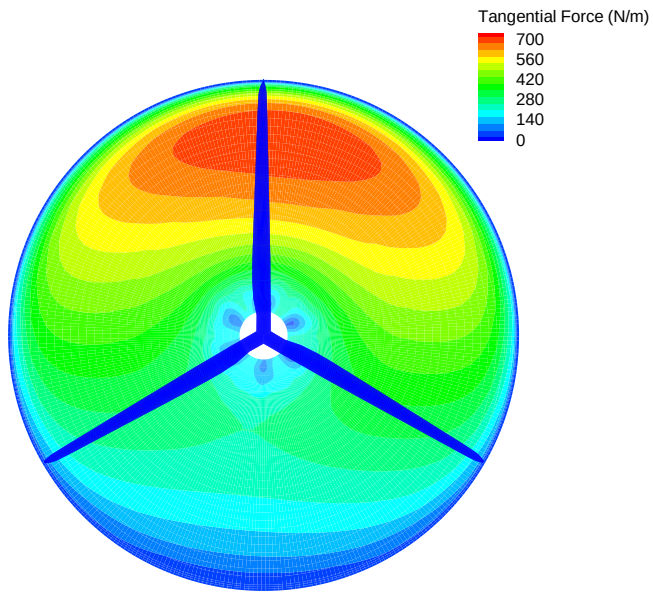

Niels N. Sørensen,
Risø DTU

Blade Normal Forces

- Hysteresis is less pronounced in the normal force.

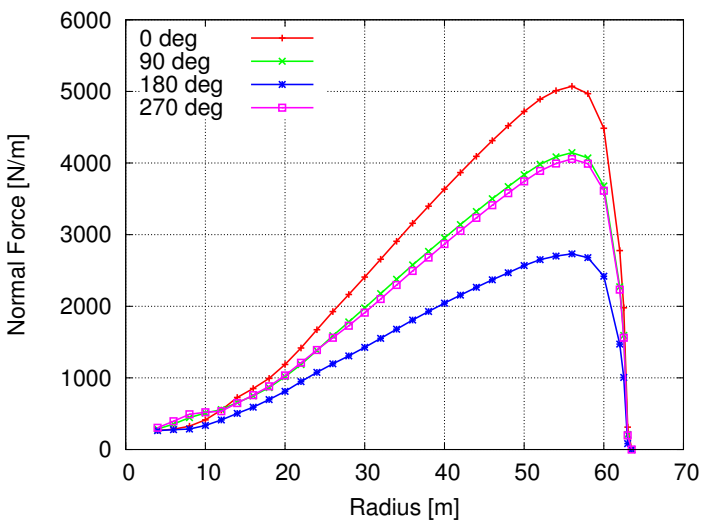

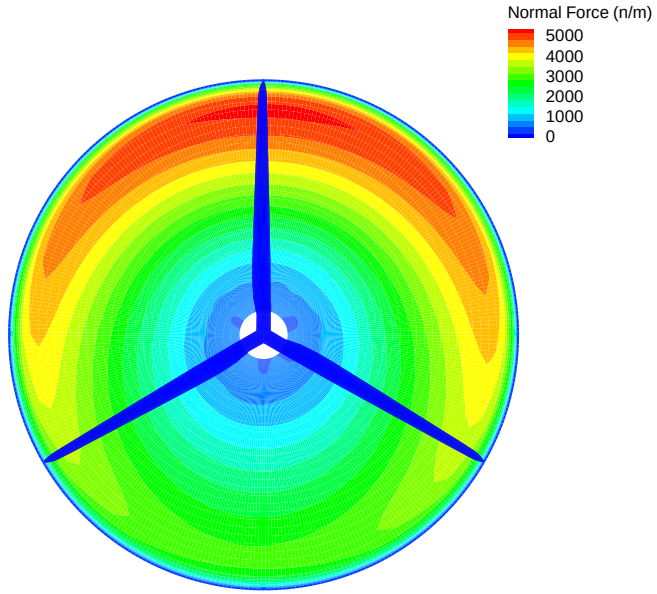

Niels N. Sørensen,
Risø DTU

Blade Normal Forces

- Hysteresis is less pronounced in the normal force.
- Good correspondence with HAWC2 except for the 180° azimuth position where HAWC2 predicts a higher normal force.

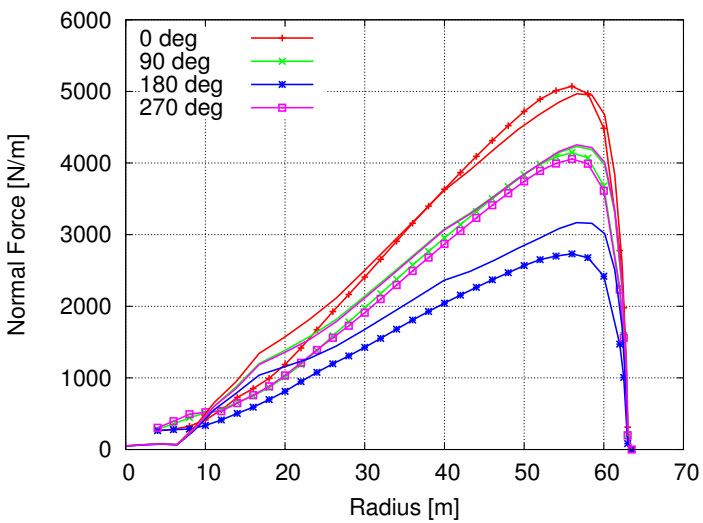

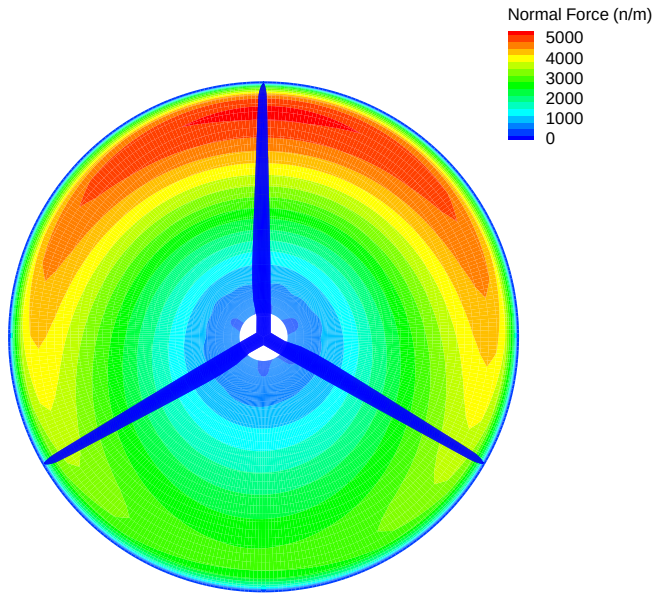

Niels N. Sørensen,
Risø DTU

Blade Normal Forces

- Hysteresis is less pronounced in the normal force.
- Good correspondence with HAWC2 except for the 180° azimuth position where HAWC2 predicts a higher normal force.
- Less favourable correspondence between ACL method and EllipSys3D for the normal force.

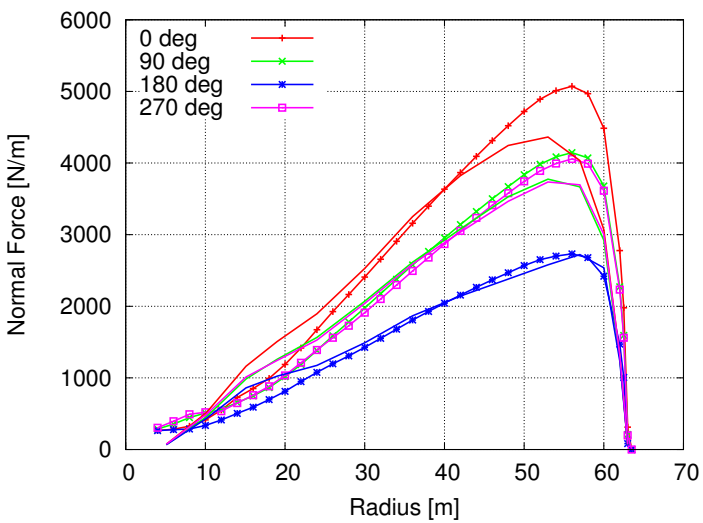

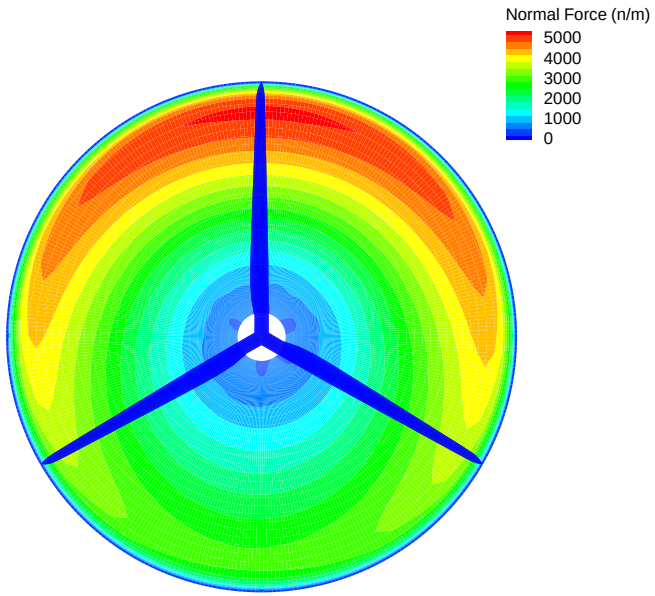

Niels N. Sørensen,
Risø DTU

Integrated Loads

- The present shear profile contains 6.6% more energy within the rotor disc compared to the uniform inflow case.
- Power production increases by 3.7%, however, after 35 revolutions at grid level 2, the solution has still not converged.

	EllipSys3D		HAWC2	
Inflow type	Power (kW)	Thrust (kN)	Power (kW)	Thrust (kN)
Uniform	1957	388	1906	
Shear	2029 (3.7%)	384 (-1.0%)	2148 (12.7%)	

Shear Profile

- Flow is accelerated considerably below the rotor due to the presence of the ground plane.
- Wake expands considerably more below the rotor than above.
- Lower part of the wake appears to be pushed upwards far downstream.

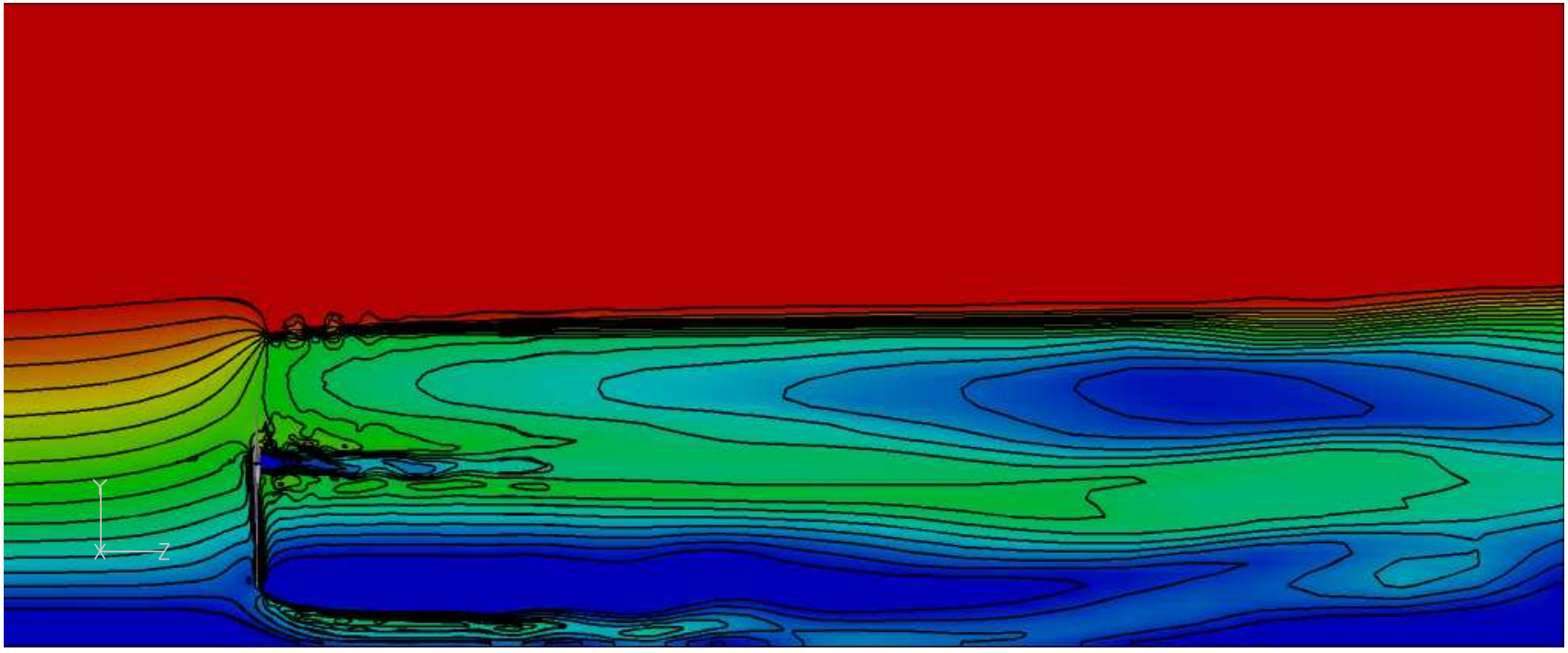

Design of rotor details

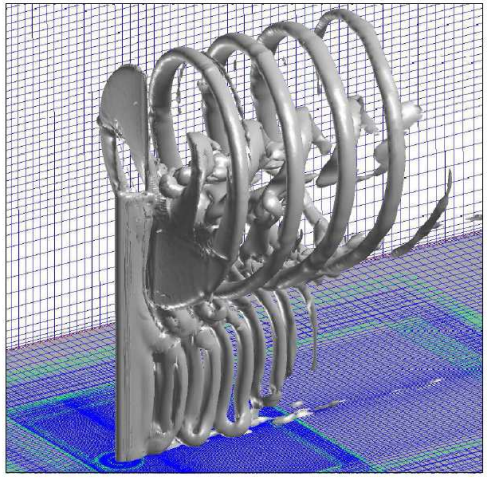

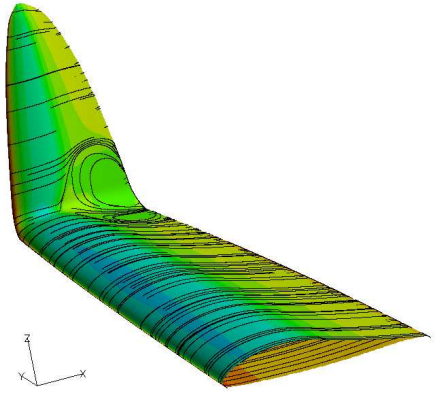

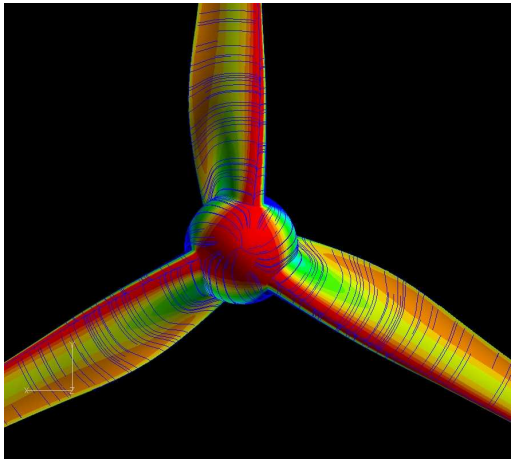

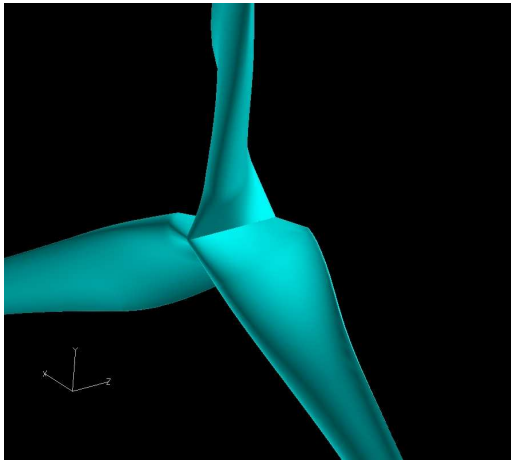

Niels N. Sørensen,
Risø DTU

Cylinder Drag Crisis

- 3D computation
- Cylinder length $2 \times D$
- Grid size 256x256x128 cells 8.4 million cells
- Resulting cell size 0.0156D
- Cell size at surface $1 \times 10^{-5} \times D$
- Re from 10 to 1e6

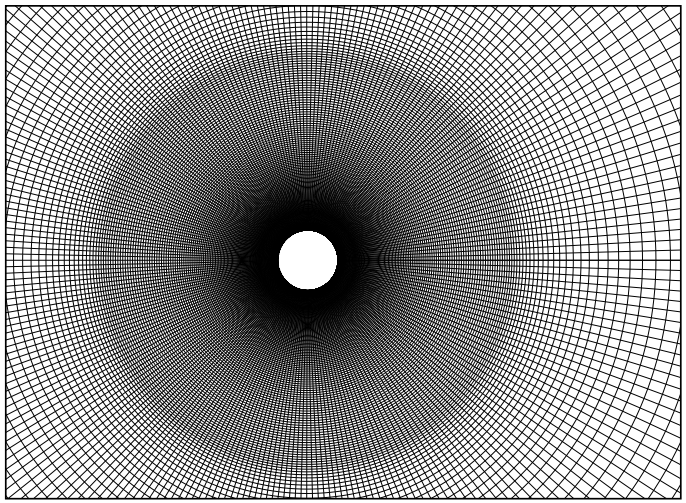

Computations are performed with the EllipSys3D flow solver:

- Second order time true computations, $\Delta t \sim 1 \times 10^{-2}$
- Convective terms by QUICK/ 4. order CDS
- Turbulence modeling based on $k - \omega$ SST model
- Transition based on $\gamma - Re_{\theta t}$ model (Tu 0.05%)

Cylinder Drag Crisis

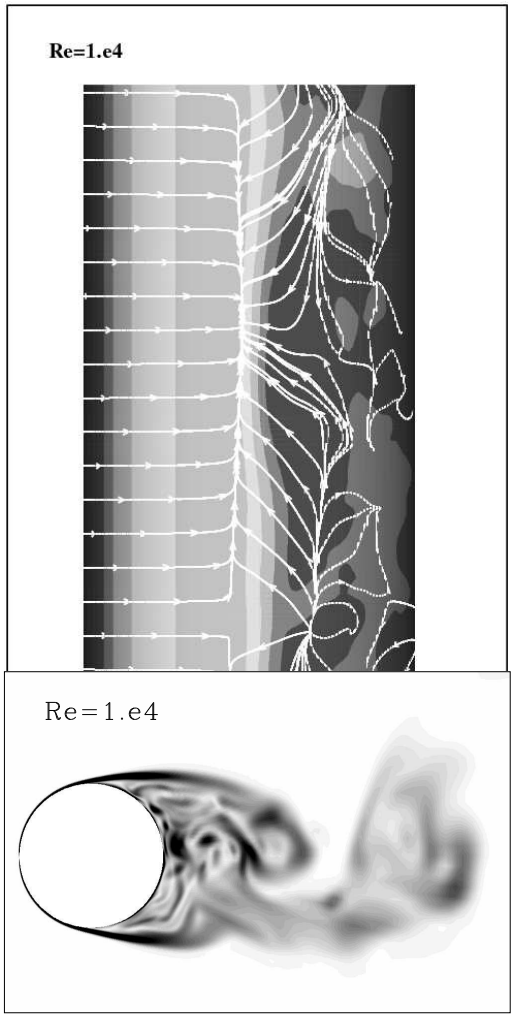

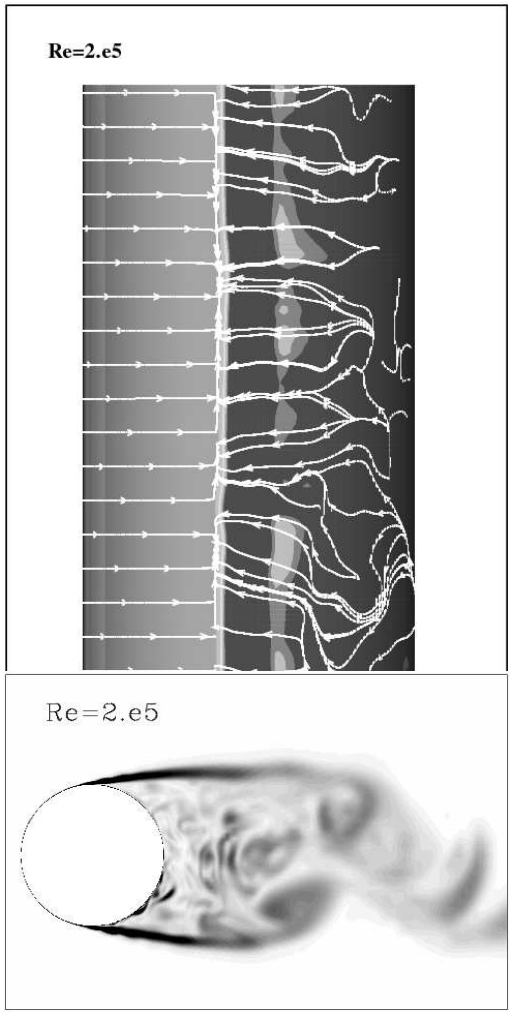

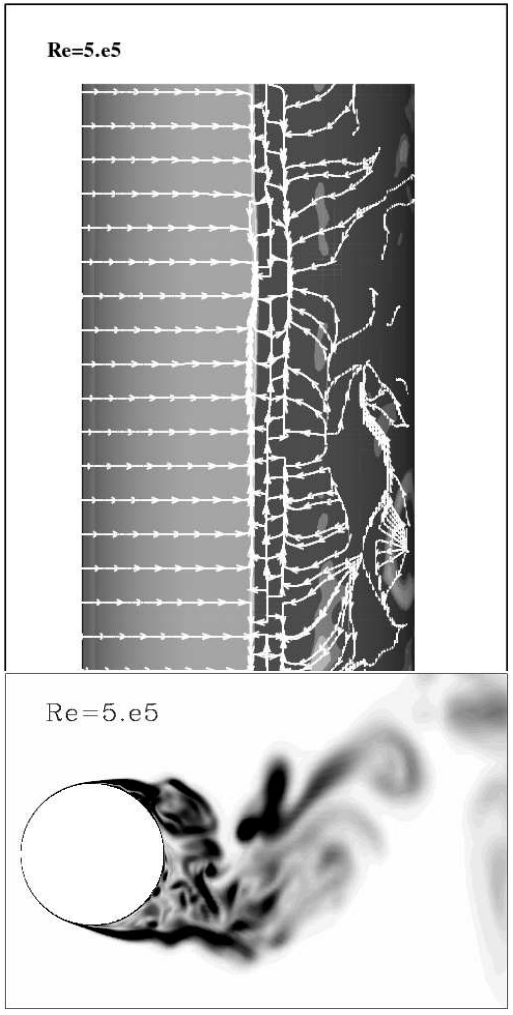

Niels N. Sørensen,
Risø DTU

The Cylinder Drag Crisis

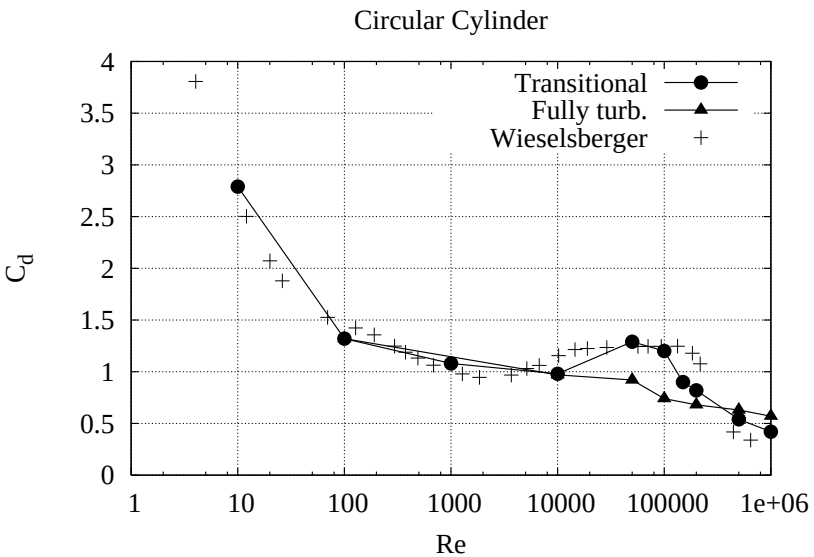

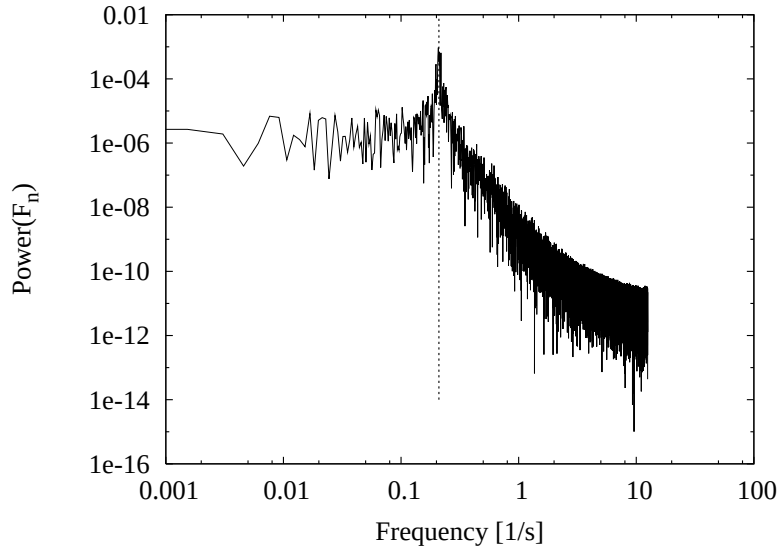

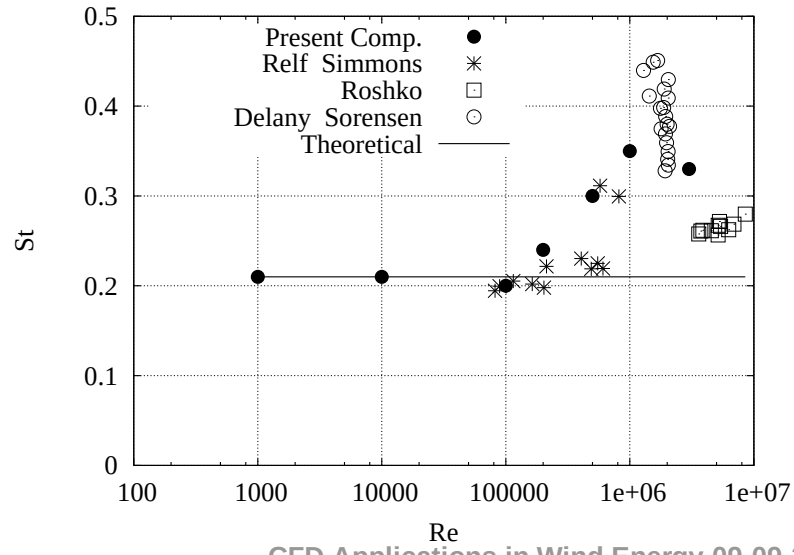

DU-96-W-351

- 3D computation
- Airfoil span length $2 \times C$
- Grid size $512 \times 256 \times 256$ cells $\sim$ 17 million cells
- Resulting cell size $0.0156 \times C$
- Cell size at surface 5×10^{-6} D or $y^+ \sim 0.5$
- Re 3×10^6
- Tu $\sim [0.05; 0.10; 0.15]$

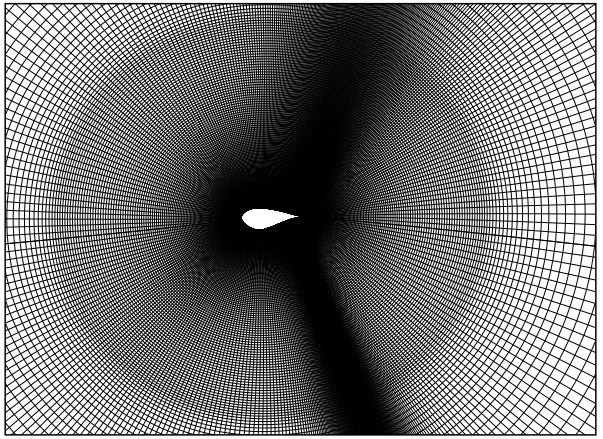

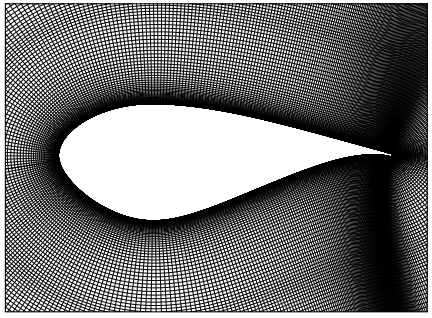

Computations are performed with the EllipSys3D flow solver:

- Second order time true computations, $\Delta t \sim 1 \times 10^{-2}$
- Convective terms by QUICK/ 4. order CDS
- Turbulence modeling based on $k - \omega$ SST model, DDES
- Transition based on $\gamma - Re_{\theta t}$ model

DU-96-W-351

The effect of the different types of modelling is clearly visible

- 2D RANS fully turbulent and transitional computations

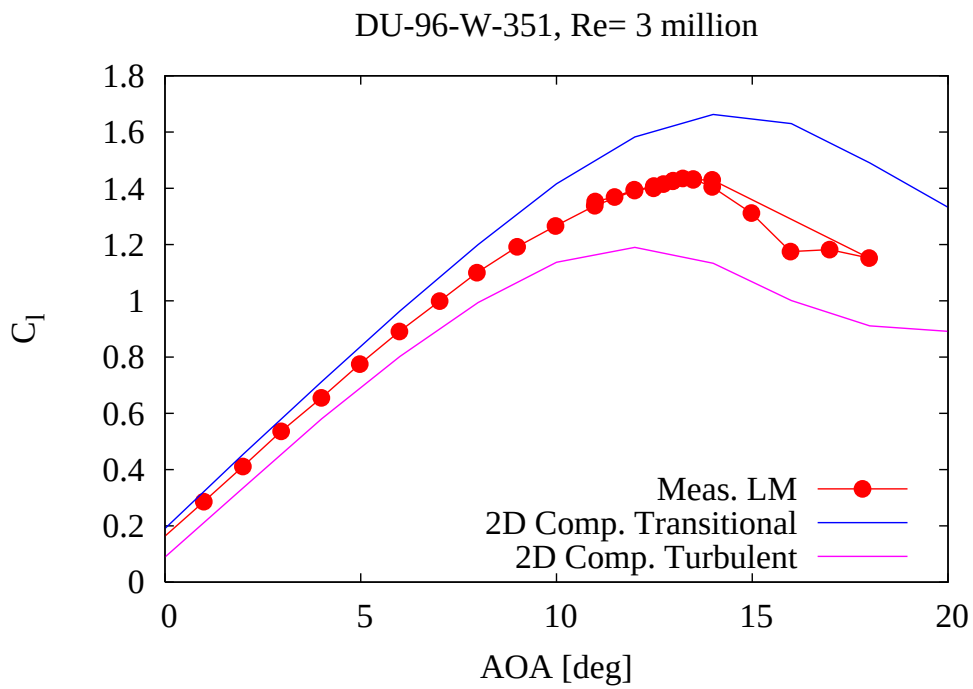

Niels N. Sørensen,
Risø DTU

DU-96-W-351

The effect of the different types of modelling is clearly visible

- 2D RANS fully turbulent and transitional computations
- 3D DDES fully turbulent computations

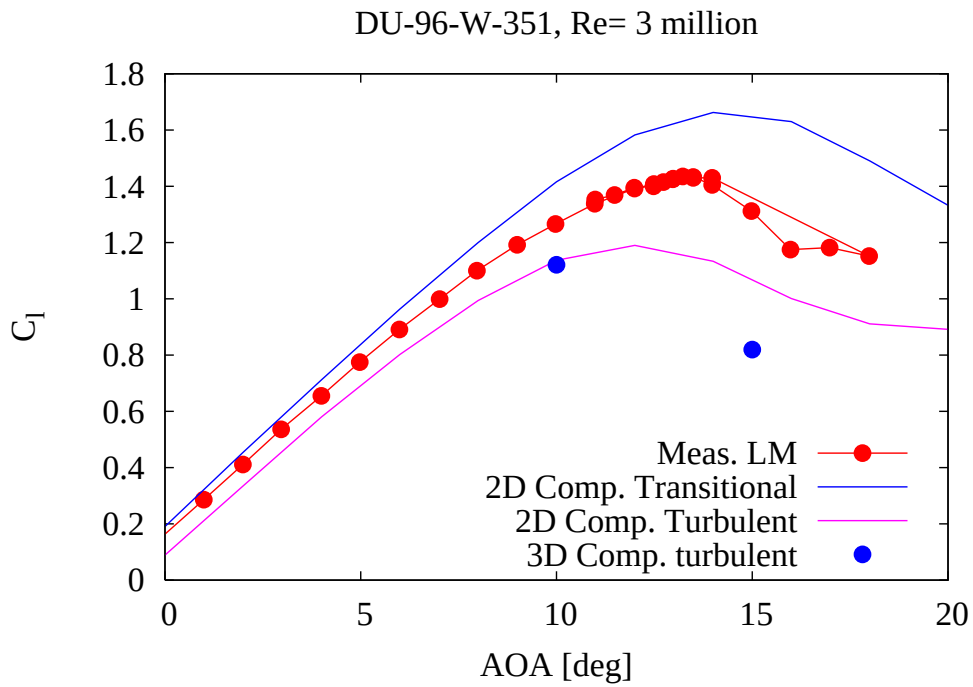

Niels N. Sørensen,
Risø DTU

DU-96-W-351

The effect of the different types of modelling is clearly visible

- 2D RANS fully turbulent and transitional computations
- 3D DDES fully turbulent computations
- 3D DDES transitional computations

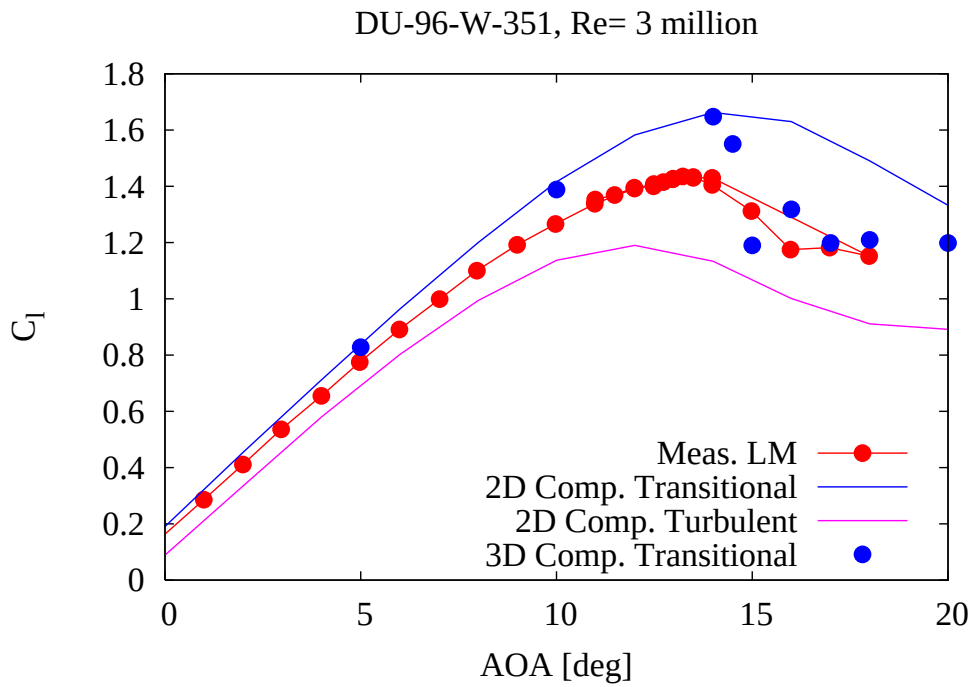

Niels N. Sørensen,
Risø DTU

DU-96-W-351

The effect of the different types of modelling is clearly visible

- 2D RANS fully turbulent and transitional computations
- 3D DDES fully turbulent computations
- 3D DDES transitional computations
- Wake behind the airfoil at AOA=18 deg

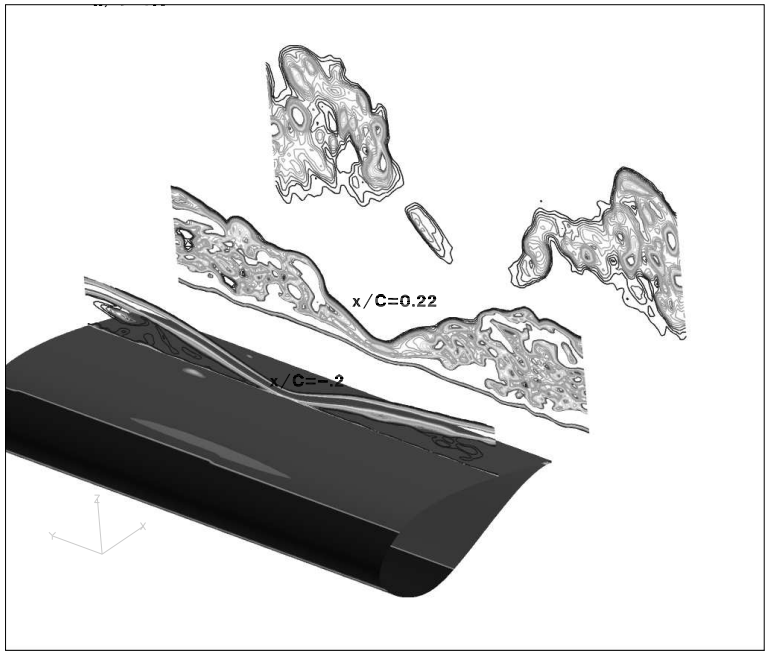

Niels N. Sørensen,
Risø DTU

The problem

- Nacelle anemometry is used in the control of a wind turbine for
- Yaw control,
- Startup/shut down,
- Power curve estimation.
- 10° yaw error $\approx$ 3% loss in power production.
- Operation with yaw error increases fatigue loads.
- Nacelle sonics are typically placed at the rear of the nacelle.
- Does it make sense to measure the yaw in the wake of the blades?

Computational Mesh

- Fully resolved rotor/nacelle geometry, tower and ground is omitted.
- Total cell count = 14.16 million cells.

Niels N. Sørensen,
Risø DTU

Computational Mesh

- Fully resolved rotor/nacelle geometry, tower and ground is omitted.
- Total cell count = 14.16 million cells.

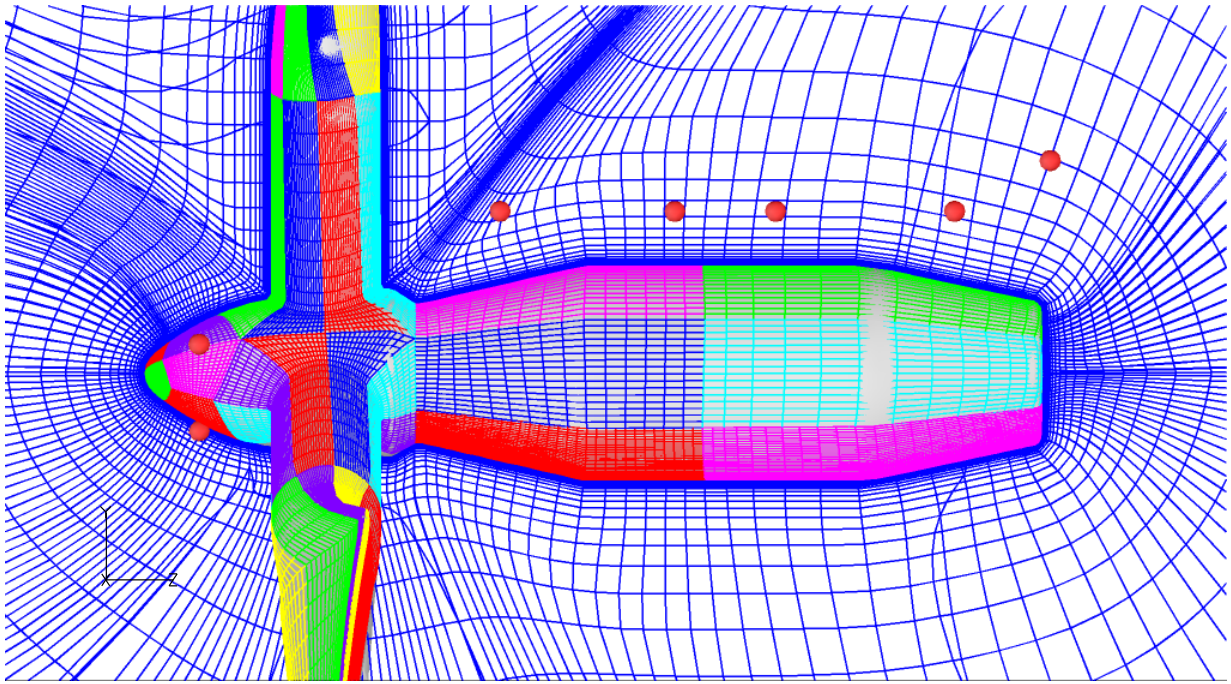

Niels N. Sørensen,
Risø DTU

Computational Mesh

- Fully resolved rotor/nacelle geometry, tower and ground is omitted.
- Total cell count = 14.16 million cells.

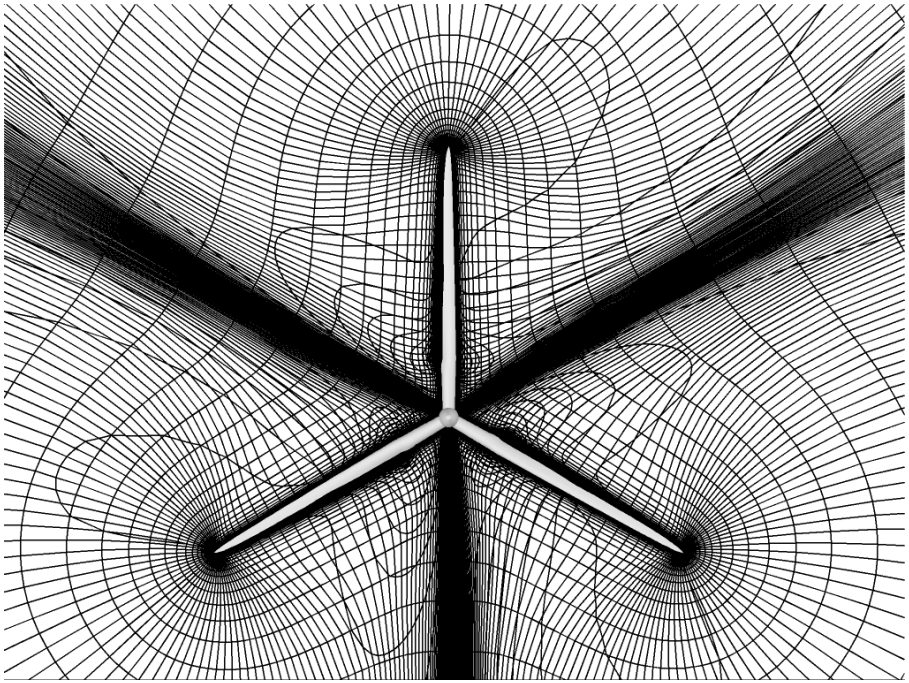

Unsteady Flow Solution

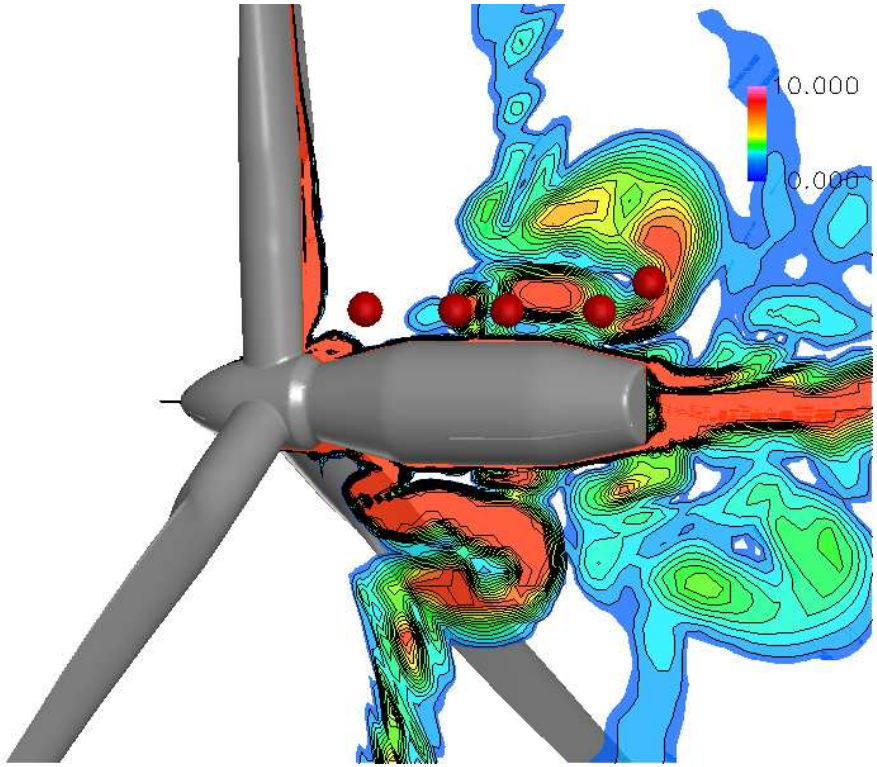

Niels N. Sørensen,
Risø DTU

Loads during standstill

Parameters:

- LM8.2, LM19.1 and two modern blades $\sim$ L=50 meter.
- Reynolds number $\frac{\rho U_\infty C}{\mu} = 1 \times 10^6$
- Second order accurate time-stepping with $\Delta t = \frac{1}{100}\frac{C}{U_\infty}$
- Turbulence modelling $k-\omega$ SST

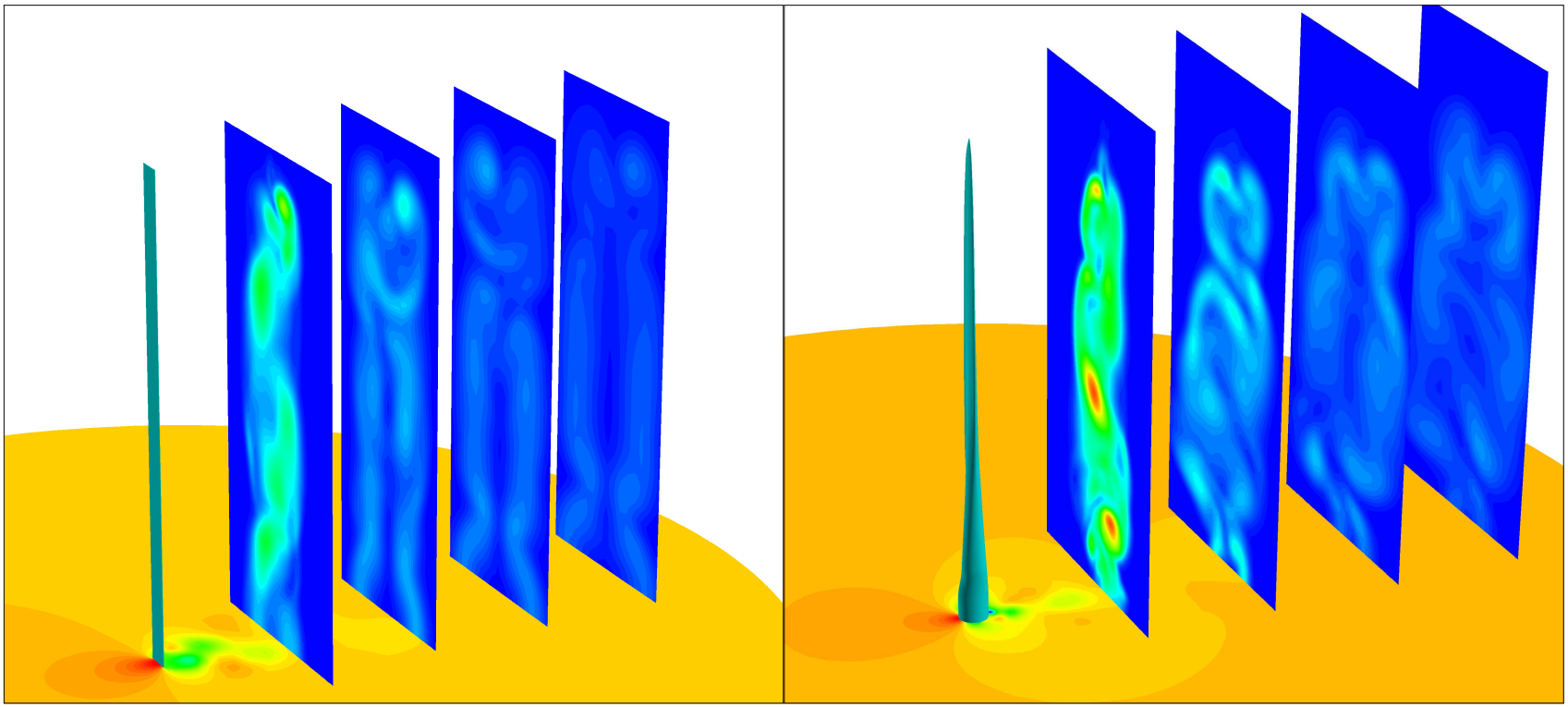

Loads during Standstill

- 256 cells around the chord
- 64 or 128 cells along the span
- 64 cells normal to the surface
- Total number of cells 1.3-2.4 million
- Outer boundary: $\sim 4\times$ Plate length
- Inner cell $y^+ \sim 2$

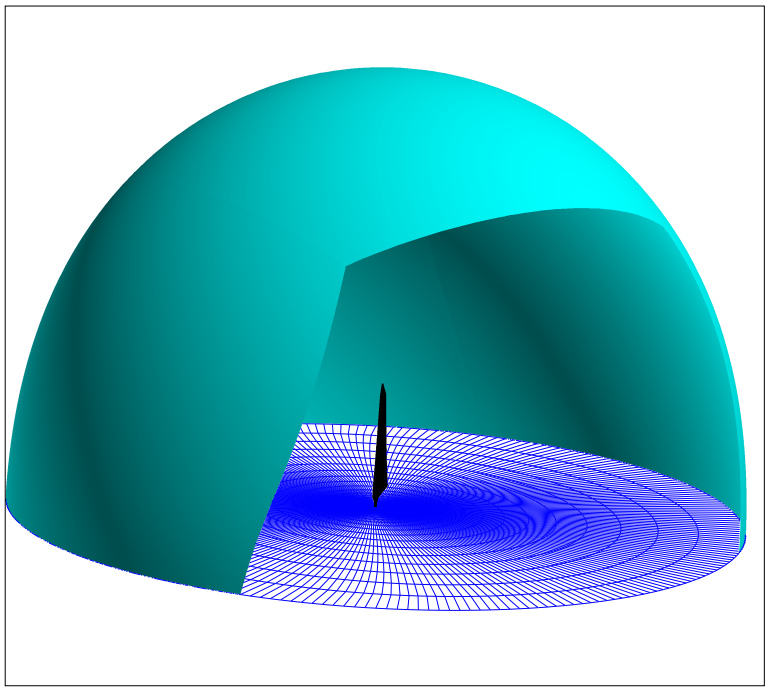

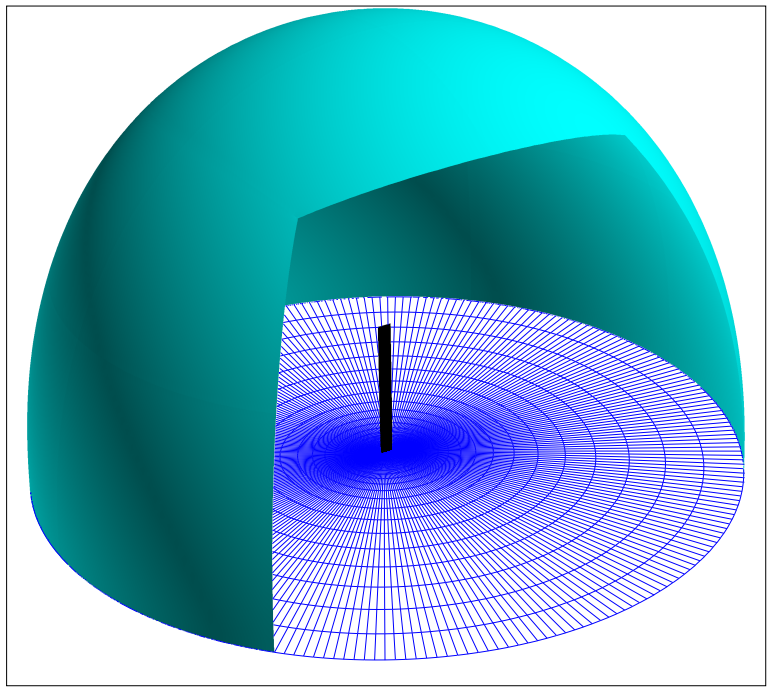

Niels N. Sørensen,
Risø DTU

Loads during Standstill

We have included three flat plates of varying aspect ratio to validate the approach

- One interesting point is the drag on the blades during standstill

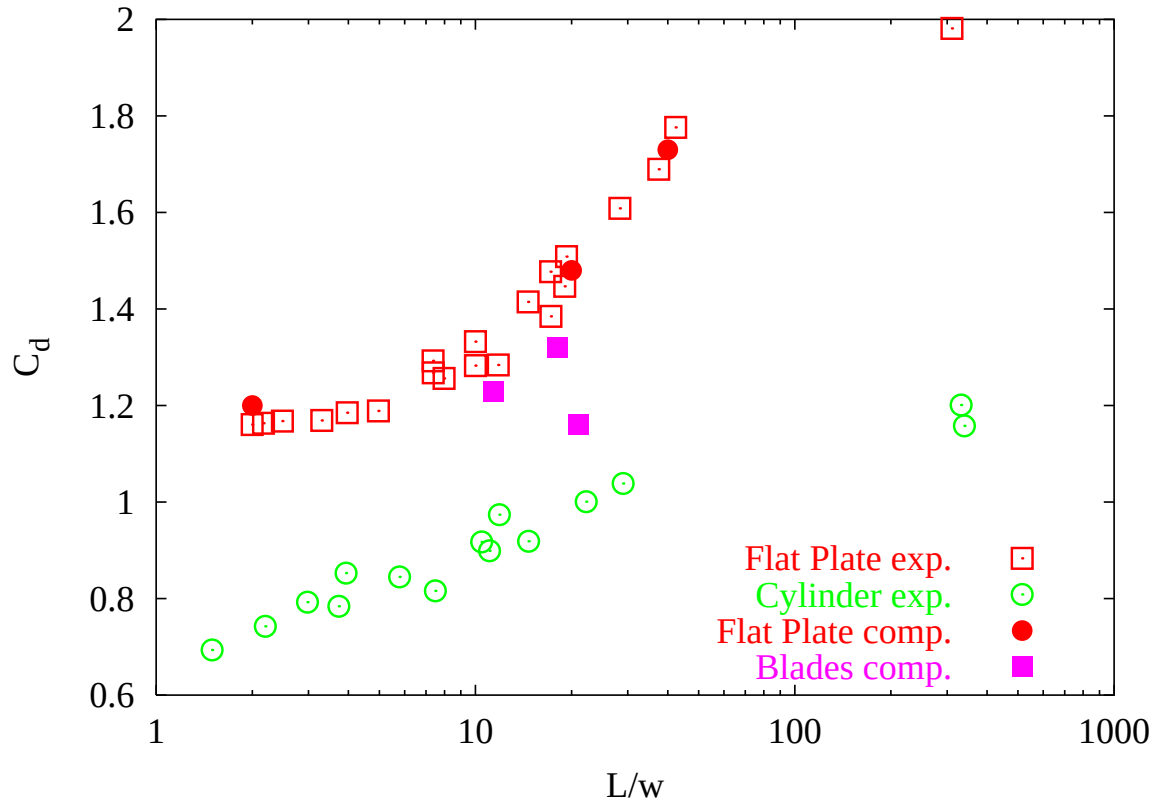

Niels N. Sørensen,
Risø DTU

Loads during Standstill

- From a load aspect the drag distribution along the blade surface is another interesting aspect

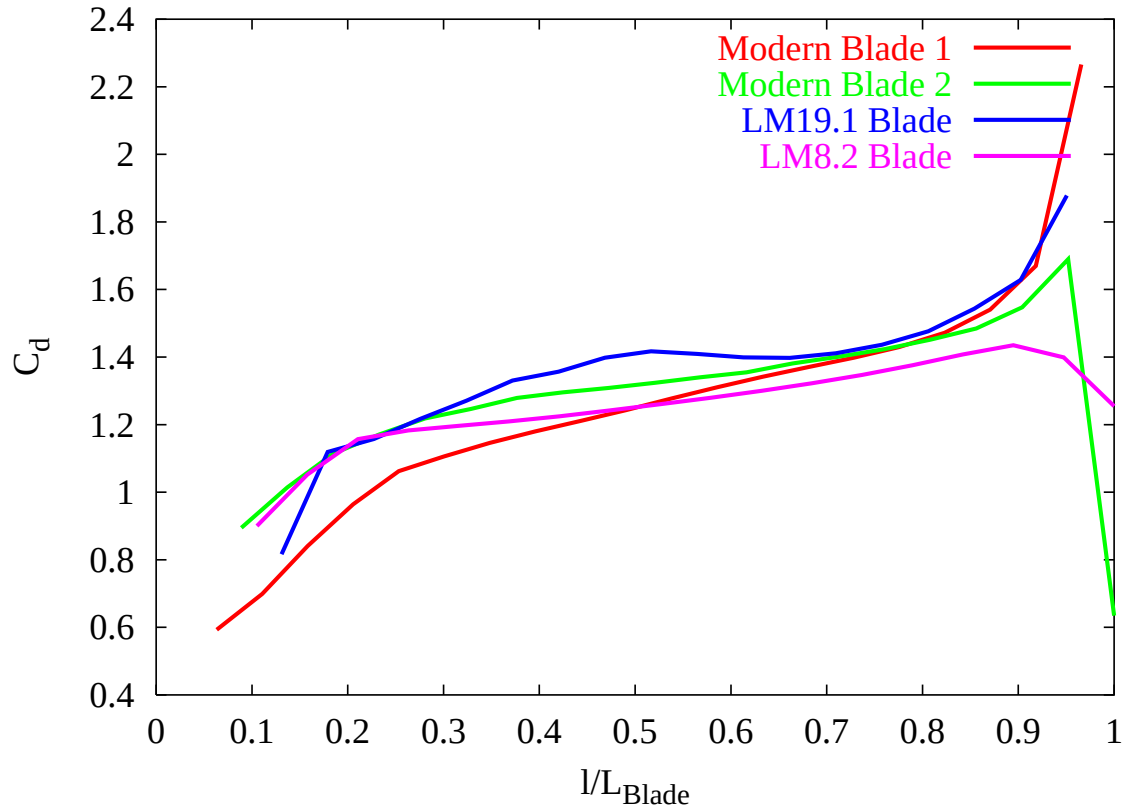

Niels N. Sørensen,
Risø DTU

Loads during Standstill

- C_d is well determined for flat plates.
- C_d for the examined blades are between 1.15-1.3.
- C_d for blades do not simply depend on the aspect ratio.
- The spanwise drag distribution shows a low value at the root and a high value at the tip.
- The use of constant C_d distribution will result in a under prediction for the flap moment for the examined blades.

The configuration

The tested configuration is based on the NREL-Phase-VI turbine during standstill

- The blade is parked straight up, zero azimuth position.
- The geometrical AOA is defined as the angle between the local chord and the test section center line
- The mean AOA given below is for the 47% section

Name	Mean Aoa [deg]	Amplitude [deg]	Pitch time [s]	Reduced freq.
47311	7.91	5.55	0.8496	0.099
47320	13.89	5.55	0.8126	0.099
47040	22.92	5.04	1.1261	0.075

Computational Method

Computations are performed with the EllipSys3D flow solver:

- Second order time true computations, using implicit scheme with sub-iterations
- Convective terms by QUICK/ 4. order CDS
- Turbulence modeling based on $k-\omega$ SST model
- Transition based on $\gamma - Re_{\theta t}$ model
- Moving mesh formulation, using prescribed motion

Four types of computations are performed

	RANS	DDES
Fully Turb.	×	×
Transitional	×	×

Computational Grid

The grid is based on a multi-block structured O-O-topology

- Distance to farfield $\sim$ 12 [m]
- Wall normal cell height $\sim y^+ < 2$
- Cells in chordwise direction 256 cells
- Cells in spanwise direction 256 cells
- Cells in normal direction 128 cells
- Total grid cell count $\sim$ 8.9 million cells

Grid and time step independence test were performed.

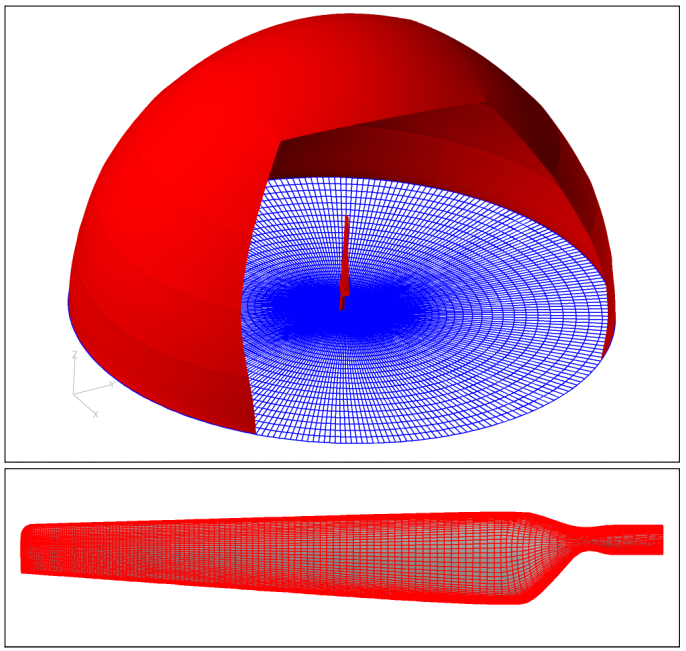

Effect of turbulence and transition modelling

- We use the medium AOA case called 47320
- We use a time step of 2×10^{-4}
- We use the fine grid 8.9 million points

r/R=0.30

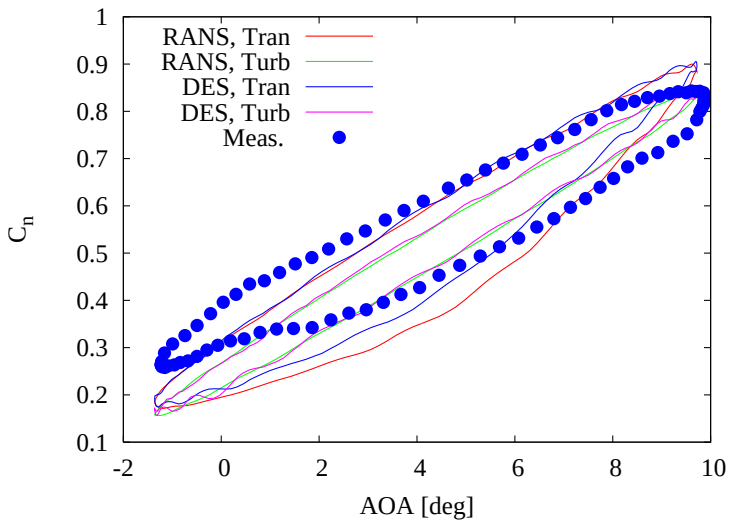

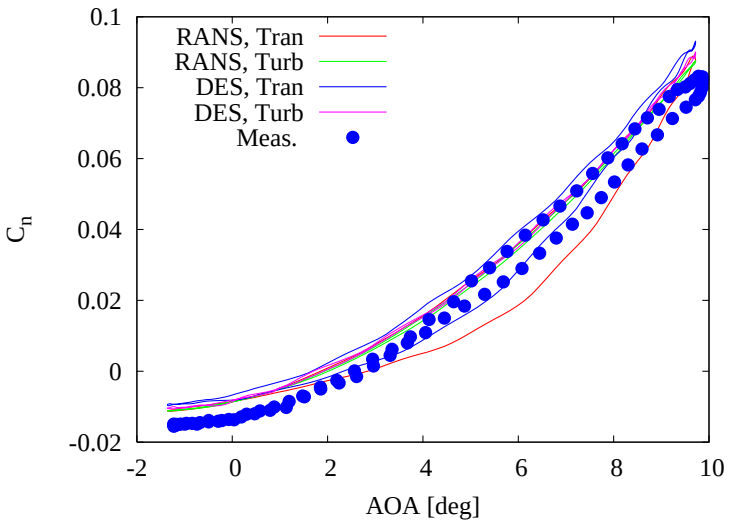

Niels N. Sørensen,
Risø DTU

Effect of turbulence and transition modelling

- We use the medium AOA case called 47320
- We use a time step of 2×10^{-4}
- We use the fine grid 8.9 million points

r/R=0.47

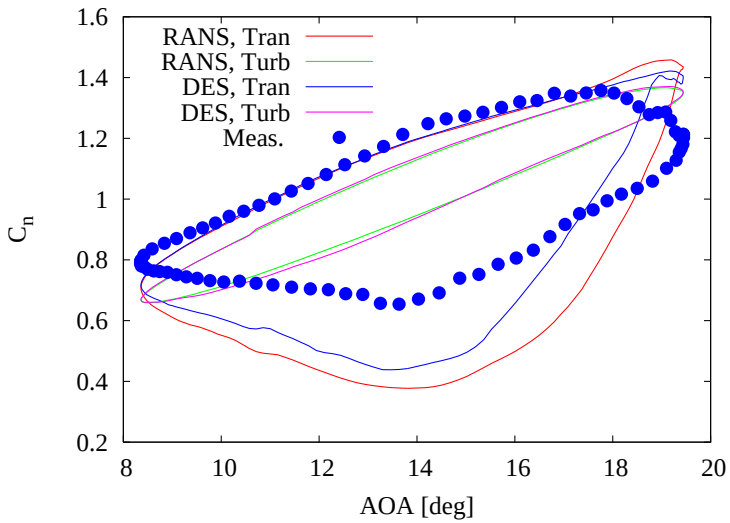

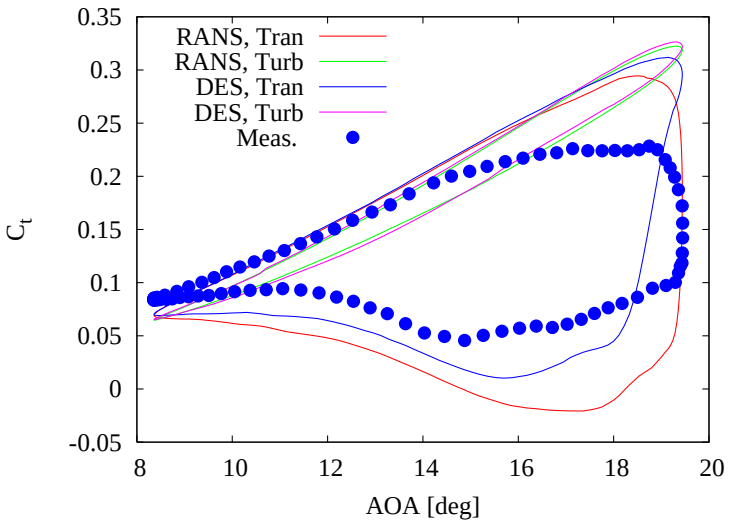

- In the present case the transition model opens the loops

Effect of turbulence and transition modelling

- We use the medium AOA case called 47320
- We use a time step of 2×10^{-4}
- We use the fine grid 8.9 million points

r/R=0.63

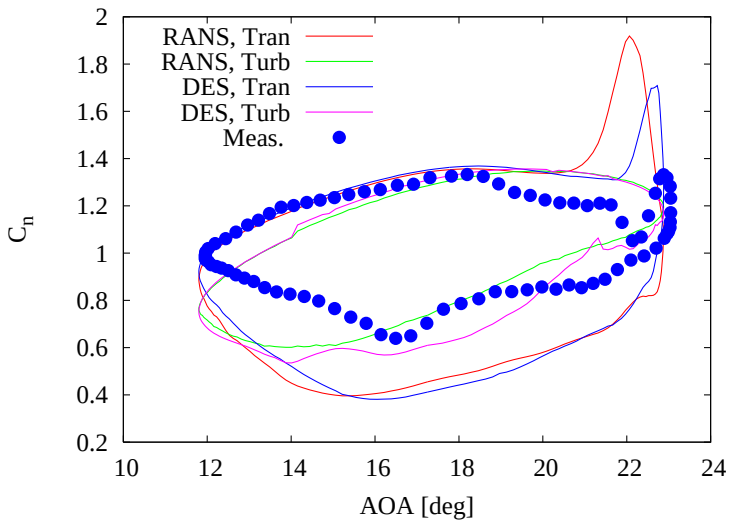

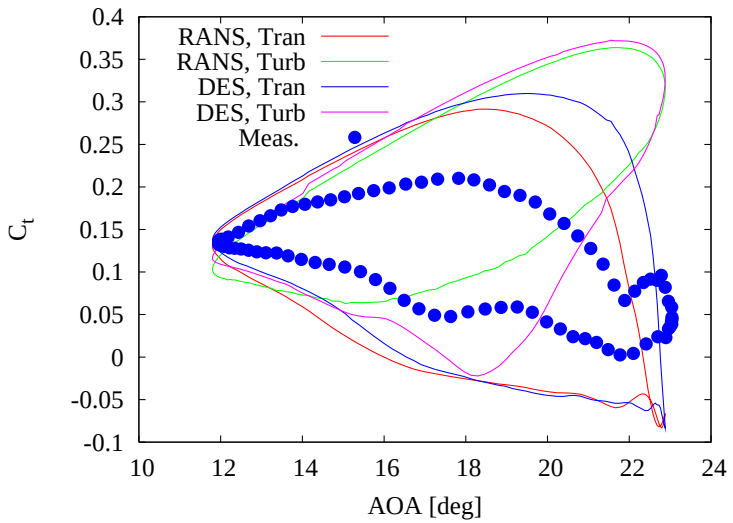

- In the present case the transition model opens the loops

Effect of turbulence and transition modelling

- We use the medium AOA case called 47320
- We use a time step of 2×10^{-4}
- We use the fine grid 8.9 million points

r/R=0.80

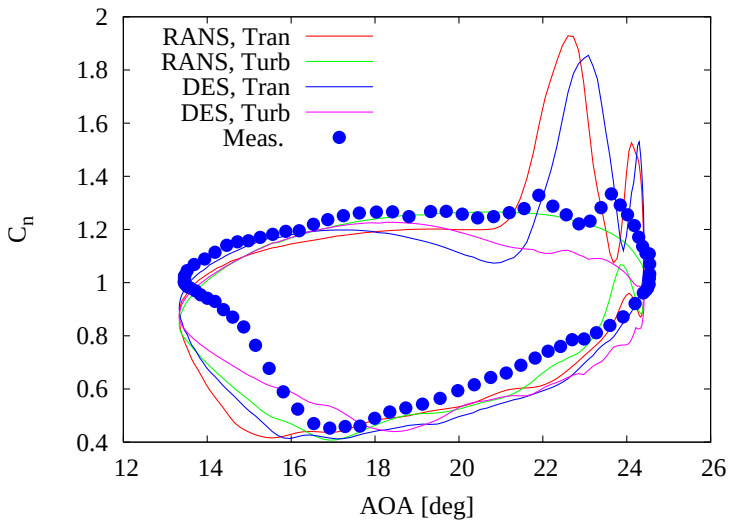

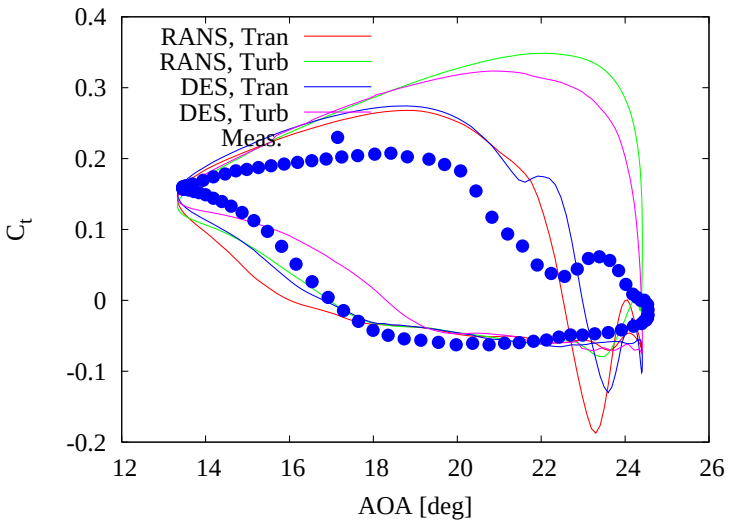

- In the present case the transition model opens the loops
- In the present case the DDES model do not help much

Niels N. Sørensen,
Risø DTU

Effect of turbulence and transition modelling

- We use the medium AOA case called 47320
- We use a time step of 2×10^{-4}
- We use the fine grid 8.9 million points

r/R=0.95

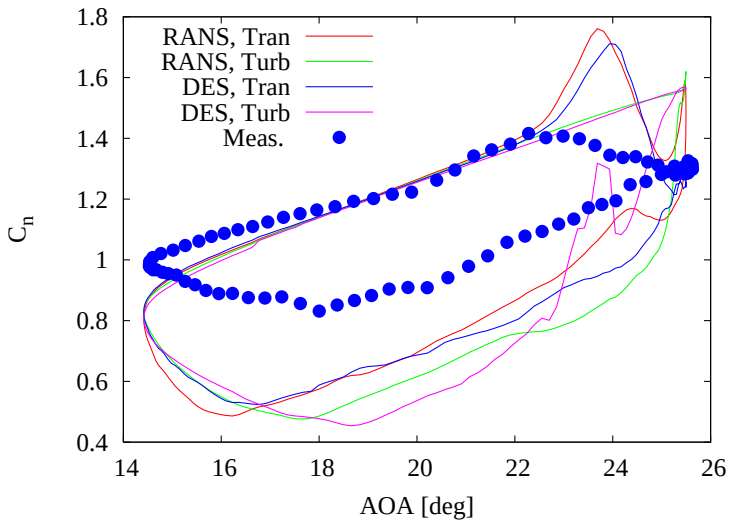

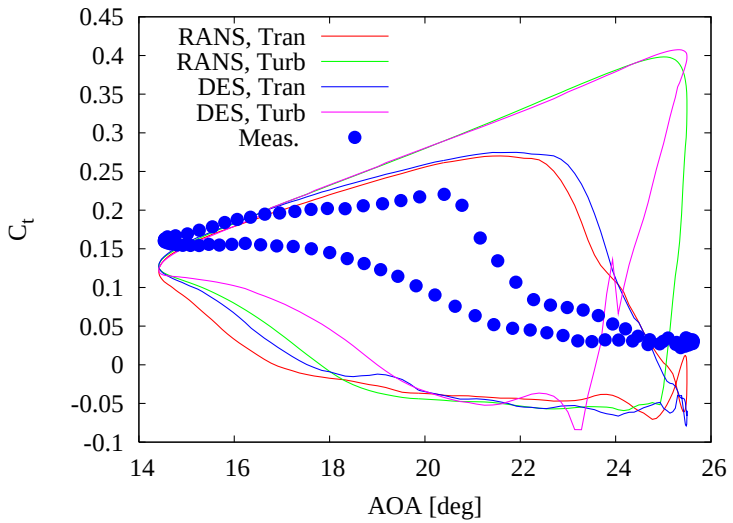

- In the present case the transition model opens the loops
- In the present case the DDES model do not help much

Niels N. Sørensen,
Risø DTU

CASE 47311, Low AOA case

r/R=0.30

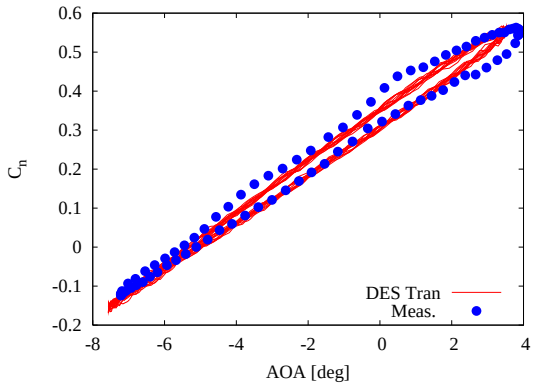

r/R=0.47

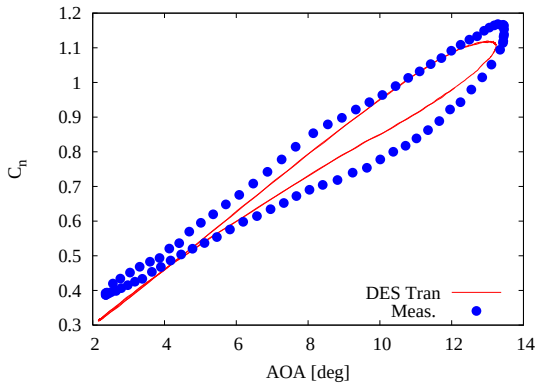

r/R=0.63

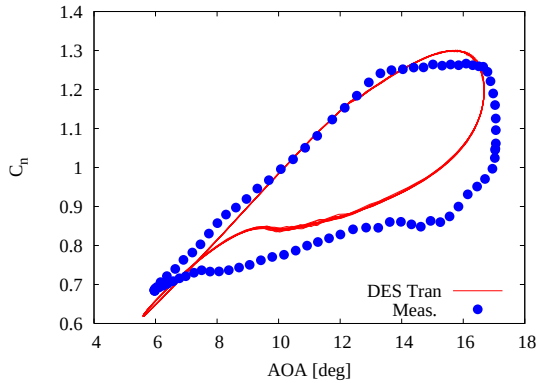

r/R=0.80

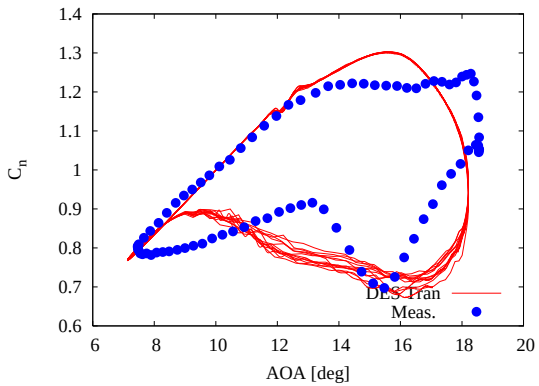

r/R=0.95

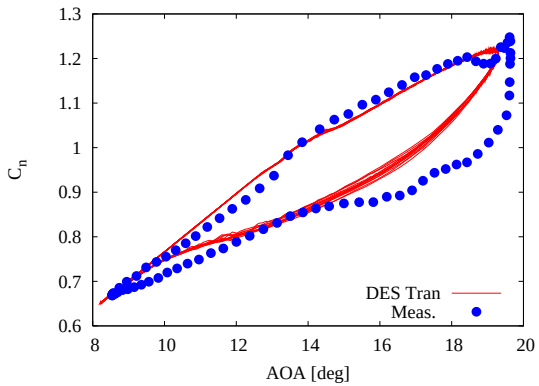

Niels N. Sørensen,
Risø DTU

Wind turbine related flow
Dynamic stall during standstill

CASE 47311, Low AOA case

r/R=0.30

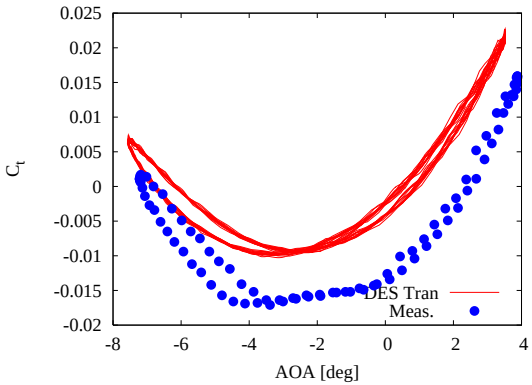

r/R=0.47

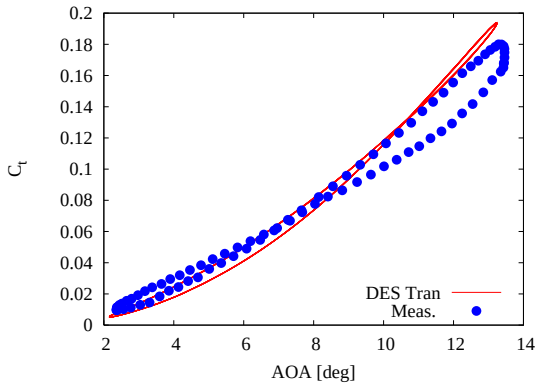

r/R=0.63

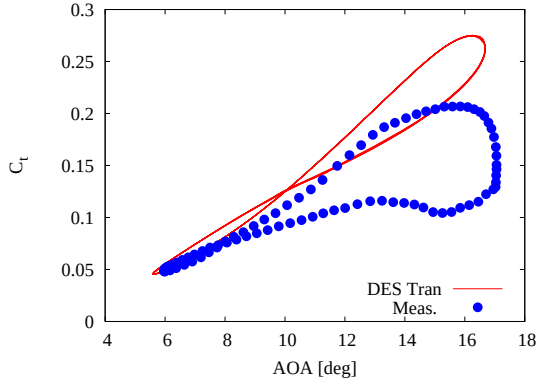

r/R=0.80

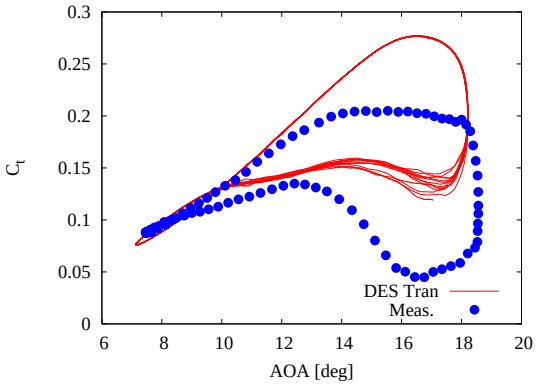

r/R=0.95

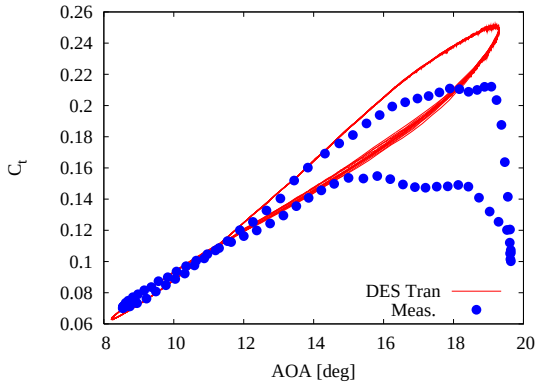

Niels N. Sørensen,
Risø DTU

CASE 47040, High AOA case

r/R=0.30

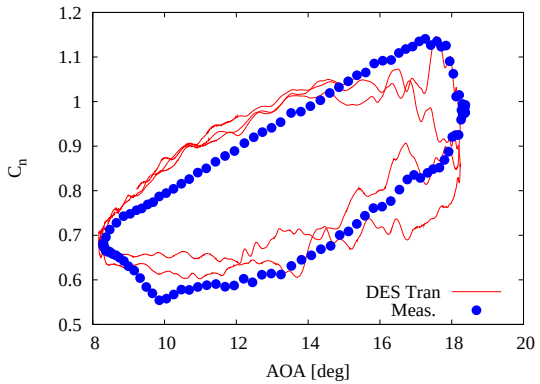

r/R=0.47

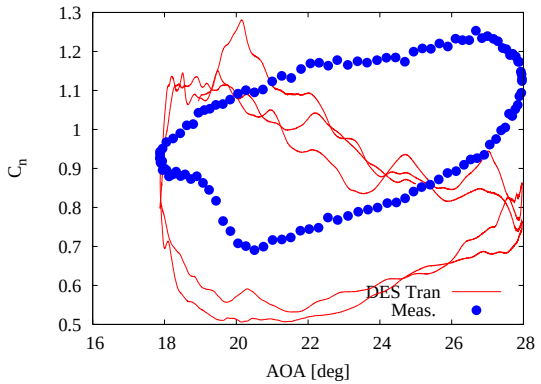

r/R=0.63

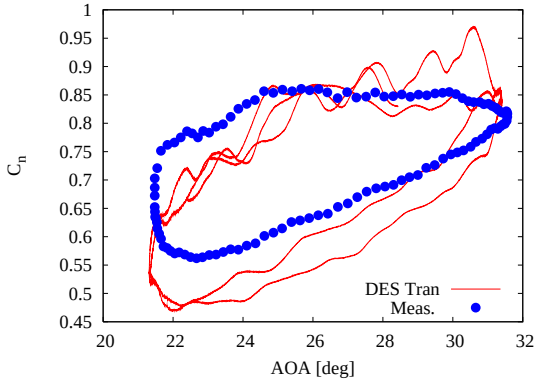

r/R=0.80

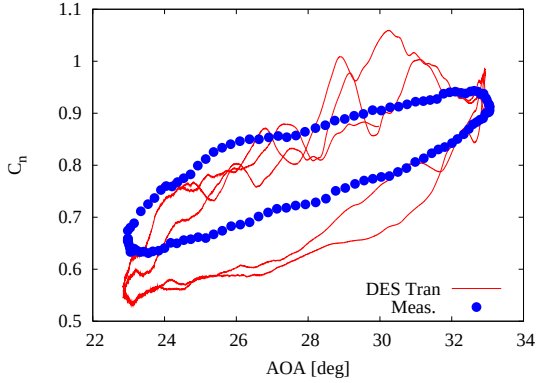

r/R=0.95

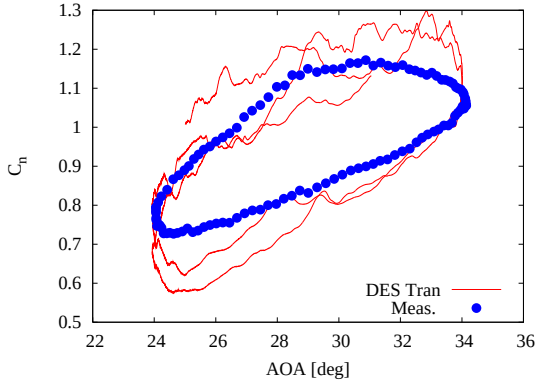

Niels N. Sørensen,
Risø DTU

CASE 47040, High AOA case

r/R=0.30

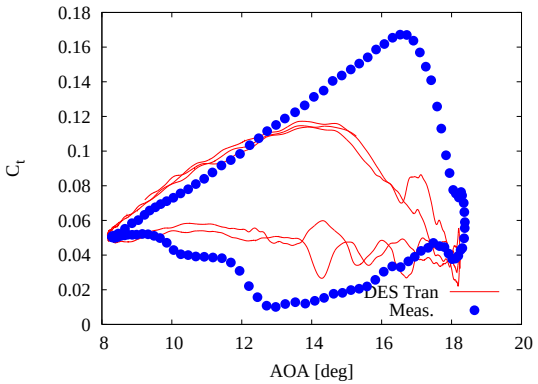

r/R=0.47

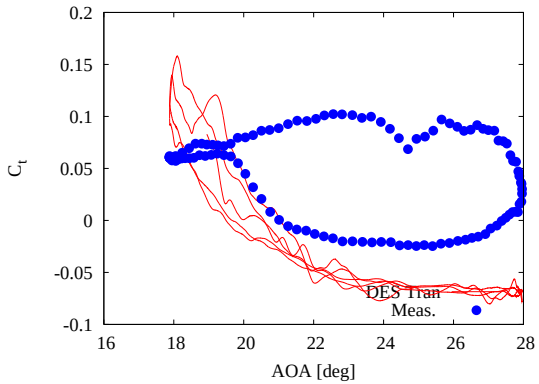

r/R=0.63

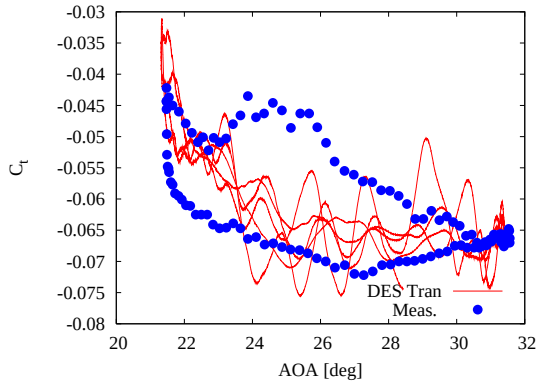

r/R=0.80

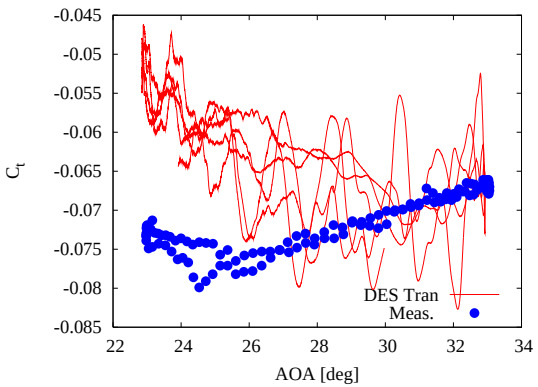

r/R=0.95

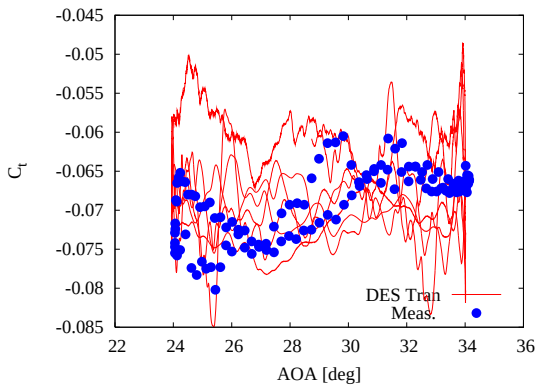

Niels N. Sørensen,
Risø DTU

Wind turbine related flow
Dynamic stall during standstill

CASE 47320, r/R=0.47

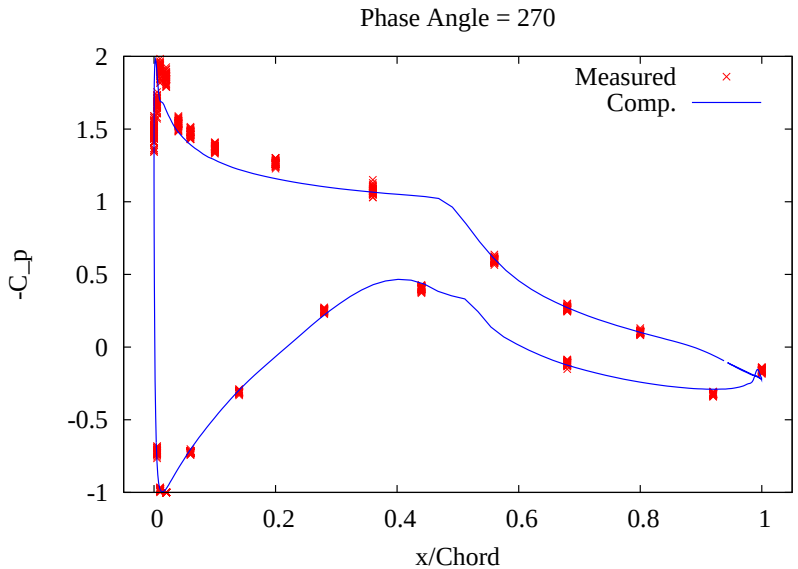

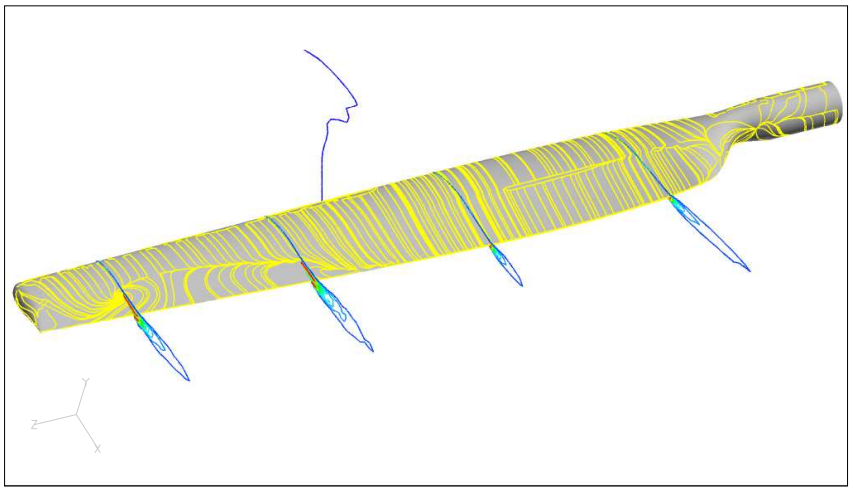

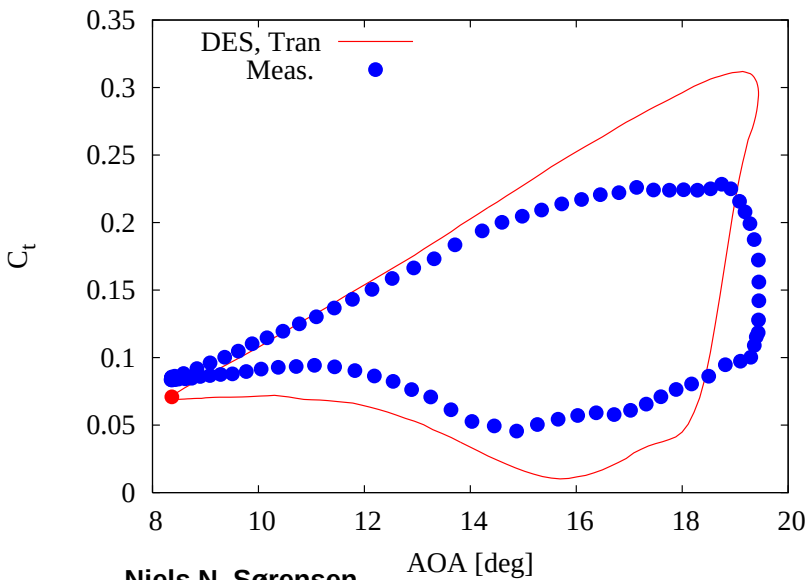

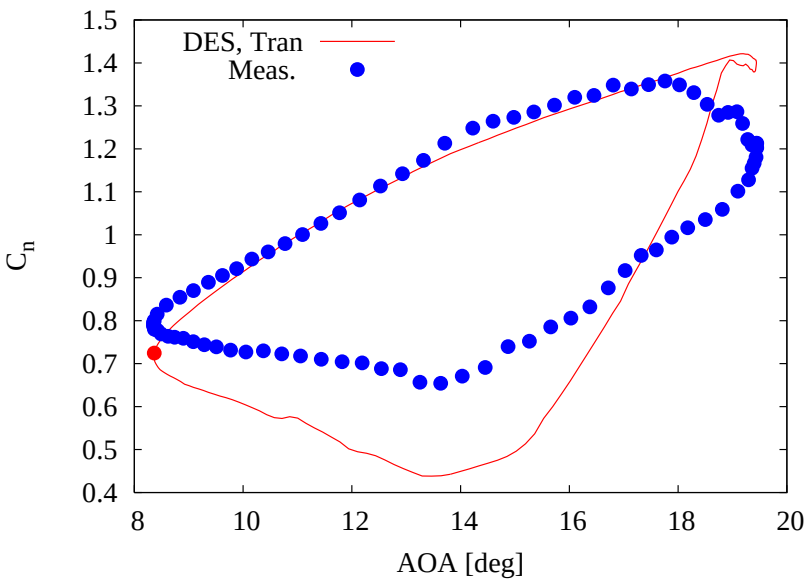

Niels N. Sørensen,
Risø DTU

Wind turbine related flow
Dynamic stall during standstill

CASE 47320, r/R=0.47

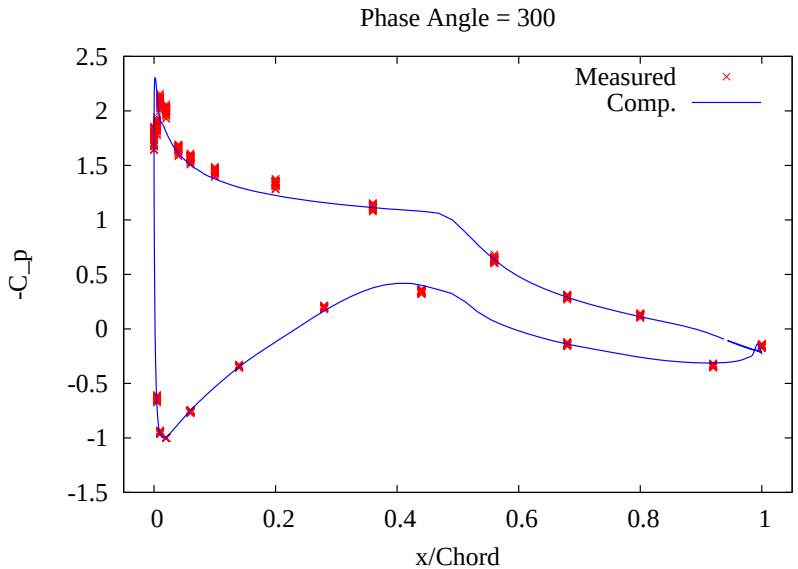

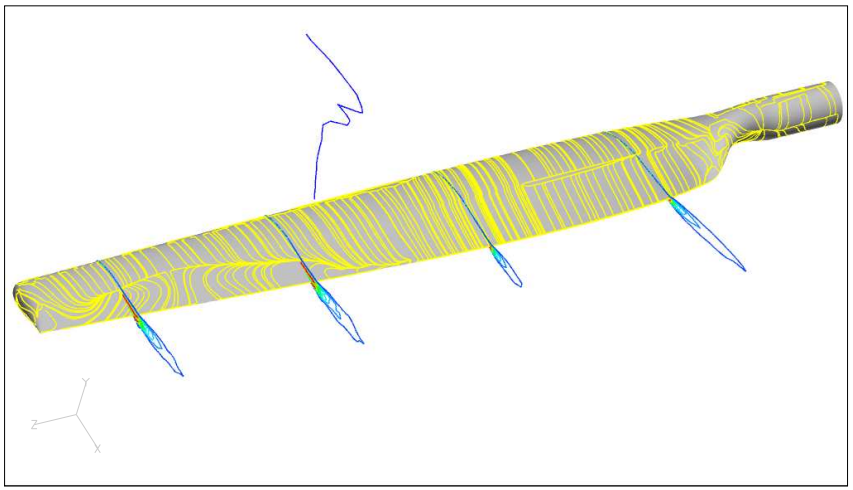

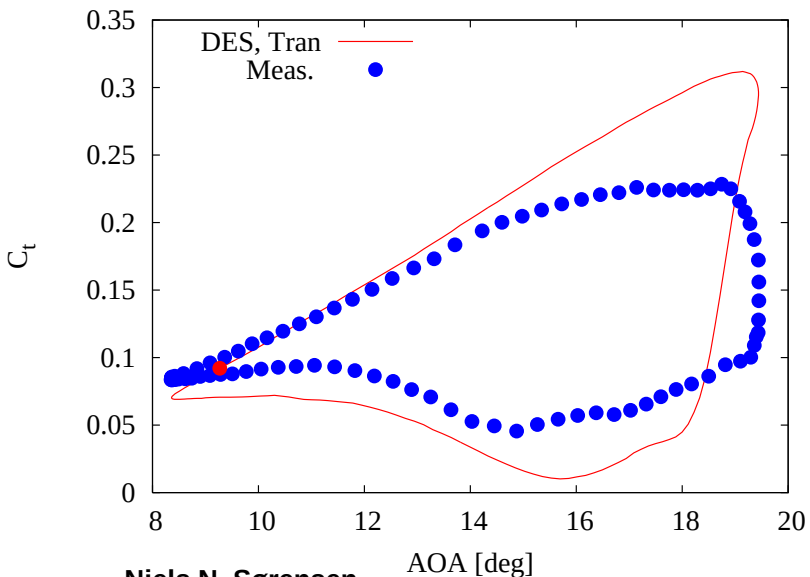

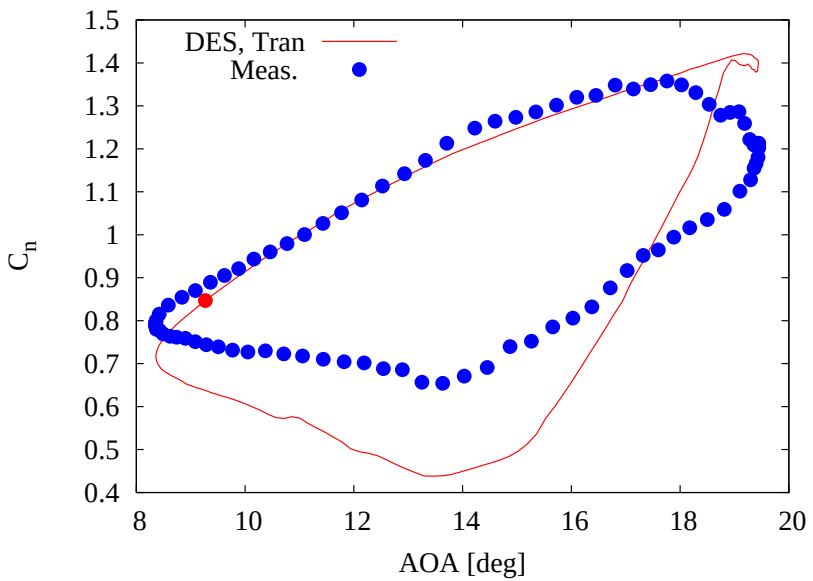

Niels N. Sørensen,
Risø DTU

Wind turbine related flow
Dynamic stall during standstill

CASE 47320, r/R=0.47

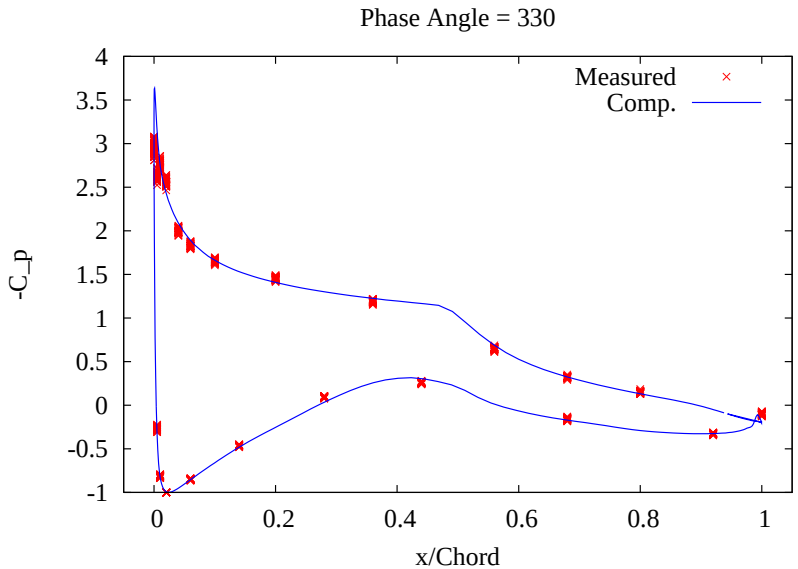

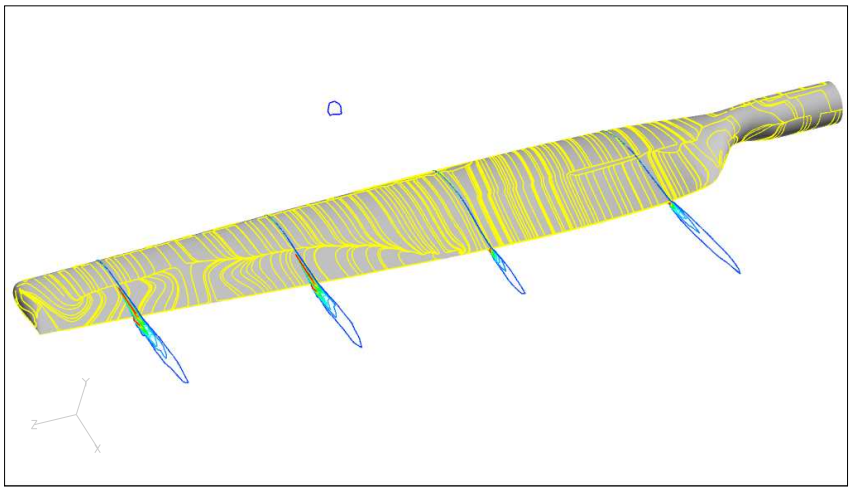

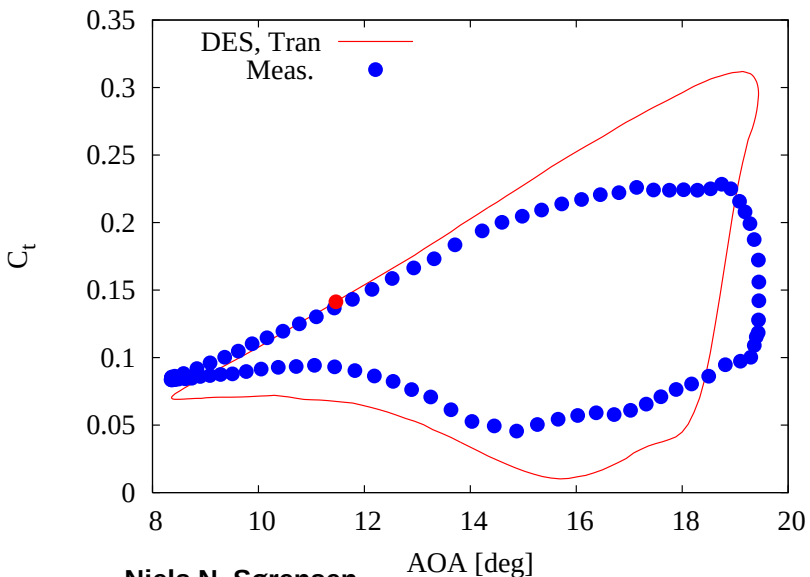

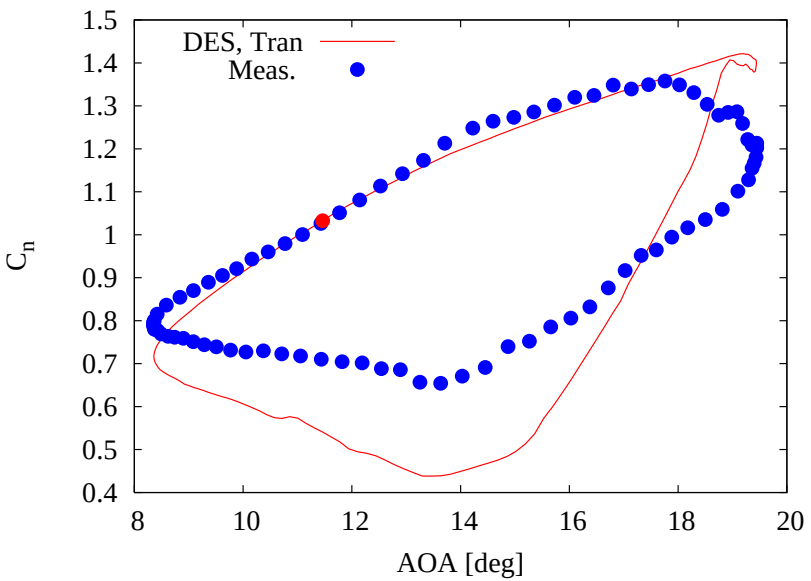

Niels N. Sørensen,
Risø DTU

Wind turbine related flow
Dynamic stall during standstill

CASE 47320, r/R=0.47

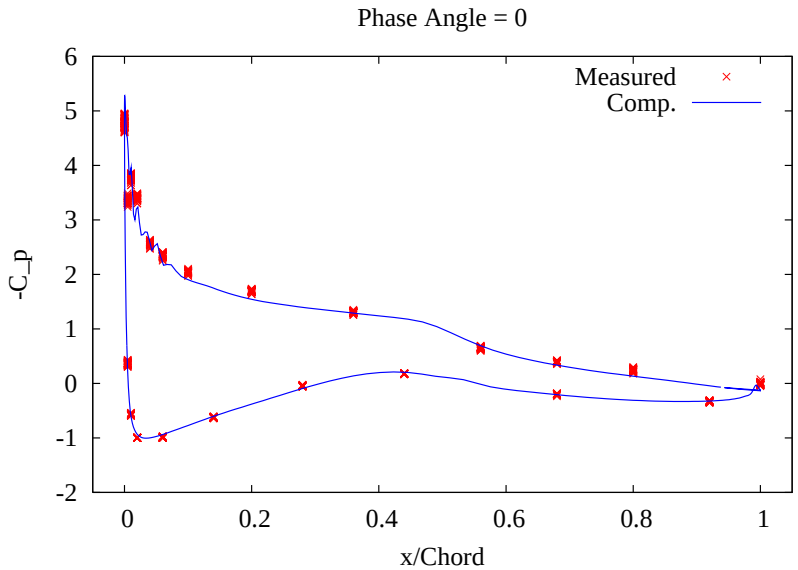

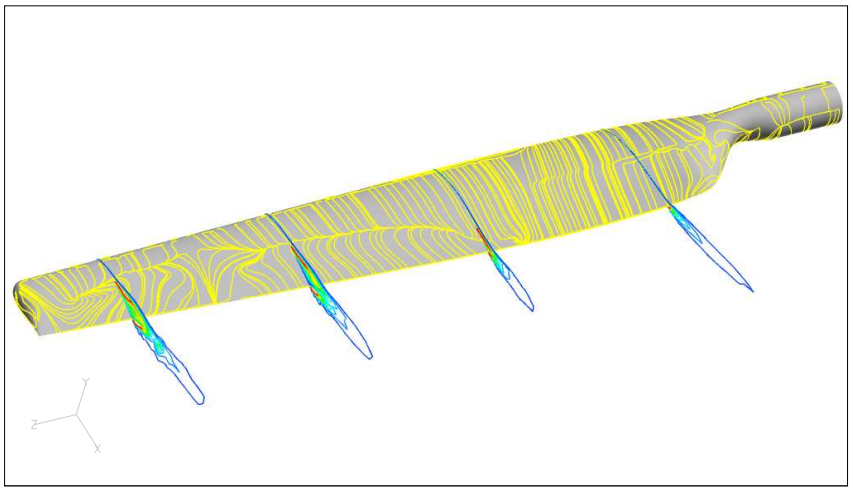

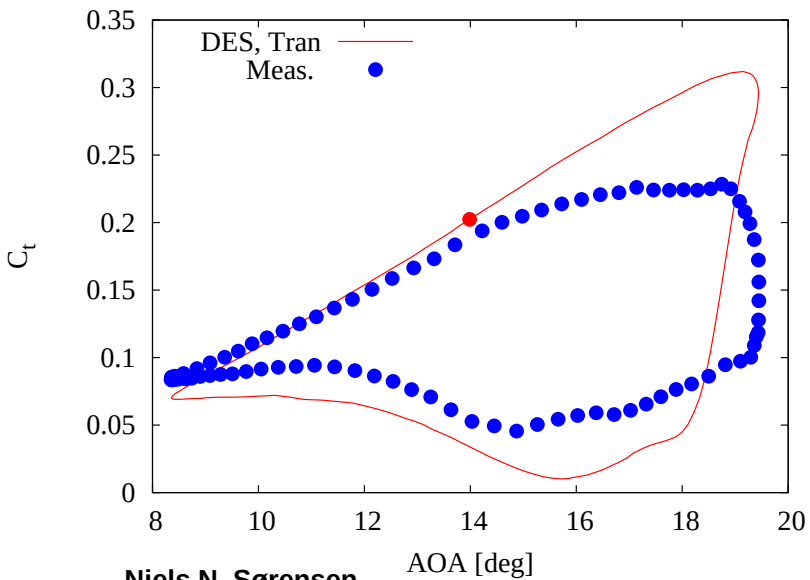

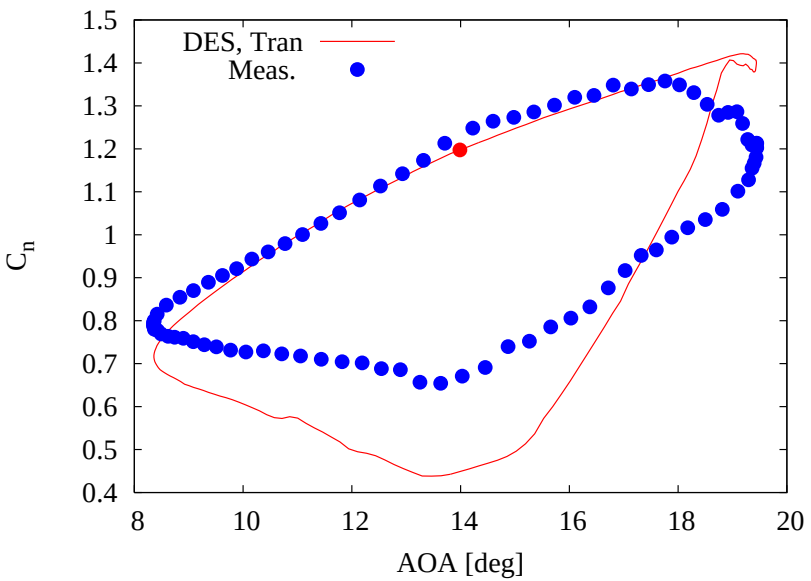

Niels N. Sørensen,
Risø DTU

Wind turbine related flow
Dynamic stall during standstill

CASE 47320, r/R=0.47

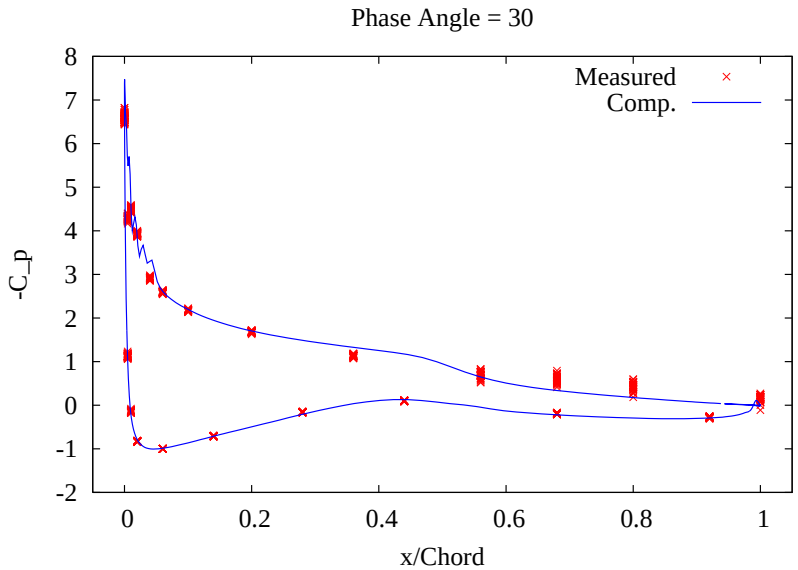

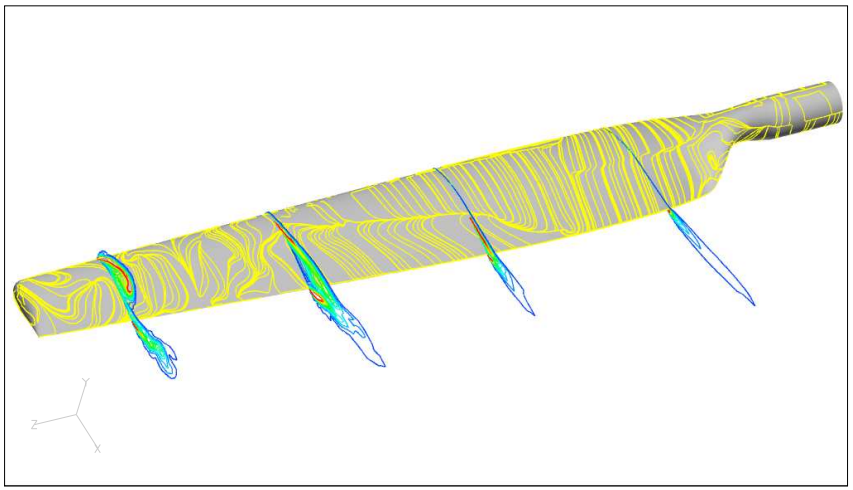

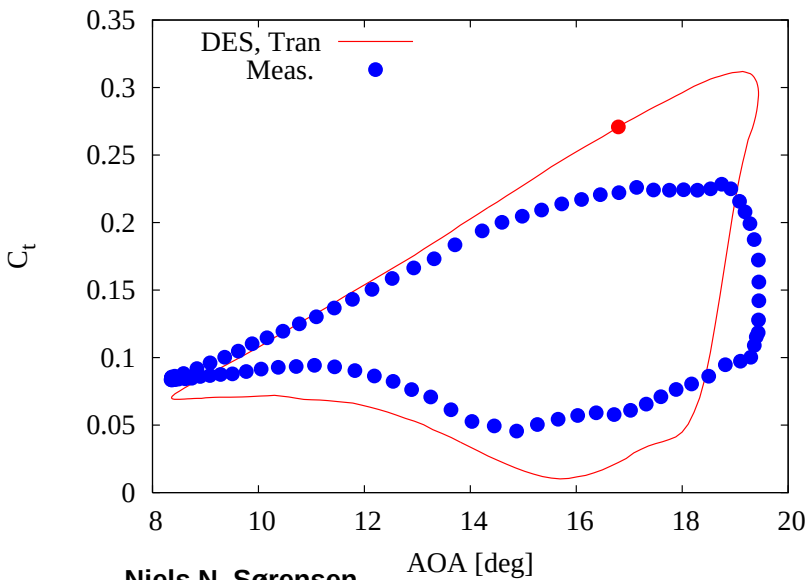

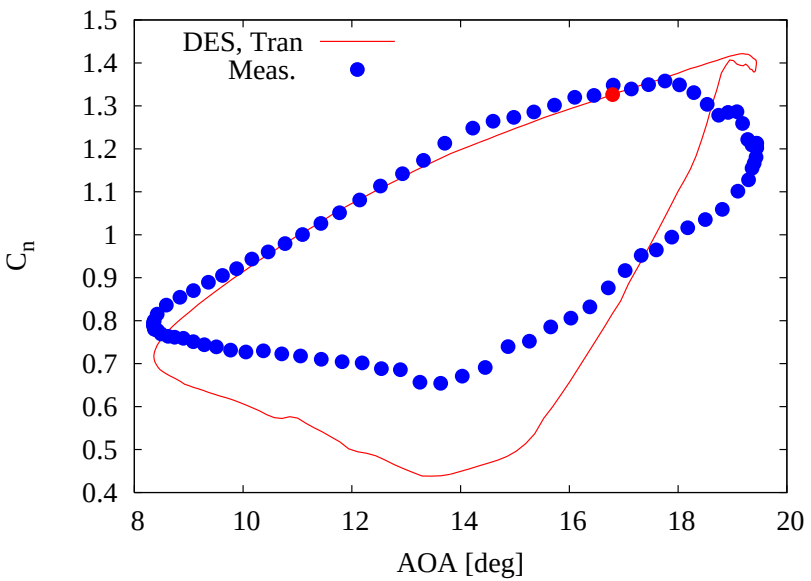

Niels N. Sørensen,
Risø DTU

Wind turbine related flow
Dynamic stall during standstill

CASE 47320, r/R=0.47

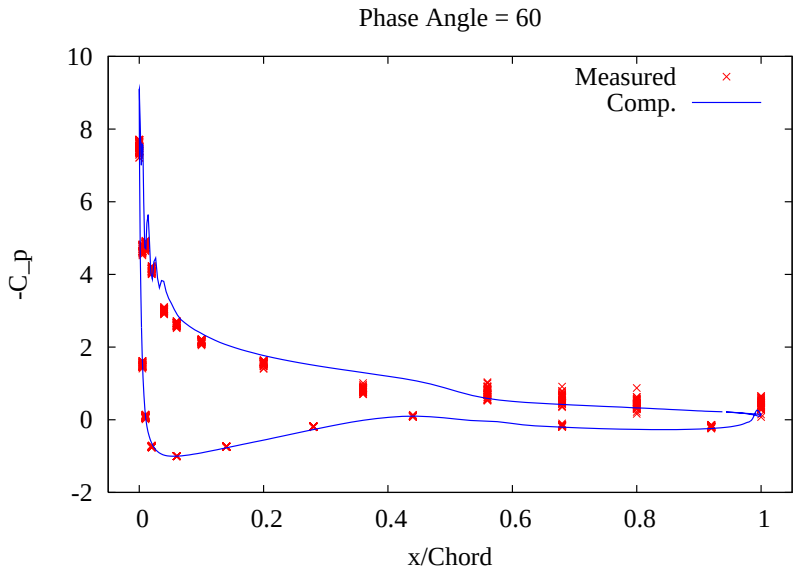

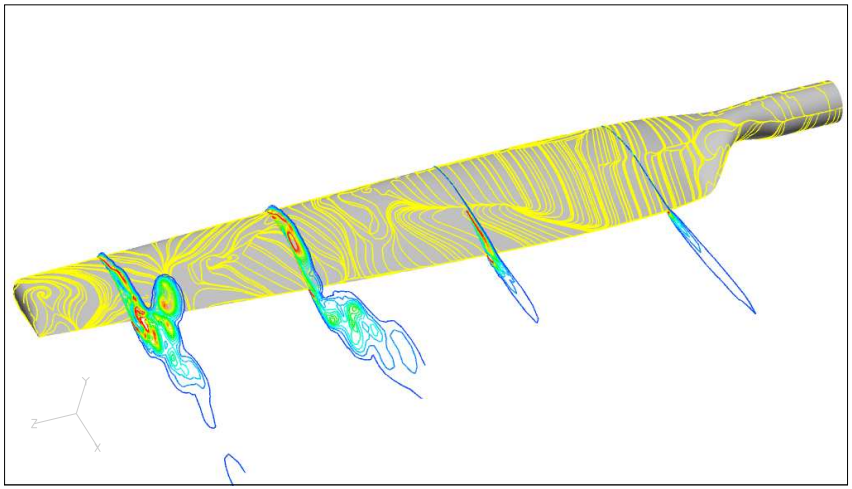

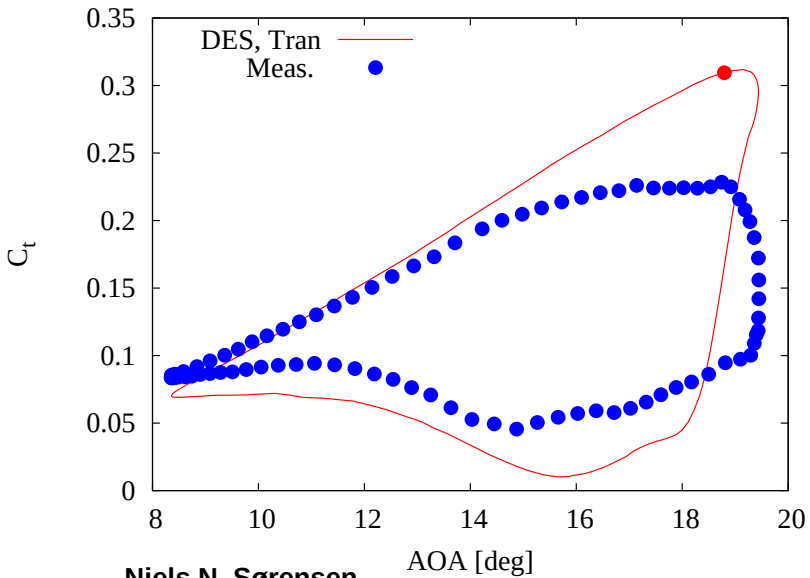

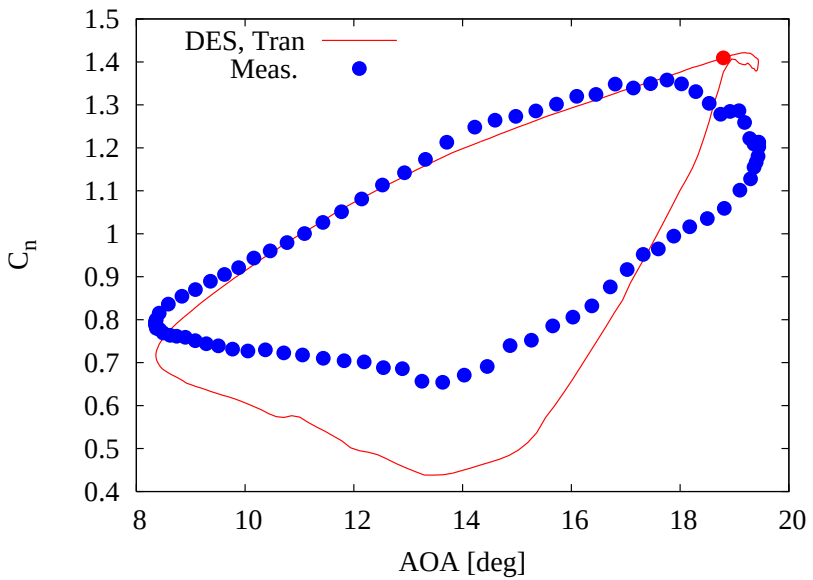

Niels N. Sørensen,
Risø DTU

Wind turbine related flow
Dynamic stall during standstill

CASE 47320, r/R=0.47

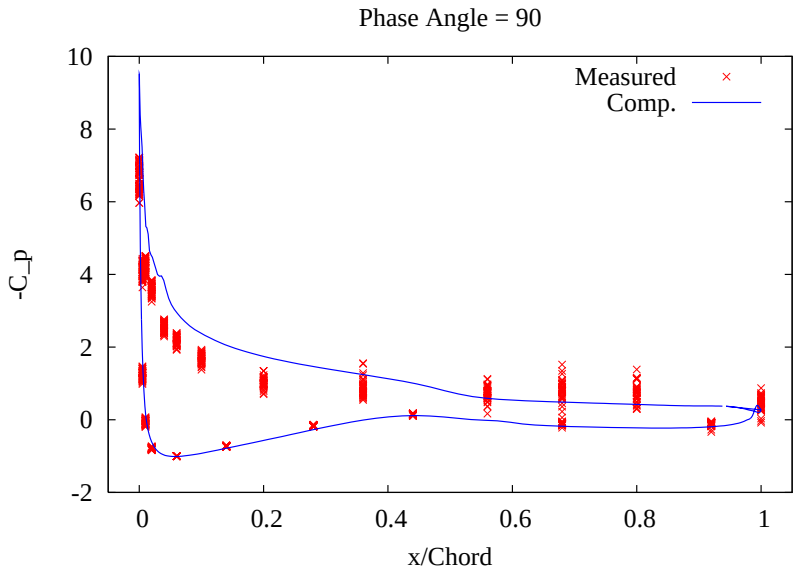

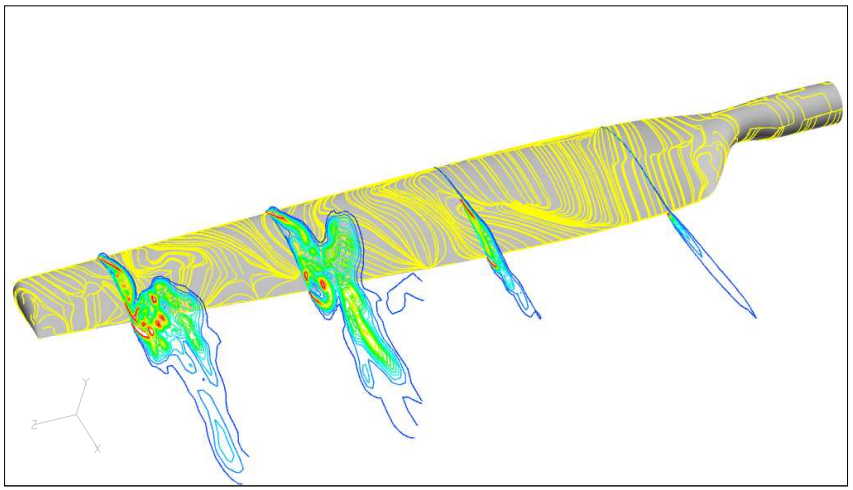

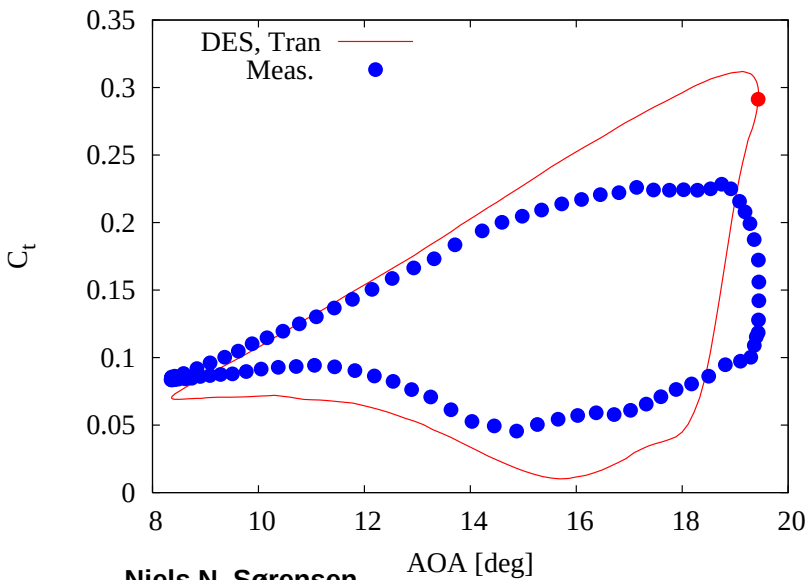

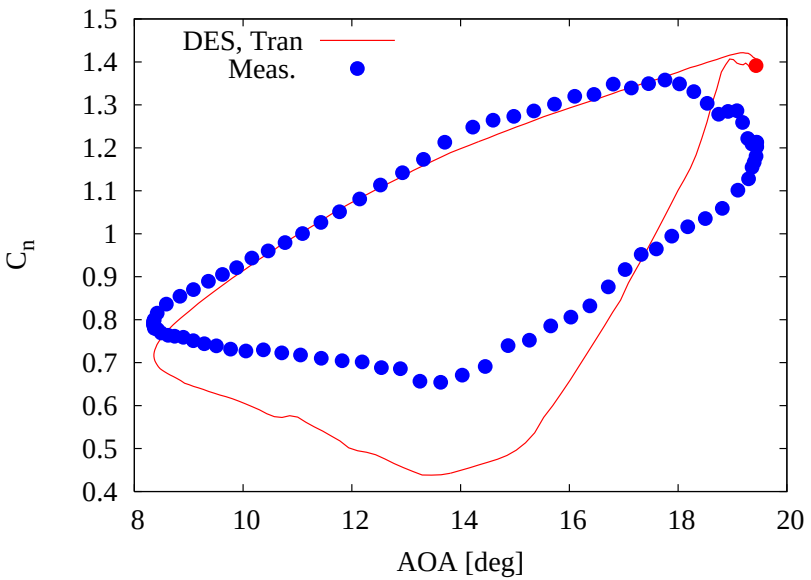

Niels N. Sørensen,
Risø DTU

Wind turbine related flow
Dynamic stall during standstill

CASE 47320, r/R=0.47

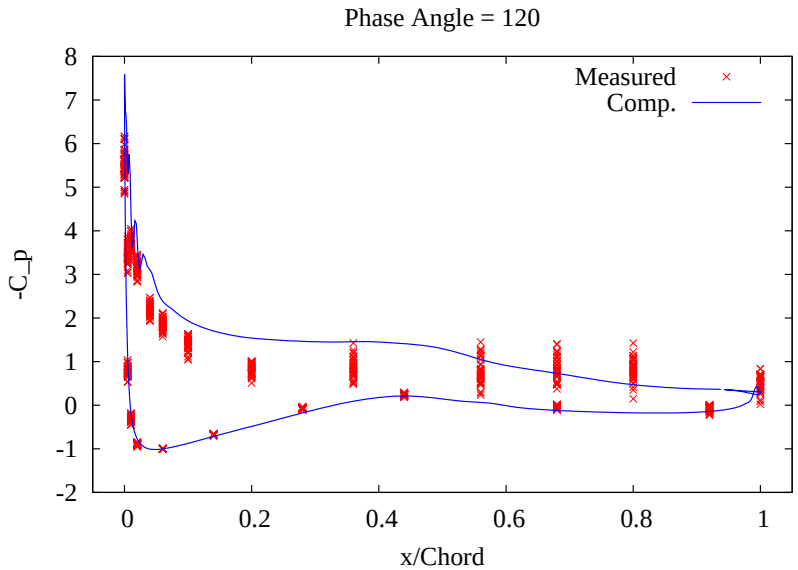

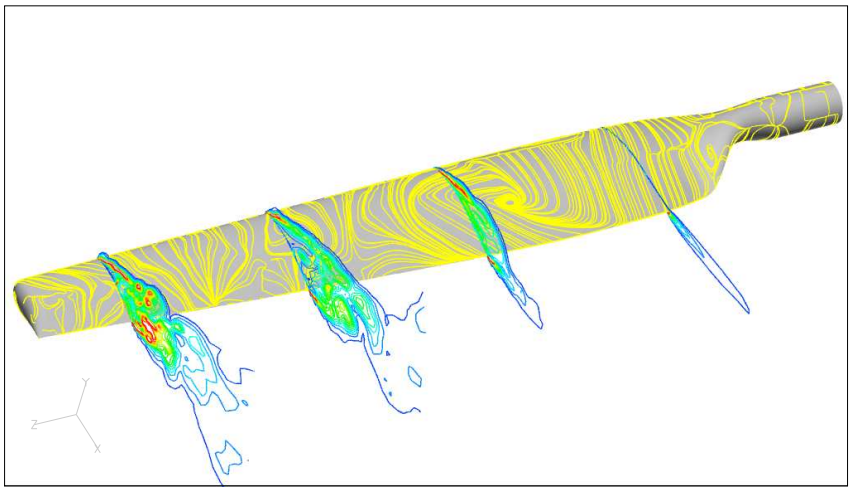

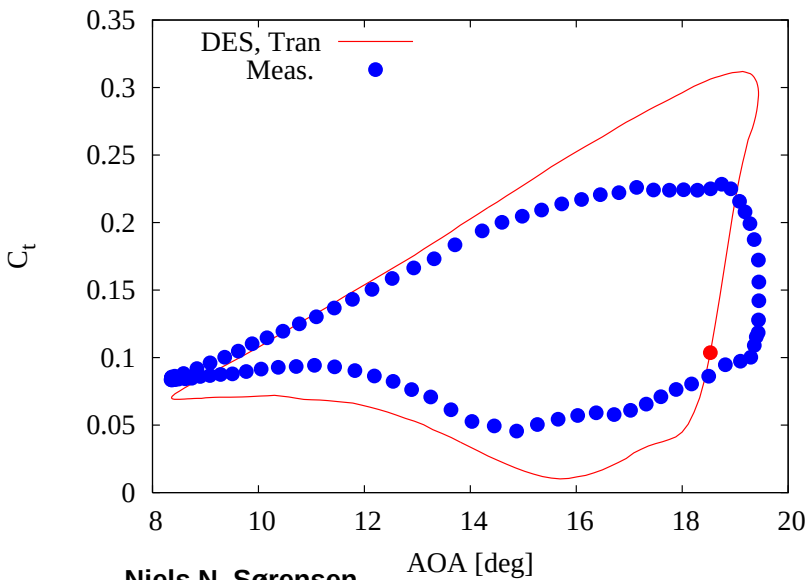

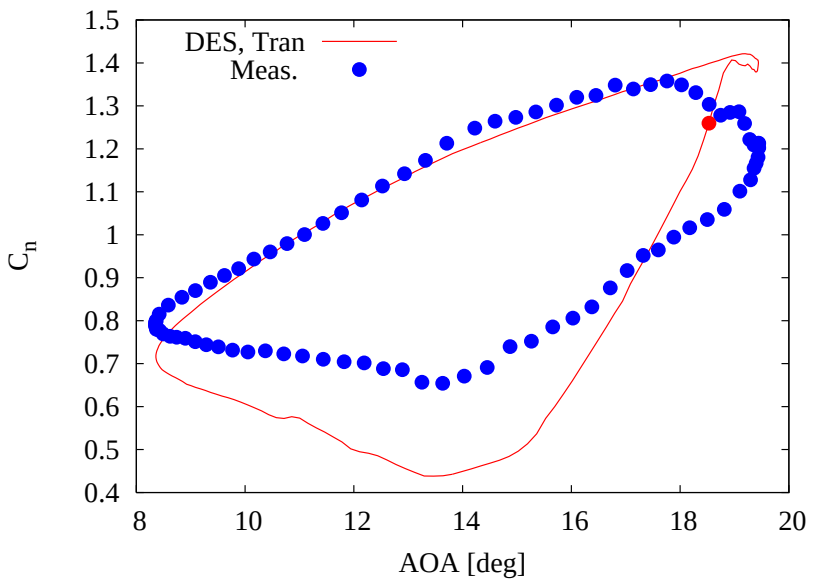

Niels N. Sørensen,
Risø DTU

Wind turbine related flow
Dynamic stall during standstill

CASE 47320, r/R=0.47

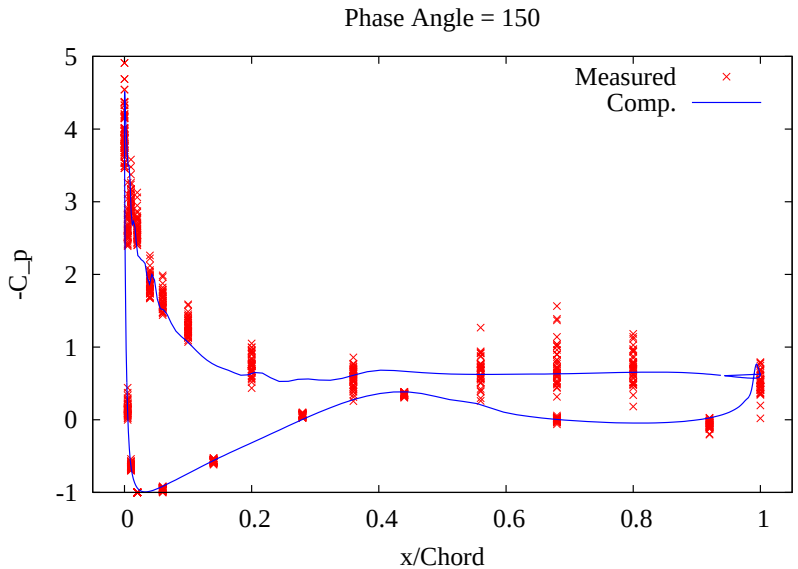

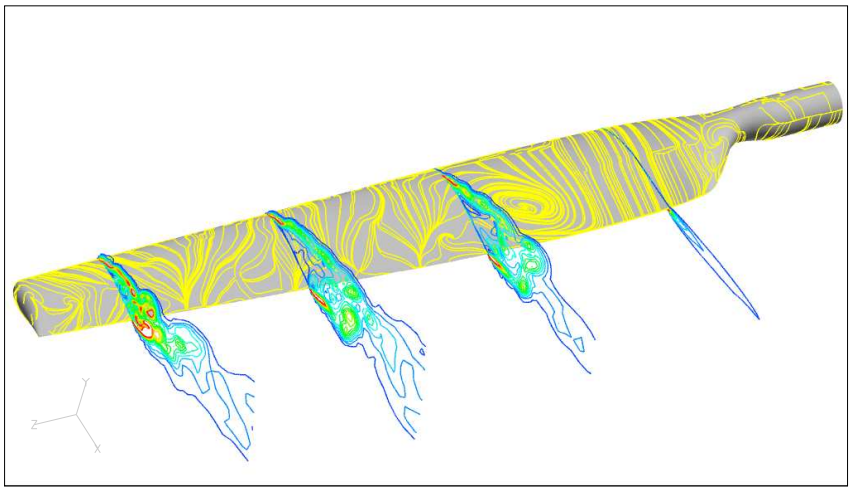

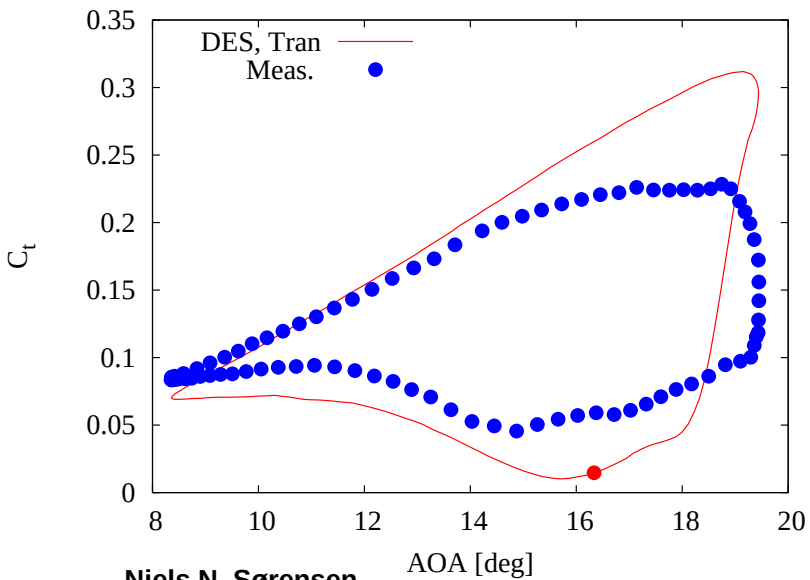

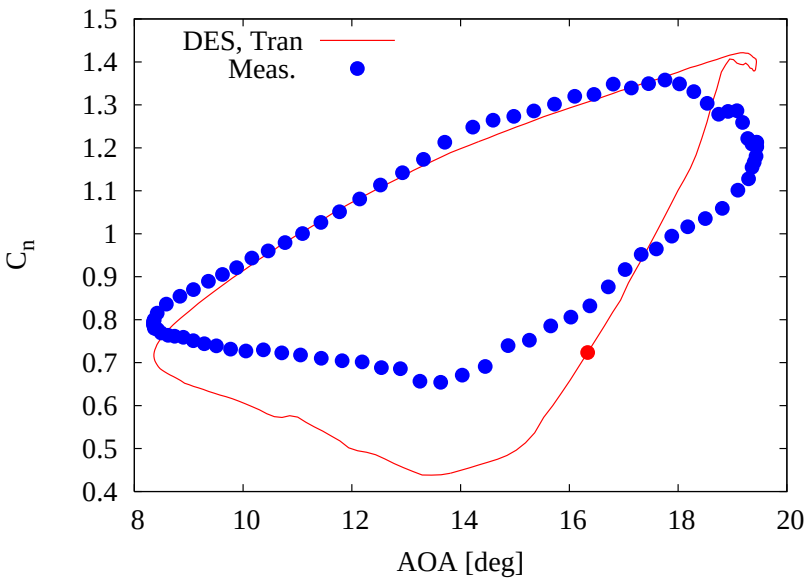

Niels N. Sørensen,
Risø DTU

Wind turbine related flow
Dynamic stall during standstill

CASE 47320, r/R=0.47

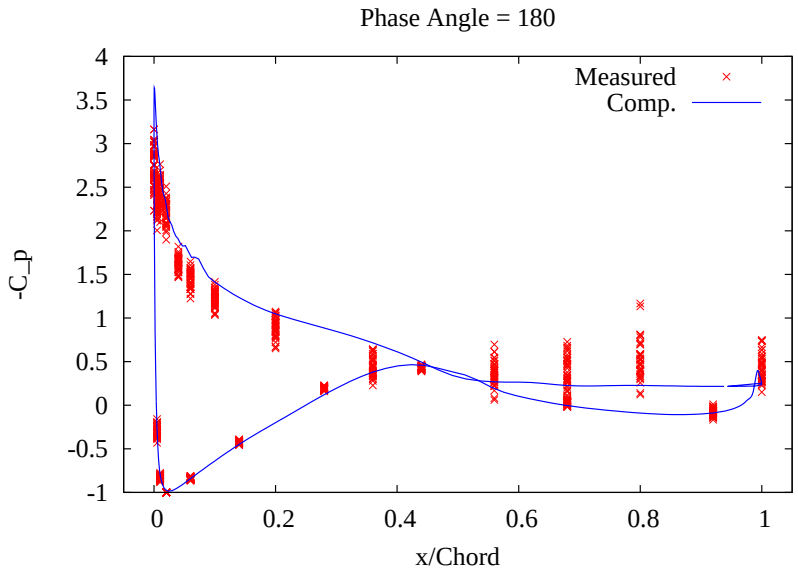

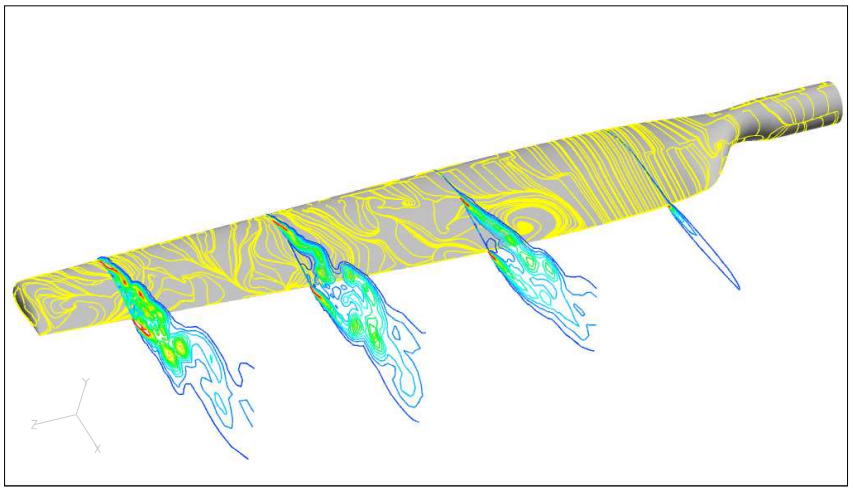

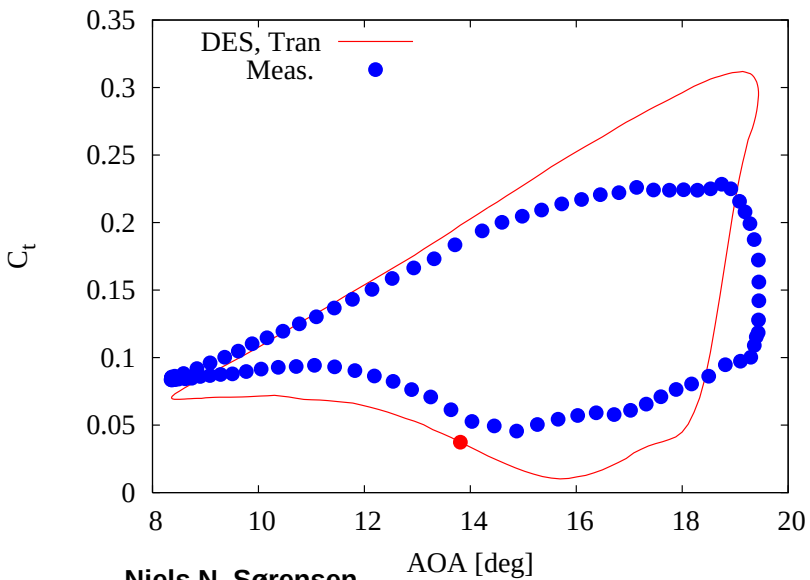

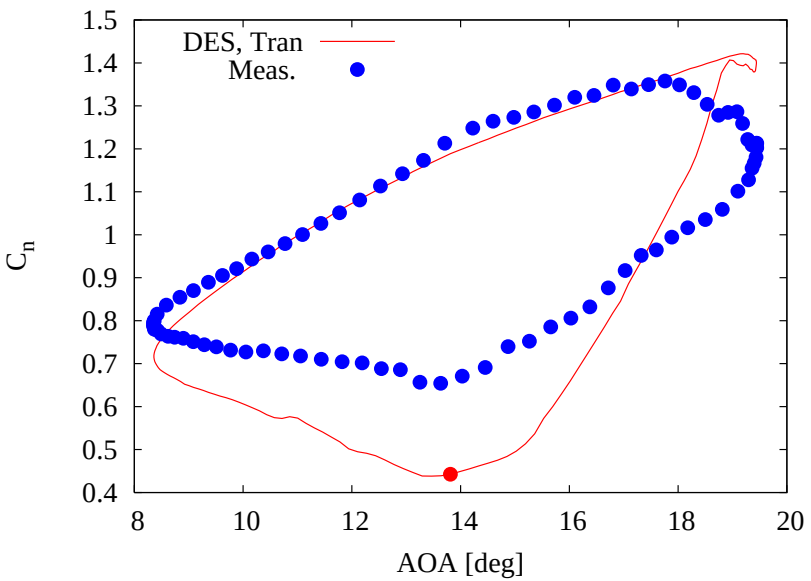

Niels N. Sørensen,
Risø DTU

Wind turbine related flow
Dynamic stall during standstill

CASE 47320, r/R=0.47

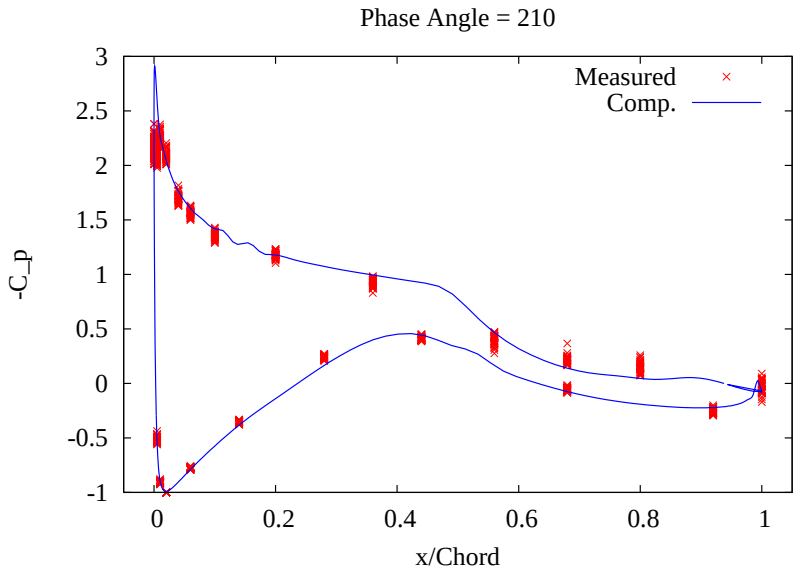

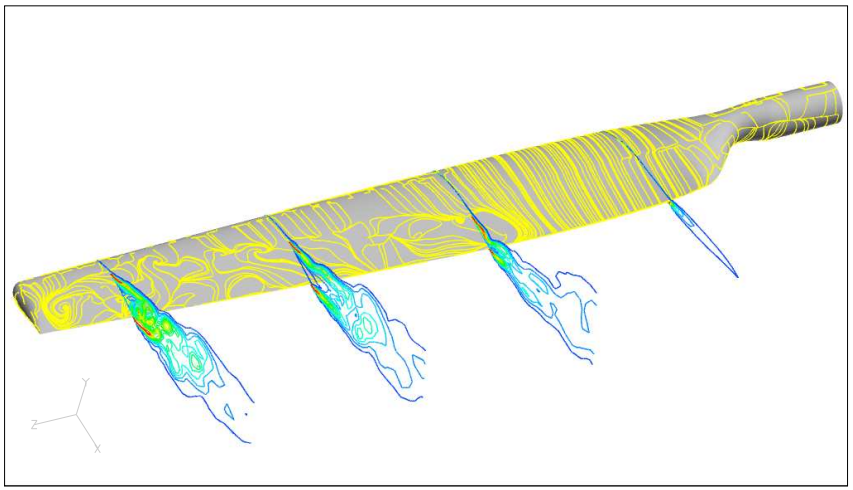

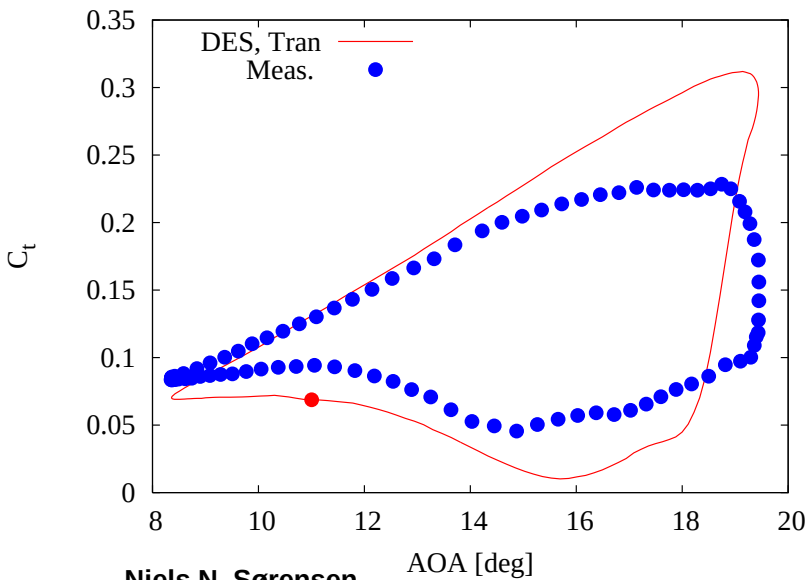

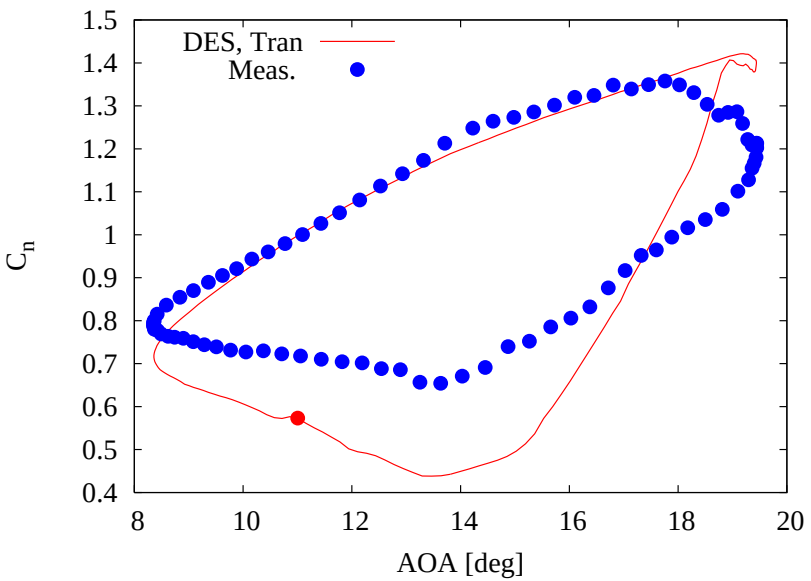

Niels N. Sørensen,
Risø DTU

Wind turbine related flow
Dynamic stall during standstill

CASE 47320, r/R=0.47

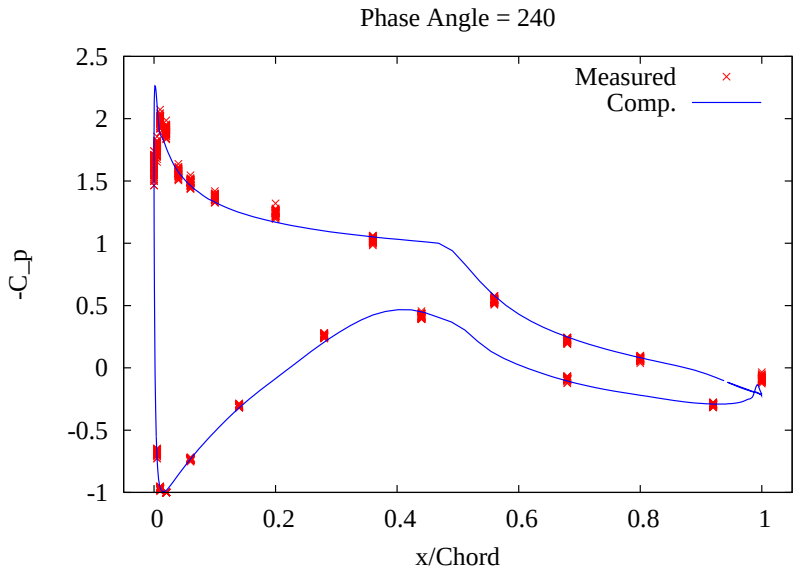

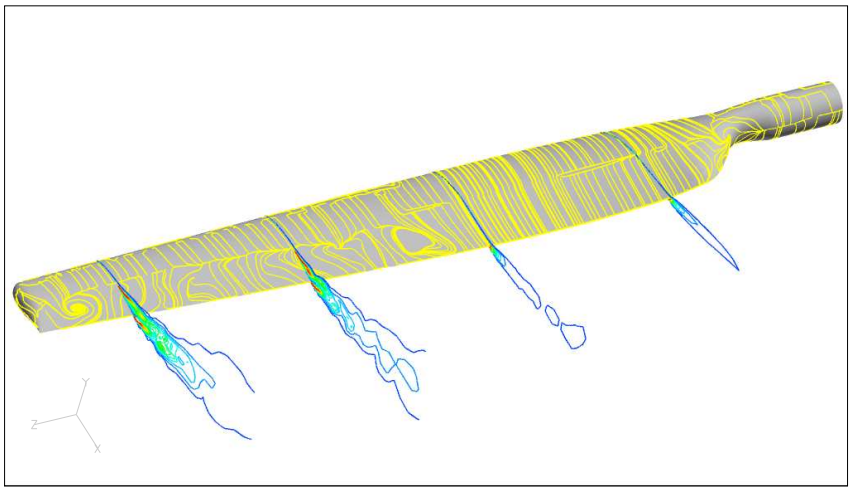

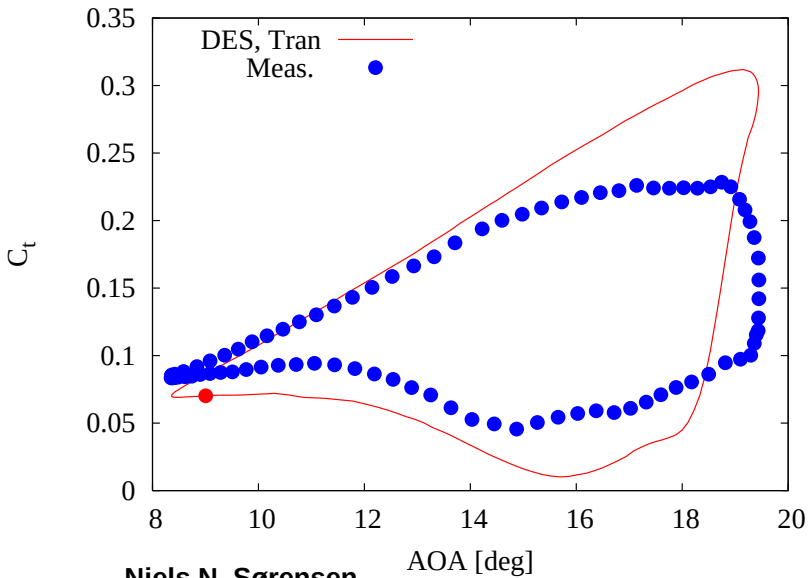

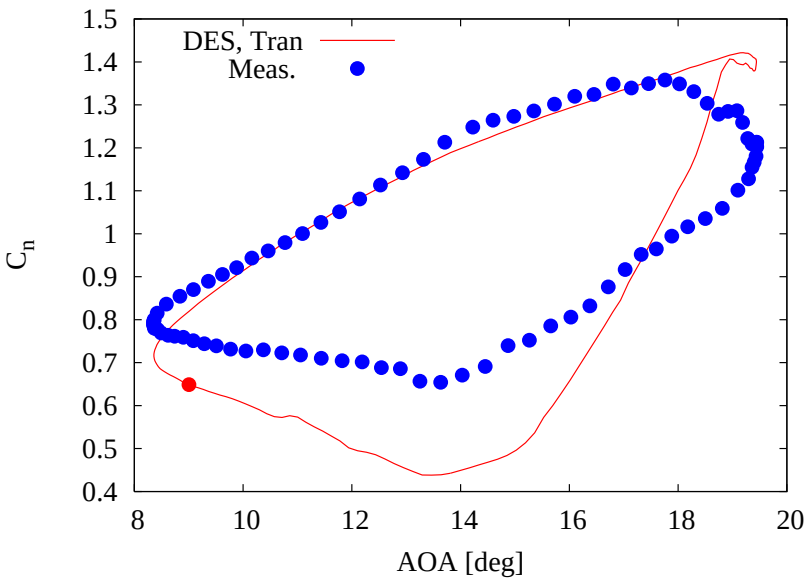

Niels N. Sørensen,
Risø DTU

Wind turbine related flow
Dynamic stall during standstill

CASE 47320, r/R=0.47

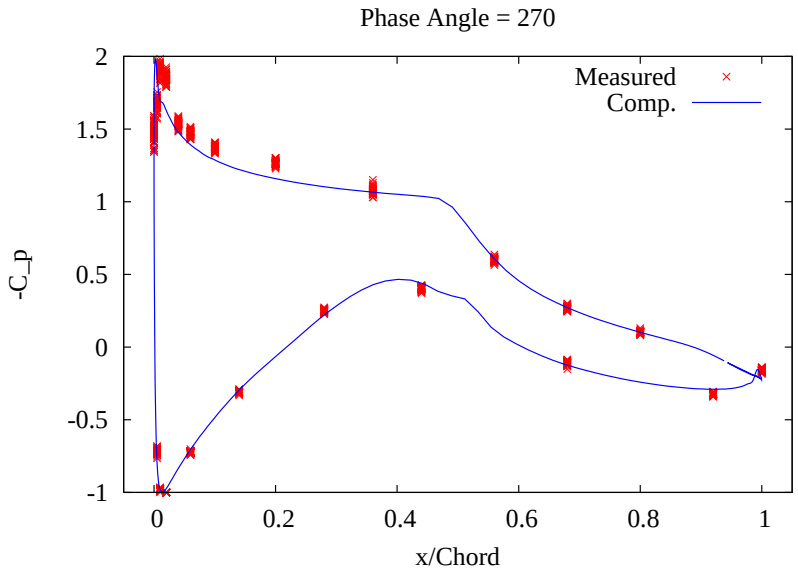

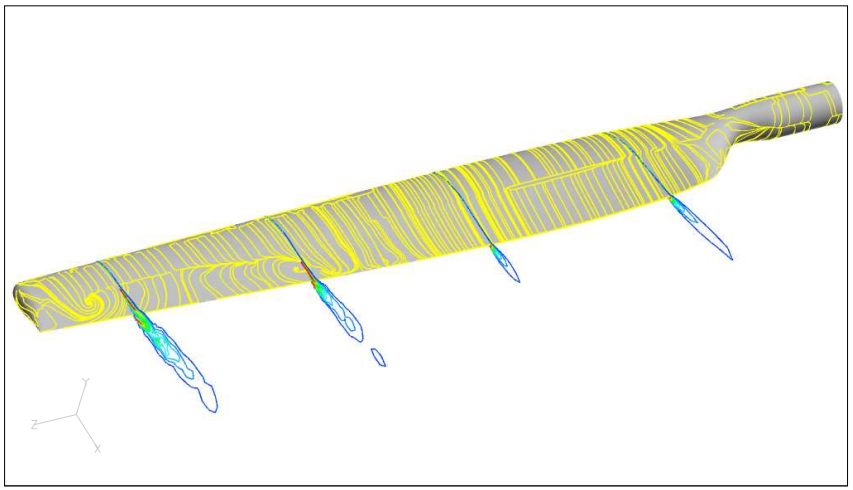

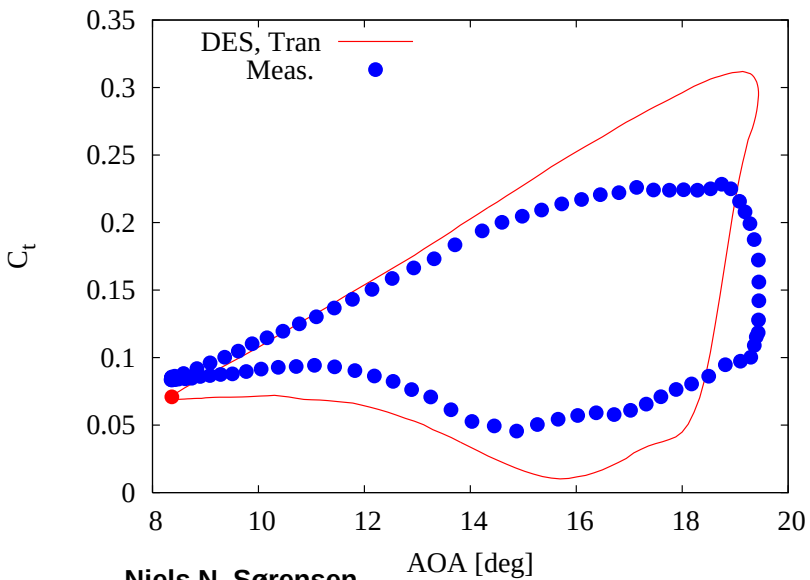

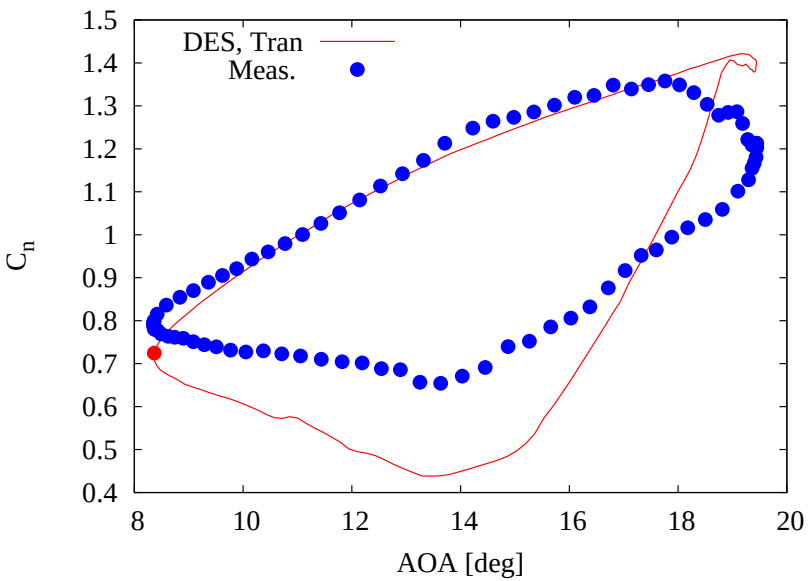

Niels N. Sørensen,
Risø DTU

Conclusion and Outlook

- I have given a series of application of CFD to wind turbine related problems
- The CFD solution is not always the absolute truth, but always a good supplement
- The most pronounced problem is the prediction of the onset of stall
- CFD can be used to shed light on fundamental problems/solution